UNIVERSIDADE D
COIMBRA

Lamyae Akrou

Numerical Aspects of the Characteristic Modes Theory

Tese no âmbito do doutoramento em Engenharia Electrotécnica e de Computadores, Ramo de Especialização em Telecomunicações orientada pelo Professor Doutor Henrique J. A. da Silva e apresentada ao Departamento de Engenharia Electrotécnica e de Computadores da Faculdade de Ciências e Tecnologia da Universidade de Coimbra

Julho de 2020

Declaration of Authorship

I, Lamyae Akrou, declare that this thesis titled, 'Numerical aspects of the characteristic modes theory' and the work presented in it are my own. I confirm that:

- This work was done wholly or mainly while in candidature for a research degree at this University.
- Where any part of this thesis has previously been submitted for a degree or any other qualification at this University or any other institution, this has been clearly stated.
- Where I have consulted the published work of others, this is always clearly attributed.
- Where I have quoted from the work of others, the source is always given. With the exception of such quotations, this thesis is entirely my own work.
- I have acknowledged all main sources of help.
- Where the thesis is based on work done by myself jointly with others, I have made clear exactly what was done by others and what I have contributed myself.

Signed: _____

Date: _____

Abstract

Nowadays, the characteristic modes theory becomes more and more popular in the electromagnetic field as a very efficient tool for analysing and solving scattering and radiation problems. Unlike the existing analysis tools, the characteristic modes analysis is based on the eigenvalues and the eigenvectors. Actually, these two key factors help enormously in gaining useful physical insights into the scatterer's modes, the modes contributions to the radiation field, and reveals which mode is dominant for each frequency sample of the frequency band being examined. Normally, the eigenvalues and the eigenvectors are derived directly from the modal decomposition of the impedance matrix of the scatterer using the real and imaginary parts of the matrix. Unfortunately, it is found that the real part of the impedance matrix doesn't fully fill full the theoretical specifications of the characteristic modes theory, which harms the numerical accuracy of the characteristic modes and reduces tremendously the total number of the obtained modes. Therefore, in order to respond to the theoretical requirements of the characteristic modes theory, a new method is proposed to treat this issue by reconstructing the real part matrix using the expansion of the Green dyadic in spherical vector waves. The new approach proved its efficiency and resulted in higher numerical accuracy, an increased number of the characteristic modes, and improved the computational speed in comparison to the conventional approach. However, after obtaining the accurate characteristic modes, the issue of how to connect the modes with each other is raised. The choice of a suitable method to perform the modes tracking is very critical to the accuracy of the analysis of the characteristic mode. Thus, the modal tracking problem is investigated also, with a main focus on the modes swapping and degenerated modes phenomena encountered in the eigenvectors correlation method. Consequently, an enhanced modal tracking method is proposed based on the difference in magnitudes between successive eigenvalues, as a criterion to establish the associations between the modes along the frequency axis. The tracking method is validated using several numerical applications, and satisfactory results are obtained. At times, to achieve a higher accuracy of the modal tracking, it is mandatory to increase the number of frequency samples resulting in a larger size of the impedance matrix. The computation of the impedance matrix at discrete frequency samples is a very time-consuming process, particularly for wideband frequency applications, therefore, the necessity to apply the impedance matrix interpolation method is highlighted. Finally, relevant concepts used throughout this dissertation are detailed in the appendices section, together with the source codes used to perform the modal decomposition, the modal tracking, and the impedance matrix interpolation.

O resumo

Atualmente, a teoria dos modos característicos se torna cada vez mais popular no campo eletromagnético como uma ferramenta muito eficiente para analisar e resolver problemas de espalhamento e radiação. Diferentemente das ferramentas de análise existentes, a análise dos modos característicos é baseada nos valores próprios e nos vetores próprios. Na verdade, esses dois fatores-chave ajudam enormemente a obter insights físicos úteis sobre os modos do dispersor, as contribuições dos modos para o campo de radiação e revelam qual modo é dominante para cada amostra de frequência da banda de frequência sendo examinada. Normalmente, os valores próprios e os vetores próprios são derivados diretamente da decomposição modal da matriz de impedância do espalhador, usando as partes reais e imaginárias da matriz. Infelizmente, verifica-se que a parte real da matriz de impedância não preenche completamente as especificações teóricas da teoria dos modos característicos, o que prejudica a precisão numérica dos modos característicos e reduz tremendamente o número total dos modos obtidos. Portanto, a fim de responder aos requisitos teóricos da teoria dos modos característicos, um novo método é proposto para tratar essa questão, reconstruindo a matriz da peça real usando a expansão da díade de Green em ondas vetoriais esféricas. A nova abordagem provou sua eficiência e resultou em maior precisão numérica, um número aumentado de modos característicos e maior velocidade computacional em comparação com a abordagem convencional. No entanto, após obter os modos característicos precisos, surge a questão de como conectar os modos entre si. A escolha de um método adequado para executar o rastreamento de modos é muito crítica para a precisão da análise do modo característico. Assim, o problema de rastreamento modal também é investigado, com foco principal nos fenômenos de troca de modos e modos degenerados encontrados no método de correlação de vetores próprios. Consequentemente, um método de rastreamento modal aprimorado é proposto com base na diferença de magnitudes entre valores próprios sucessivos, como critério para estabelecer as associações entre os modos ao longo do eixo de frequência. O método de rastreamento é validado usando várias aplicações numéricas, e resultados satisfatórios são obtidos. Às vezes, para obter uma precisão mais alta do rastreamento modal, é obrigatório aumentar o número de amostras de frequência, resultando em um tamanho maior da matriz de impedância. O cálculo da matriz de impedância em amostras de frequência discreta é um processo muito demorado, particularmente para aplicações de frequência de banda larga, portanto, é destacada a necessidade de aplicar o método de interpolação da matriz de impedância. Finalmente, os conceitos relevantes usados ao longo desta dissertação são detalhados na seção de apêndices, juntamente com os códigos-fonte usados para realizar a decomposição modal, o rastreamento modal e a interpolação da matriz de impedância.

Acknowledgements

In the first place, I would like to express my sincere gratitude to my supervisor Dr. Henrique José Almeida da Silva, associate professor at the University of Coimbra, for his efforts, time, and guidance throughout these years. Although he left this world, he will remain a very distinguishable person who taught me many precious values, and to whom I am deeply grateful.

My thankfulness goes also to Dr. Miloslav Čapek, associate professor at the Czech Technical University, and his teamwork and all the members of the Department of Electromagnetic field, for the welcoming and fruitful collaboration during my research stay in Prague, Czech Republic.

Special thanks are due to professors Dr. Maria do Carmo and Dr. Tiago Morgado for their precious help in reviewing this dissertation report.

I am grateful to Dr. Jorge Dias, Dr. Carlos Fernandes, Dr. Mario Silveirinha, and Dr. Henrique Salgado for accepting to be part of the jury committee, and for their time and efforts to evaluate this work, and for valuable suggestions.

I am thankful to Dr. Andre Mendes for his assistance in the administrative issues.

I am particularly grateful for Dr. Teresa Gomes, Dr. Tony Almeida, and Dr. Paulo Coimbra with whom I have had the pleasure to take courses during the first year of my studies in Coimbra.

I am very thankful to Abdelmalek Essaadi University, National Center for Scientific and Technical Research in Morocco, and Erasmus Mundus – Al Idrisi II scholarship for financial support.

I would also like to thank all the members of staff at the Department of Electrical and Computer Engineering in Coimbra, for their assistance and valuable technical support.

Many thanks go to all members of the Mathworks forum, Stack Exchange forum, LaTex, Academic Phrasebank of Manchester University, Word hippo, Thesaurus, Power thesaurus, Word Counter, Google translate, Merriam webster, Grammarly, Reverso, and to all similar websites providing help in coding and editing.

Last but not least, I am profoundly grateful to all my family members for all the support and encouragement through my entire life, and for their patience, sacrifices. You have been always a source of motivation and inspiration, thank you.

Dedicated to my dearest sister Bouchra.

Contents

List of Figures

List of Tables

Abbreviations

AEFIE	**A**ugmented **E**lectric **F**ield **I**ntegral **E**quation
AMFIE	**A**ugmented **M**agnetic **F**ield **I**ntegral **E**quation
A(S)MFIE	**A**pproximate **S**ymmetric **M**agnetic **F**ield **I**ntegral **E**quation
CFIE	**C**ombined **F**ield **I**ntegral **E**quation
CM	**C**haracteristic **M**odes
CMA	**C**haracteristic **M**odes **A**nalysis
CMT	**C**haracteristic **M**odes **T**heory
EFIE	**E**lectric **F**ield **I**ntegral **E**quation
GEP	**G**eneralized **E**igenvalue **P**roblem
MFIE	**M**agnetic **F**ield **I**ntegral **E**quation
MiMo	**M**ulti-**I**nput- **M**ulti-**O**utput
MoM	**M**ethod **o**f **M**oments
MS	**M**odal **S**ignificance
PEC	**P**erfect **E**lectric **C**onductor
PO	**P**hysical **O**ptics
RWG	**R**ao-**W**ilton-**G**lisson basis functions
SIE	**S**urface **I**ntegral **E**quation
SSIE	**S**ingle **S**ource **I**ntegral **E**quation
TE	**T**ransverse **E**lectric
TM	**T**ransverse **M**agnetic
VIE	**V**olume **I**ntegral **E**quation

Physical Parameters

Angular frequency	ω	in radian per second (rad/s)
Conductivity	σ	in siemens per meter (S/m) or (Ω^{-1}/m) or (mho/m)
Electric charge density	ρ_e	in coulombs per meter cubed $(Coul/m^3)$
Electric current density	J	in amperes per meter squared (A/m^2)
Electrical field	E	in volts per meter (V/m)
Electric flux density	D	in coulombs per meter squared $(Coul/m^2)$
Magnetic charge density	ρ_m	in webers per meter cubed (Wb/m^3)
Magnetic current density	M	in volts per meter squared (V/m^2)
Magnetic field	H	in amperes per meter (A/m)
Magnetic flux density	B	in webers per meter squared (Wb/m^2)
Permeability	μ	in henries per meter (H/m)
Permittivity	ϵ	in farad per meter (F/m)
Speed of light in vacuum	c	in meter per second $(2.997\ 924\ 58 \times 10^8\ ms^{-1})$
Wave impedance	η	in ohms (Ω)
Wave number	k	in reciprocal meters (m^{-1})

Chapter 1

Introduction

Nowadays, characteristic modes theory (CMT) is considered as a very promising field of study, particularly for antenna design optimization. Its mathematical formulation was first done by Garbacz [1] by making use of the scattering matrix. His goal was to find a proper field representation of the modal expansion type, which can simplify the solution of scattering problems for arbitrarily shaped scatterers. He came to the conclusion that each perfectly conducting body possesses a particular set of surface currents called "characteristic modes" and corresponding radiated fields which characterize the body shape independently of any specific excitation. The work of Garbacz inspired Harrington and Mautz to investigate the characteristic modes theory. Actually, the basics of the theory were already established by Garbacz for conducting bodies, unfortunately without practical numerical implementation [1]. Hence, they proposed the use of the method of moments (MoM) [2–4] to perform the numerical implementation of the theory based on the impedance matrix instead of the scattering matrix [5, 6]. In fact, they presented a simpler formalism of the theory, with explicit formulas for determining the mode currents and fields for conducting bodies. Shortly, they extended the theory to dielectric and magnetic bodies in [7] using the volume integral equation, which included the case of lossy materials. Later, the authors presented an alternative to the volume formulation using the equivalent surface currents [8]. After that, Harrington and Mautz have driven their research work to investigate the possible uses of the characteristic modes such as controlling the radar scattering by reactive loading for wire objects [9], and radiation pattern synthesis and optimization of radar cross-section for loaded N-port scatterers [10, 11]. The two researchers also applied the theory for aperture problems [12]. In short, their work was mostly on the applications of the characteristic modes theory, whereas Garbacz' work was mainly directed toward the development of the theory itself. He and his colleague Inagaki went into defining a new set of characteristic modes (known as Inagaki modes), where the region of observation is over more general regions than the

body surface and the sphere at infinity [13]. Later, Inagaki and Garbacz and Pozar took advantage of the orthogonality properties of Inagaki modes to investigate antenna pattern synthesis and optimization problems [14]. Subsequently, Liu, Garbacz and Pozar proposed a new formalism to the theory in [15], where the resulting "generalized characteristic modes" set presents many appealing features compared to Inagaki modes, such as reducing both the pattern error in pattern synthesis and the computational time. A recent study by Etheir and McNamra shed light on the efficiency of the generalized modes set in guiding the antenna design process, specifically, multi-input-multi-output (MIMO) antennas used for mobile communications [16]. However, it is rare to find other research works exhibiting the potential of the generalized modes. In effect, the majority of researchers went into investigating the characteristic modes derived from diagonalizing the impedance matrix. The characteristic modes were used in solving several vexing problems in antenna design, such as small antenna placement over a supporting structure. This problem was firstly addressed by Newman in [17], where he considered the antenna as a probe, and not as a radiator. He demonstrated that the radiation resistance and efficiency of a small antenna can be substantially increased by properly chosen the antenna location over the supporting structure. Analogically, Austin and Murray in [18] used characteristic modes of both the antenna and the structure (a vehicle) in optimizing the antenna performance and generating the desired radiation pattern. Subsequently, their work motivated Strohschein to study the characteristic modes response of a wireless device while varying the antenna placement, with the dimensions of the antenna and the wireless device comparable to the wavelength. His study highlighted how the characteristic modes of the isolated antenna and the device are modified as the antenna and the device become collocated [19]. Furthermore, many other applications of the CMT were proposed such that made by Hilbert et al. [20], where the authors proved the usefulness of the theory in understanding the antenna operation even when dealing with electrically large and complicated structures such as a log-periodic dipole antenna. In the meantime, Kabalan and his research team focused their efforts on investigating the apertures problems, where a variety of electromagnetic structures were investigated to gain more physical insights into the electromagnetic penetration process through an aperture separating two different mediums [21–25].

Later, despite all these prominent research works and the promising applications of the theory, the TCM has fallen into disuse for several years, possibly this stems from the limited capabilities of computer systems at that time. Nevertheless, a considerable effort in recent years has been devoted to recover and shed light on the potential of the CMT in solving radiating and scattering problems (see Fig 1.1), with a major focus on antenna design optimization for personal mobile communication devises. Since its re-emergence, numerous publications on the mobile handset antenna designs have been released [26–29], where the CMT has found many applications in antenna shape synthesis [30–36],

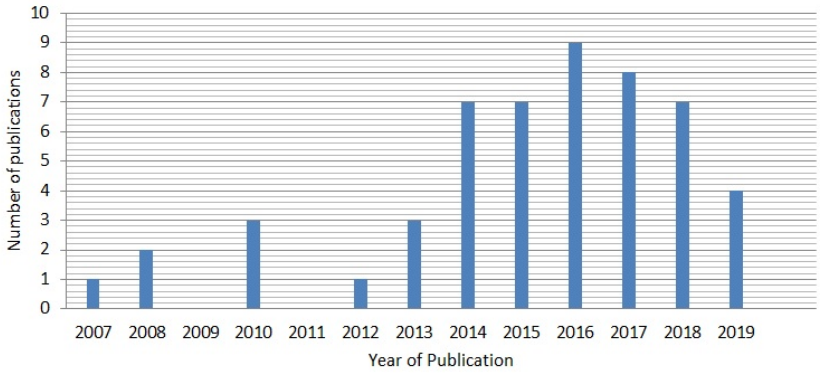

FIGURE 1.1: The number of scientific publications on the characteristic modes theory, the statistics are generated using "Web of Science" citation database, using the search terms: "characteristic modes theory" or "characteristic modes decomposition" or "impedance matrix decomposition" or "modal tracking" or "characteristic modes analysis". Retrieved October 17, 2019, from https://apps.webofknowledge.com.

and in MiMo antennas design [16, 37–41], besides the reconfigurable antennas [42][43, chap.5], and antennas based on meta-materials [44–46], in addition to some applications in extracting the equivalent circuit model of antennas [31, 47, 48]. Actually, the use of CMT in antennas design yielded great achievements, most prominently are the bandwidth enhancement and the improvement of the radiation efficiency of antennas. Part of these accomplishments is due to taking into consideration the chassis' modes and the chassis-antenna coupling [26, 32, 49–51]. Worth noting is that the widely adopted approach to implement the CMT is Harrington and Mautz's approach [5], where the MoM is substantially used. Actually, the MoM forms a good partner to the CMT, where the results accuracy can be improved based on the particular choice of basis and testing functions to be used. Most often, local basis functions are applied to MOM problems [4], namely, the Rao-Wilton-Glisson (RWG) basis functions [52]. Typically, RWG basis functions are used for conducting bodies and homogeneous penetrable materials in conjunction with the surface integral equation (SIE) method [8, 53, 54]. Whereas, the Schaubert-Wilton-Glisson (SWG) basis functions are used for inhomogeneous dielectric bodies together with the volume integral equation (VIE) [55]. It is valuable to note that there are very scarce implementations of the CMT using the VIE method [56], as it requires a high number of the MoM unknowns compared to the SIE implementations which are the most adopted, yet many computational complexities are still encountered in the application of the theory for electrically large bodies. Foremost, the storage problem of the MOM matrix and the potentially long computation time. Solutions to these challenges might be found through the use of MoM matrix interpolation [57, 58] or even through the use of Multilevel Fast Multiple Method algorithm for large scale problems [59] [4, chap.8]. Furthermore, the modal tracking is another major problem of the CMT. Usually, this issue is detected while observing the variation of the characteristic modes

along with the frequency axis, where the modes present sometimes unjustified behavior, i.e., they can appear or disappear all of a sudden. This becomes more and more severe for complex structures. Different tracking approaches were proposed to solve this problem. The majority of these approaches are based on computing the correlation coefficient between some specific modal quantities such as the eigenvectors, or the modal fields [60–64]. The use of hybrid methods based on the extrapolation of the eigenvalues and correlation of the eigenvectors was also investigated [65, 66]. While, the authors in [67] proposed the use of the characteristic modes orthogonality to perform the tracking. Notably, all the above mentioned tracking methods have been tested using conducting bodies. In fact, it is seldom to find modal tracking applied for dielectric objects as it was done in [68, 69].
In this thesis, some of the above-mentioned problems of the characteristic modes theory will be examined with some solutions to overcome these difficulties.

1.1 Objectives

The principle goal of the present thesis is to review the basics of the characteristic modes theory for both perfectly conducting bodies and dielectrics and investigate some of the critical issues encountered in its numerical implementation, with a main focus on the conducting bodies. To that end, the following points are going to be addressed:

- The main surface integral equations used to perform the numerical implementation of the characteristic modes theory.
- Overcoming the deficiency issue of the real part of the impedance matrix.
- The improvement of the modal tracking results.
- The use of the impedance matrix interpolation to accelerate the computations.

1.2 Thesis Outline

The present work is divided into seven chapters, where a literature review on the characteristic modes theory was given in Chapter 1. While Chapter 2 presents the mathematical formulation of the characteristic modes theory for conducting bodies based on the electric field integral equation (EFIE) and for dielectrics both with and without losses using the volume integral equation (VIE). Moreover, Chapter 3 contains the most common surface integral equation formulations used in performing the numerical

implementations of the characteristic modes theory to analyse conducting and dielectric bodies. The formulations presented therein do not consider losses and invoke the surface equivalence principle. Whereas, Chapter 4 is dedicated to shedding light on the shortcoming of the real part of the impedance matrix and present a new method to reformulate the characteristic modes theory using spherical vector waves. The work contained in Chapter 4 is based on the journal paper [70], which was conducted in cooperation with Prof. Miloslav Čapek from Czech Technical University in Prague. Furthermore, Chapter 5 mainly concerns the characteristic modes tracking issue, namely, the swapping modes and degenerated modes problems encountered in the eigenvectors correlation-based methods, and presents an enhanced method to perform modal tracking using eigenvalues only. Thereafter, Chapter 6 reviews the MoM matrix interpolation approach and highlights its efficiency in accelerating the impedance matrix filling time. Chapter 7 draws the main conclusions of this work and provides some ideas for future work. Finally, some relevant concepts used throughout this work are detailed in the appendices, together with the source codes used to perform the modal decomposition, the modal tracking, and the impedance matrix interpolation.

1.3 Main Contributions

The scientific contribution of this thesis can be summarized as follows:

- Increasing the accuracy of the characteristic modes by rebuilding the real part matrix using the expansion of the Green dyadic in spherical vector waves[1].
- The development of an enhanced modal tracking approach using the difference in magnitude between contiguous eigenvalues.

[1]This is the result of a collaboration work [70], to which the author of this thesis contributed by writing the $[S]$ matrix implementation code by making use of the spherical wave functions used to build the theoretical background presented in [70]. Meanwhile, Vit Losenicky performed the $[S]$ matrix implementation in Matlab using the M and N functions presented in [71] for comparison purposes. Further, the author used the Advanpix Matlab toolbox to transform the $[S]$ matrix implementation into an arbitrary precision code. Moreover, the author developed the modal decomposition code using Python. While Doruk Tayli derived the expressions and performed the Python multi-precision implementation. Whereas, the manuscript with the figures and tables was prepared mostly by Doruk Tayli and Miloslav Čapek, while recommendations were given by both Lukas Jelinek and Mats Gustafsson to improve the implementations and the manuscript. These were the main tasks of the co-authors as far as the author is aware.

1.4 List of Publications

L. Akrou, Corrections to "Enhanced Modal Tracking for Characteristic Modes", IEEE Transactions on Antennas and Propagation, vol. 68 (5), p. 4161-4162, 2020.

L. Akrou, H.Silva, "Enhanced Modal Tracking for Characteristic Modes", IEEE Transactions on Antennas and Propagation, Vol. 67 (1), 356-360, Jan 2019.

D. Tayli, M. Capek, **L. Akrou**, V. Losenicky, L. Jelinek, and M. Gustafsson, "Accurate and Efficient Evaluation of Characteristic Modes", IEEE Transactions on Antennas and Propagation, Vol. 66 (12), 7066-75, Dec 2018.

Miloslav Capek, Doruk Tayli, **Lamyae Akrou**, Vit Losenicky, Lukas Jelinek, Mats Gustafsson, "Accurate Evaluation of Characteristic Modes", 12^{th} European Conference on Antennas and Propagation (EUCAP), 2018.

Chapter 2

Characteristic Modes Theory

2.1 Introduction

Nowadays, the characteristic modes theory (CMT) constitute an appealing approach for predicting the behavior of an arbitrarily shaped structure immersed in an electromagnetic field. This theory was originally proposed by Garbacz [1], and later refined by Harrington and Mautz [5][6]. Mainly, it is based on properly defining the relationship between the surface currents over the structure and the scattered fields without considering any feeding. Its mathematical formulation starts by delineating the impedance operator, from which a generalized eigenvalue problem [72, 73] is derived. Solving the resulting generalized eigenvalue problem provides new information, namely, eigenvalues and eigenvectors, which are very important in understanding the radiation and scattering mechanisms. By virtue of the eigenvectors' orthogonality, the characteristic modes form a useful basis set in which to expand the currents and the scattered fields or the radiated fields. A detailed derivation of the CMT formulation for both conductors and dielectrics will be given in the next sections following the approach given in [5][6].

2.2 Definition of Characteristic Modes

Inevitably, the most important concept in the theory is that of the characteristic modes. Garbacz and Tupin [74] define the characteristic modes as a basis set that allows to expand the currents and fields scattered or radiated by a perfectly conducting obstacle under harmonic excitation. According to the authors this set possesses orthogonality properties both over the obstacle surface and the enclosing sphere at infinity, and succinctly relate the scattering operator and impedance operator representations of the obstacle. Also, the authors stated that the characteristic modes exhibit interesting

mathematical properties which may be interpreted physically in terms of radiated and net stored powers. However, the above definition is pertaining to conducting bodies only. Later, a more general definition which extends to include other materials was given by Harrington and Mautz in [7], where they define the characteristic modes as:

"*For loss-free bodies, the modes consist of a set of real characteristic sources which diagonalize the generalized network matrix for the body, and a set of characteristic fields which diagonalize the scattering matrix. Most of the properties of these modes remain the same as those of the corresponding modes for perfectly conducting bodies. For lossy bodies, the corresponding modes have complex characteristic sources. However, in the lossy case there also exists a set of real characteristic sources which diagonalize the generalized network matrix, but their fields do not diagonalize the scattering matrix*".

Theoretically, these definitions determine the nature of the eigenvalues, eigenvectors, and the characteristic fields of the body which should be obtained when applying the characteristic modes theory to a specific case study.

2.3 Formulation of CMT for Conductors

Basically, CMT for perfect electric conductor (PEC) bodies is developed from the electric field integral equation (EFIE) [75]. The reason is that EFIE is applicable to both closed and open structures [76]. Therefore, let consider a metallic in an impressed electric field E^i. The total field is the summation of the incident field E^i and the scattered field E^s such that [77]

$$E = E^i + E^s \tag{2.1}$$

Next, by applying the boundary conditions on the surface S of the metallic body, the tangential component of the total electric field vanishes, resulting in [5, 77]

$$L_{tan}(J) = E^i_{tan} = -E^s_{tan} \tag{2.2}$$

Where, equation (2.2) is the operator[1] equation of the current J on the surface S. In accordance with [5], $-L(J)$ gives the electric intensity at any point in space due to the current J on S, and have the dimensions of the impedance operator Z, hence [5]

$$Z(J) = L_{tan}(J) \tag{2.3}$$

[1] For a definition of the concept of an operator see [1, chap.2]

Actually, the operator L can be expressed as [5]

$$L(J) = j\omega A(J) + \nabla\phi(J) \tag{2.4}$$

with $A(J)$ standing for the magnetic vector potential, and $\phi(J)$ representing the electric scalar potential, given by [5]

$$A(J) = \mu \oiint_S J(\boldsymbol{r}')g(\boldsymbol{r}, \boldsymbol{r}')\,\mathrm{d}s' \tag{2.5}$$

$$\Phi(J) = \frac{-1}{j\omega\epsilon} \oiint_S \nabla' \cdot J(\boldsymbol{r}')g(\boldsymbol{r}, \boldsymbol{r}')\,\mathrm{d}s' \tag{2.6}$$

$$g(\boldsymbol{r}, \boldsymbol{r}') = \frac{\exp(-jk \mid \boldsymbol{r} - \boldsymbol{r}' \mid)}{4\pi \mid \boldsymbol{r} - \boldsymbol{r}' \mid} \tag{2.7}$$

Here $g(\boldsymbol{r}, \boldsymbol{r}')$ is the Green's function of free space [78], and J is the surface current on S, where ϵ, μ, and k are the electric permittivity, the magnetic permeability and the wave number of vacuum, respectively, while ω is the angular frequency, and j is the imaginary unit number, whereas $\boldsymbol{r}$ and $\boldsymbol{r}'$ denote the field point and the source point, with s' related to $\boldsymbol{r}'$. Hence, by substituting (2.5) and (2.6) in (2.2) the tangential component of the incident field can be written as

$$E^i_{tan} = j\omega\mu \oiint_S J(\boldsymbol{r}')g(\boldsymbol{r}, \boldsymbol{r}')\,\mathrm{d}s' + \nabla\left(\frac{-1}{j\omega\epsilon} \oiint_S \nabla' \cdot J(\boldsymbol{r}')g(\boldsymbol{r}, \boldsymbol{r}')\,\mathrm{d}s'\right) \tag{2.8}$$

The equation (2.8) is the electric field integral equation (EFIE) [76], and its matrix form is obtained using the Method of Moments (MoM) [2–4]. In fact, the implementation of the MoM implies that the studied structure is segmented into small triangular elements. Then, a suitable basis functions and testing functions are chosen. Here, the testing functions are taken to be the same as the expansion functions, this is known also as the Galerkin testing procedure [3]. Frequently, the Rao-Wilton-Glisson (RWG) basis functions are used to model the PEC surfaces [52], owing to their simplicity, and their divergence conforming property (i.e. they have a finite divergence) that makes the representation of the current physical [75]. Consequently, the surface current expansion can be expressed as follows [6]

$$J = \sum_n^N I_n f_n \tag{2.9}$$

Here, I_n are the unknown coefficients to be determined, while N is the total number of basis functions (i.e., the inner edges), and f_n are the RWG expansion functions defined

in Appendix A. Additionally, a proper inner product is defined as [75, p.24]

$$< f_m, E^i_{tan} >= \iint_S f_m \cdot E^i_{tan} \, \mathrm{d}s \tag{2.10}$$

Therefore, taking the inner product of (2.2) with each testing function f_m results in the following set of linear equations [77]

$$\sum_n^N I_n < f_m, L_{tan}(f_n) >=< f_m, E^i_{tan} > \tag{2.11}$$

Henceforth, the subscript 'tan' will be omitted as the inner product concerns only the tangential components on the surface S. Equation (2.11) can be rewritten in matrix form equation resulting in [77]

$$[Z][I_n] = [< f_m, E^i >] \tag{2.12}$$

with the impedance matrix $[Z]$ given by [77]

$$[Z] = [< f_m, L(f_n) >] \tag{2.13}$$

and $[I_n]$ is the matrix containing the unknown coefficients I_n to be determined. Accordingly, the impedance matrix elements can be derived as [6, 77]

$$Z_{mn} = \oiint_S \mathrm{d}s \oiint_S \left[j\omega\mu \Big(f_m \cdot f_n \Big) + \frac{1}{j\omega\epsilon} \Big(\nabla' \cdot f_m \Big) \Big(\nabla \cdot f_n \Big) \right] g(\boldsymbol{r}, \boldsymbol{r}') \, \mathrm{d}s' \tag{2.14}$$

Where, the entries of the impedance matrix describes the electromagnetic coupling between different edge elements. Therefore, if the edge elements m and n are considered as finite small electric dipoles, then Z_{mn} represents the contribution of dipole n to the electric current of dipole m [79]. The obtained impedance matrix is diagonalized using the following weighted eigenvalue equation [5],

$$[Z][I_n] = (1 + j\lambda_n)[M][I_n] \tag{2.15}$$

where λ_n are the eigenvalues, while $[I_n]$ are the eigenvectors (also called eigenfunctions), and M is a weight operator chosen to be the real part of the operator Z. Actually, any choice of M would result in diagonalizing Z, but chosen $M = R$ grant the orthogonality property of the radiation patterns [5]. Subsequently, the impedance matrix is expressed in function of its real and imaginary parts, i.e.,

$$[Z] = [R + jX] \tag{2.16}$$

Therefore, by substituting (2.16) into (2.15) a simplified equation is derived as [1, 5]

$$[X][I_n] = \lambda_n[R][I_n] \tag{2.17}$$

The resulting equation (2.17) is known as the generalized eigenvalue problem [72], it can be numerically solved using the 'eig' function from Matlab [80] and Python [81] (for more details see Appendices B and C).
Theoretically, the obtained eigenvalues λ_n are real numbers and range from $-\infty$ to $+\infty$, with those of smallest magnitude being more important for radiation and scattering problems (see Fig. 2.1) [5], but practically they are not real, if it is the case, only the real values are considered. The usefulness of the eigenvalues can be better perceived using their physical meaning, which can be summed up as it follows [30]

- when $\lambda_n > 0$, the mode can be considered inductive, i.e. stores magnetic energy.
- when $\lambda_n < 0$, the mode can be considered capacitive, i.e. stores electrical energy.
- when $\lambda_n = 0$, the mode can be considered at resonance and can be called externally resonant.
- when $\lambda_n \to \infty$, the mode doesn't radiate any power and can be considered at internal resonance.

Consequently, the eigenvalues related to a mode n, can be expressed as the quotient of stored power and radiated power, or alternatively, in terms of the magnetic and electric energies, W_m^n and W_e^n, respectively, and the angular frequency ω, leaving [30, 76, 82]

$$\lambda_n = \frac{P_{stored,n}}{P_{radiated,n}} = \frac{2\omega(W_m^n - W_e^n)}{P_{radiated,n}} \tag{2.18}$$

In the meanwhile, due to the wide range of the eigenvalues, other quantities have been derived, namely, the characteristic angles [1, 17], and the modal significance [18], which map the eigenvalues into the limited ranges $]90^o, 270^o[$ (see Fig. 2.2), and $]0, 1]$ (see Fig. 2.3), respectively. Where, the characteristic phases, known as characteristic angles, indicates the phase difference between a characteristic current and the associated characteristic field [33], and it is given by [17]

$$\alpha_n = 180^o - tan^{-1}(\lambda_n) \tag{2.19}$$

Hence, modes with characteristic angles near 180^o are considered as good or effective radiators, while modes with characteristic angles near 90^o or 270^o are deemed ineffective radiators [17]. Regarding the modal significance, it is inferred that the more is the

modal significance is closer to 1, the more efficiently the mode resonates and radiates when excited [33]. The expression of the modal significance MS_n is given by [18]

$$MS_n = \left| \frac{1}{1 + j\lambda_n} \right| \tag{2.20}$$

Interestingly, a tentative has been made in [83] to define a more accurate formula of the modal significance by making use of the maximum of the mode' current density, however, it is restricted to radiation problems only.

Further, another useful parameter can be extracted from the representation of the curves of the modal significance which is the radiation bandwidth of the characteristic modes defined as [31]

$$BW = \frac{f_U - f_L}{f_{res}} \tag{2.21}$$

where f_{res} is the resonance frequency of the characteristic mode, while f_U and f_L are the upper and lower frequencies computed with respect to the MS_{HP} measure, which represent the the modal significance at half of the power radiated at resonance, and it is given by [31]

$$MS_{HP} = \left| \frac{1}{1 + j\lambda_n} \right| = \frac{1}{\sqrt{2}} = 0.707 \tag{2.22}$$

Moreover, a modal quality factor corresponding to each characteristic mode can be easily computed for narrow band radiators using the radiation bandwidth parameter as [31]

$$Q_{rad} = \frac{1}{BW} \tag{2.23}$$

In addition, the eigenvectors $[I_n]$ are assumed to be real, and normalized to radiate unit power, i.e., [6]

$$\begin{aligned} < J_n, RJ_n > &= < \sum_i I_{i,n} f_i, R \sum_j I_{j,n} f_j > \\ &= \sum_{i,j} I_{i,n} I_{j,n} < f_i, R f_j > \\ &= [I_n^T][R][I_n] = 1 \end{aligned} \tag{2.24}$$

Here, $(^T)$ denotes the transpose. It is worth mentioning that normalization ensures the uniqueness feature of the characteristic currents J_n [34], and it is optional, otherwise, if currents are not normalized, the factor $< J_n, RJ_n >$ must be properly introduced into the theory [5]. Furthermore, the characteristic currents must fulfil the orthogonality

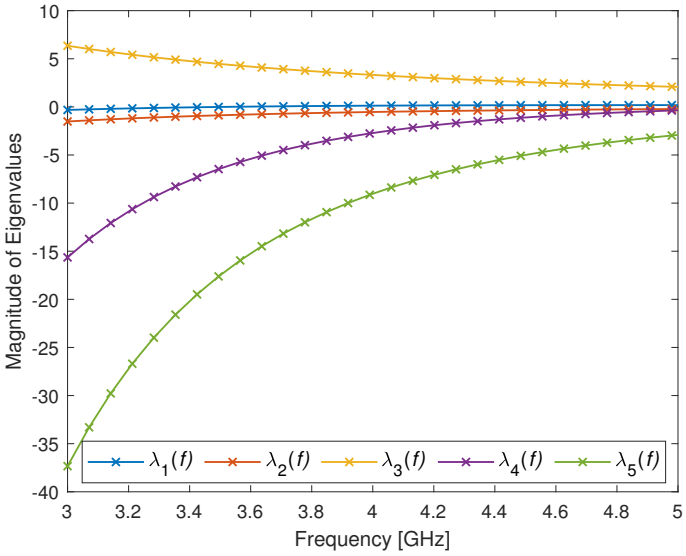

FIGURE 2.1: Example of the eigenvalues plot for a metallic plate ($L = 30$ mm, $W = 40$ mm along with the frequency bandwidth [3 GHz – 5 GHz]).

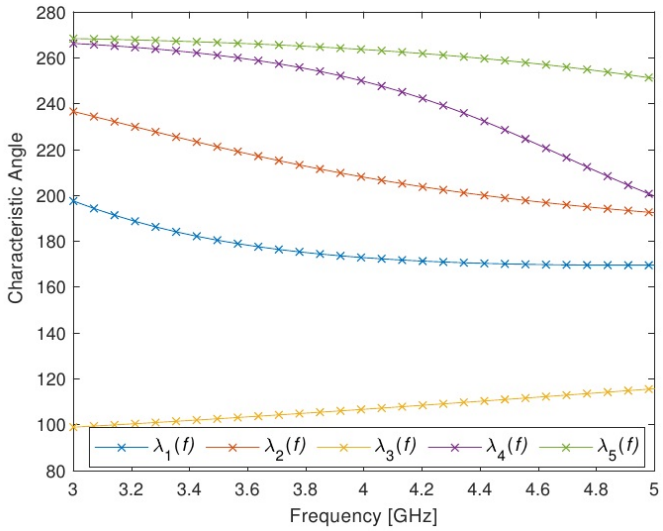

FIGURE 2.2: Example of the characteristic angles plot for a metallic plate ($L = 30$ mm, $W = 40$ mm along with the frequency bandwidth [3 GHz – 5 GHz]).

properties described by Harrington and Mautz in [5], i.e.,

$$< J_m, RJ_n > =< J_m^*, RJ_n >= \delta_{mn} \tag{2.25}$$

$$< J_m, XJ_n > =< J_m^*, XJ_n >= \lambda_n \delta_{mn} \tag{2.26}$$

$$< J_m, ZJ_n > =< J_m^*, ZJ_n >= (1 + j\lambda_n)\delta_{mn} \tag{2.27}$$

Where δ_{mn} is the Kronecker delta function (i.e., equals 0 if $m \neq n$ and 1 if $m = n$), while the asterisk symbol (*) denotes the complex conjugate.

Conventionally, the electric and magnetic fields generated by a characteristic current are

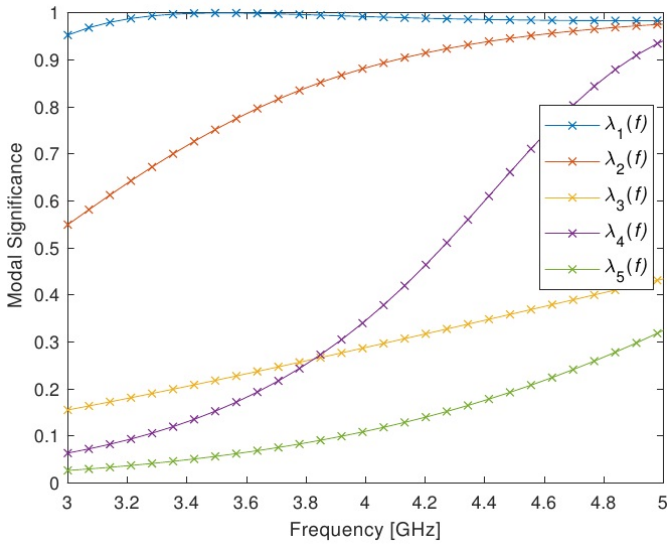

FIGURE 2.3: Example of the modal significance plot for a metallic plate ($L = 30$ mm, $W = 40$ mm along with the frequency bandwidth [3 GHz − 5 GHz]).

denominated characteristic fields, and they also satisfy the orthogonality relationships such that [5]

$$\frac{1}{\eta}\oiint_{S_\infty} \overrightarrow{E}_m \cdot \overrightarrow{E}_n^* \, \mathrm{d}s = \delta_{mn} \tag{2.28}$$

$$\eta \oiint_{S_\infty} \overrightarrow{H}_m \cdot \overrightarrow{H}_n^* \, \mathrm{d}s = \delta_{mn} \tag{2.29}$$

Where the explicit formulas of the the characteristic far fields $\overrightarrow{E}_n$ and $\overrightarrow{H}_n$ are given in [5] as

$$\overrightarrow{E}_n = \eta \overrightarrow{H}_n \times \overrightarrow{n} = \frac{-j\omega\mu}{4\pi \boldsymbol{r}} e^{-jk\boldsymbol{r}} \overrightarrow{F}_n(\theta, \phi) \tag{2.30}$$

with η is the intrinsic impedance of space, $\overrightarrow{n}$ and (θ, ϕ) are the unit radial vector and the angular coordinates on the sphere at infinity S_∞, while $\overrightarrow{F}_n$ is a complex vector representing the characteristic pattern.

2.4 Formulation of CMT for Lossless Dielectrics

According to [1], any material either it is a conductor, a dielectric or a magnetic possess a set of characteristic modes to expand the induced currents and the far-fields. Starting from this fact, Harrington and Mautz extended the characteristic modes theory to dielectric and magnetic bodies. Firstly, the volume integral equation (VIE) was used for the formalism of the characteristic modes theory [7]. Then, the surface integral equation

(SIE) was proposed in [8]. In this section, the VIE formulation will be used to derive the mathematical expressions of the CMT for dielectrics following the procedure in [7]. Analogically to the PEC bodies, the induced current J and the impressed electric field E^i are related through the impedance operator Z [7], such that

$$Z(J) = E^i \tag{2.31}$$

where the impedance operator Z is given by [7]

$$Z = Z_V + (j\omega \triangle \epsilon)^{-1} \tag{2.32}$$

Here, $\triangle\epsilon = \epsilon_V - \epsilon$, where ϵ_V is the electrical permittivity of the body, whereas the linear operator Z_V associate the scattered field E^s and the induced polarization current. Worth mentioning that Z_V is depending only on the shape of the body volume V, and can be expressed as [7]

$$Z_V(J) = -E^s \tag{2.33}$$

Therefore, Z_V can be explicitly expressed using the magnetic and electric potentials, A and Φ as it follows [7]

$$Z_V(J) = j\omega A(J) + \nabla\Phi(J) \tag{2.34}$$

Moreover, the induced polarization current J is defined by [7]

$$J = j\omega \triangle \epsilon(E^i + E^s) \tag{2.35}$$

Similarly, an inner product is defined over the body volume as [7]

$$< f_m, E^i >= \iiint_V f_m \cdot E^i \, \mathrm{d}v \tag{2.36}$$

Identically to the conducting bodies, the resulting generalized eigenvalue equation is expressed using the real and imaginary parts of the impedance matrix $[Z]$ such that [7]

$$[X][I_n] = \lambda_n[R][I_n] \tag{2.37}$$

Again, $[X]$ and $[R]$ are assumed to be real and symmetric. Also, all the eigenvalues are presumed to be real, for the characteristic currents they can be chosen real, and they fulfil the orthogonality relationships as in (2.25). Analogically, the case of magnetic bodies is a totally dual problem to the case of dielectrics, with the starting operator equation is in terms of the impressed magnetic field and the induced magnetization current, further details can be found in [7].

2.5 Formulation of CMT for Lossy Dielectrics

For the sake of completeness and self-consistency of the theory, the lossy materials case was also mathematically formulated in [7]. Hence, the theoretical formulation provided in Section 2.4 will be slightly altered. To begin with, the electric current, both conduction, and polarization is defined by [7]

$$J = (\sigma + j\omega \triangle \epsilon)(E^i + E^s) \tag{2.38}$$

where, σ represents the losses, and E^s is the scattered field defined by (2.33), whereas the incident field E^i is given by the modified operator equation such that [7]

$$E^i = (Z_V + Z_M)(J) \tag{2.39}$$

Again, Z_V is given by (2.34), while Z_M is expressed using [7]

$$Z_M(J) = (\sigma + j\omega \triangle \epsilon)^{-1}(J) \tag{2.40}$$

Clearly, Z_M depends mainly on the constitutive parameters. Furthermore, Z_V and Z_M are symmetric operators, and they can be re-written in terms of their real and imaginary Hermitian parts [7], i.e.,

$$Z_V = R_V + jX_V \tag{2.41}$$

$$Z_M = R_M + jX_M \tag{2.42}$$

To perform the diagonalization of the impedance operator formed by the summation of Z_V and Z_M, Harrington and Mautz proposed in [7] the following weighted eigenvalue equation given by

$$[Z_V + Z_M][I_n] = (1 + j\lambda_n)[R_V][I_n] \tag{2.43}$$

which, by substituting Z_V by its expression from (2.41), is reduced to [7]

$$[X_V - jZ_M][I_n] = \lambda_n[R_V][I_n] \tag{2.44}$$

Equation (2.44) contains the eigenvalue problem corresponding to the loss-free case, in addition to the effect of the constitutive parameters of the body represented by Z_M.

Consequently, the resulting eigenvalues and eigenvectors of (2.44) may be complex. Additionally, the orthogonality relationships are altered as it follows [7]

$$< J_m, R_V J_n > = \delta_{mn} \tag{2.45}$$

$$< J_m, (X_V - Z_M) J_n > = \lambda_n \delta_{mn} \tag{2.46}$$

$$< J_m, (Z_V + Z_M) J_n > = (1 + j\lambda_n) \delta_{mn} \tag{2.47}$$

Worth mentioning that equation (2.45) guarantees the orthogonality of the radiation fields [7]. In the same context, Harrigton and Mautz proposed another generalized eigenvalue equation for cases where only the spectral solution is needed, by considering only the real and imaginary parts of the matrices $[Z_V]$ and $[Z_M]$, i.e., [7]

$$[X_V + X_M][I_n] = \lambda_n [R_V + R_M][I_n] \tag{2.48}$$

Hence, the matrices $[X_V + X_M]$ and $[R_V + R_M]$ are real and symmetric, and the eigenvalues λ_n are real, while the eigenvectors can be chosen real [7]. However, the use of equation (2.48) will damage the orthogonality property of the far fields, resulting in [7]

$$\frac{1}{\eta} \oiint_{S_\infty} E_m^* \cdot E_n \, \mathrm{d}s + < I_m, R_M I_n >= \delta_{mn} \tag{2.49}$$

2.6 Characteristic modes analysis implementation

Principally, as have been demonstrated in the previous sections, the characteristic modes are obtained through the characteristic modes analysis (CMA) which is very close to the MoM but without considering any feeding structure [33]. The first numerical implementation of the characteristic modes theory has been made by Harrington and Mautz for PEC bodies. Thereafter, implementations for dielectric bodies were developed either as self-efforts or as commercial computational electromagnetic software packages [84]. Where the eigenvalues together with the eigenvectors are the main parameters examined, followed by the modal significance and the characteristic angles. The numerical implementation of the theory has some principal and common steps for both PEC bodies and dielectrics. Firstly, a meshed structure in free space must be considered in the presence of an impressed electric field (or magnetic field). Subsequently, the mathematical formulation of the theory obtained using the surface currents and the induced field is transformed into its matrix by making use of the MoM. Furthermore, a generalized eigenvalue problem is formulated using the real and imaginary parts of the impedance matrix. Thereafter, the characteristic modes are obtained by solving the resulting generalized eigenvalue equation for each frequency sample in the frequency band

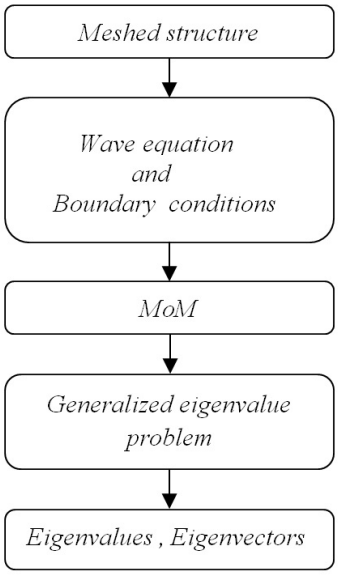

FIGURE 2.4: Flowchart of the characteristic modes analysis.

under consideration (see Appendices B and C). A summary of the aforementioned steps is detailed in Fig. 2.4.

2.7 Conclusion

In this chapter, it has been shown that the characteristic modes theory offers a great convenience into the analysis and understanding of the radiation and scattering mechanisms from arbitrarily shaped bodies, without the need to specify any feeding structure. The theory can be applied to bodies both with and without losses. The mathematical formulation of the theory consists of expressing the problem as a generalized eigenvalue problem. The main parameters obtained from solving the generalized eigenvalue equation are the eigenvalues and the eigenvectors. For conductors, the eigenvalues are used to determine the state of the mode, i.e. either it is capacitive or inductive or at resonance, which is the desirable state. While the eigenvectors are assumed to be real, and they are used to expand the surface currents and the radiated fields. However, for lossless dielectrics the eigenvalues are presumed to be real, and the characteristic currents can be chosen real. Moreover, for lossy dielectrics the constitutive parameters of the body must be taken into consideration when formulating the generalized eigenvalue problem. Therefore, the resulting eigenvalues and the eigenvectors may be complex which renders the study of such bodies using the characteristic modes theory very challenging.

Chapter 3

Surface Integral Equations

3.1 Introduction

This chapter is devoted to shedding light on the main surface integral equations commonly used to implement the characteristic modes theory. Generally, the surface integral equations are used in formulating the scattering problems. Usually, this type of integral equations is used along with the equivalence principle [85] to further simplify the formalism of the problem under consideration, where the original problem is subdivided into two separate problems, one of which is equivalent to the interior region of the original problem, and the other one is equivalent to the exterior region of the problem. Normally, the unknowns to be sought for are the currents over the surface of a scatterer. Therefore, an approximate solution of the surface currents is obtained through building a surface integral equation, and this is performed by making use of the surface equivalence principle as aforementioned, the source-field relationships derived from Maxwell's equations, and the boundary conditions for the electric and magnetic fields [86, p.51].
Admittedly, some integral equations are more efficient than the others in approximating the numerical solution for a given problem. For instance, the electrical field integral equation (EFIE) proved to be more suitable for conducting surfaces [75], whereas the Poggio-Miller-Chang-Harrington-Wu-Tsai (PMCHWT) formulation is found to be more appropriate for homogeneous dielectric surfaces [8, 87, 88]. Likewise, some of the surface integral equations are found to be suffering from the internal resonances problem [89–91]. Actually, It is commonly known that the internal resonances problem becomes noticeable at the frequencies which coincide with the internal resonances of the body, where the solution of the integral equation is not unique, and the matrix form of the integral equation is ill-posed [92]. Fortunately, several solutions were proposed to alleviate the severity of this issue, hence allowing the improvement of the efficiency and accuracy

of surface integral equations. These solutions along with the formalism of the integral equations will be detailed in the following sections.

3.2 Magnetic Field Integral Equation Formulation

The magnetic field integral equation (MFIE) is a widespread space-frequency domain integral equation, also called the second-kind Fredholm integral equation or the Fredholm alternative. It was originally derived by Maue in 1949 together with the electric field integral equation (EFIE). These two equations were mainly intended to obtain the surface current density on a perfect electric conductor (PEC) in free space when excited by arbitrary incident harmonic fields [93]. The MFIE is mainly based on the extinction theorem (see Appendix E), moreover, the scatterer must be a closed surface. Its formulation is derived in the same way as the EFIE (see Sec.2.3), i.e., by applying the boundary conditions on the surface of the body. Consequently, the MFIE for a perfect electric conductor (PEC) object read [93]

$$\hat{n} \times H^i(\boldsymbol{r}) = \pm\frac{1}{2}J(\boldsymbol{r}) - \hat{n} \times p.v. \oiint_S \nabla' g(\boldsymbol{r}, \boldsymbol{r}') \times J(\boldsymbol{r}')\, \mathrm{d}s', \quad \boldsymbol{r} \in S \tag{3.1}$$

Here, $\hat{n}$ is the unit normal vector to the surface. Noting, $p.v.$ in the equation above denotes the Cauchy principal value of the integration. The positive sign in the term $\frac{1}{2}J(\boldsymbol{r})$ is used for exterior scattering or radiating problems, while the negative sign applies for interior (cavity) problems [93]. It is worth noting that in case of scattering or radiating problems the incident fields are implicitly considered to be generated by sources applied outside the body surface S, and those for the interior problems are assumed to be generated by sources inside S [93].

Apparently, the MFIE is well-posed as it contains only one spatial derivative, hence its degree of singularity is lower than the EFIE, which contains two spatial derivatives [94]. In fact, this could make it more popular than EFIE, but unfortunately, this is not the case as it works only for closed surfaces, while EFIE is applicable for both open and closed surfaces [75]. Further, the MFIE has another drawback is that its solution is far less accurate than the EFIE [95], which also can explain the reasons why it is less commonly used for practical applications such as CMT. Nevertheless, some attempts have been made to address the formalism of CMT based on MFIE for PEC bodies in [96] followed by [76, 97], where the generalized eigenvalue problem is expressed as [97]

$$[Z][I_n] = j(1 + j\lambda_n)[X][I_n] \tag{3.2}$$

or after simplification of the common terms as [97]

$$[R][I_n] = -\lambda_n[X][I_n] \tag{3.3}$$

From (3.3), it is obvious that the roles of the real part $[R]$ and the imaginary part $[X]$ of the impedance matrix $[Z]$ are switched in comparison to the CMT based on EFIE. Theoretically, this approach should produce results equivalent to those obtained from the EFIE, however, the numerical results may differ [4, 96]. Unfortunately, both the EFIE and the MFIE fail to converge to a unique solution for closed scatterers when the resonance frequency of the incident electromagnetic wave is in the neighborhood of an internal resonance of the structure under consideration. This can be explained as the lack of proper boundary conditions which can force the interior fields to vanish [91]. Several solutions were proposed to solve this problem. For instance, Mohsen et al. proposed to correct the inaccurate surface currents on the conducting bodies at resonance frequencies by adding a correction term, which is the resonant mode current multiplied by an unknown complex factor. A conducting sphere was used to validate the method, and excellent agreement was obtained between the correction factor technique (CFT) and the exact Mie series solutions [98]. While, Yaghjian went into correcting the surface integral equations, which consider only the tangential boundary conditions, and added the normal boundary conditions. His approach resulted in a new set of equations called the "augmented integral equations" [93]. Another widespread approach consists in the use of a linear combination of the two equations, i.e., MFIE and EFIE, to overcome the problem of non-uniqueness of the solution at these internal resonances. These two latter approaches will be further detailed in the following sections 3.3, 3.5.

3.2.1 Approximate Symmetric MFIE

Another alternative for the MFIE was first proposed in 1990 by Correia and Barbosa, called "the approximate symmetric MFIE" [99]. This formulation is based on the symmetrization of the MFIE. The process begins by observing that the first term of MFIE is symmetric (i.e $\frac{1}{2}J$), while the second term is not. This can be better seen by rewritten equation (3.1) in operator form[1], i.e.,[99]

$$\hat{n} \times H^i = \frac{1}{2}J + L_H J \tag{3.4}$$

[1]The authors of [99] did not take into consideration the Cauchy principal value in (3.1)

Therefore, by making use of the Galerkin's method, the elements of the MoM matrix can be written as [99]

$$Z_{mn} =< f_n/2, f_m > + < L_H f_n, f_m > \tag{3.5}$$

The authors in [99] assumed that the contribution of the second term ($< L_H f_n, f_m >$) to the MoM matrix elements is at least one order of magnitude less than the first term ($< f_n/2, f_m >$), hence the matrix will not greatly change if averaging is performed. Therefore, they averaged the matrix elements by making use of the symmetry of the inner product and the properties of the adjoint operator as follows:

$$\begin{aligned} Z^{'}_{mn} &= \left(Z_{mn} + Z_{nm}\right)/2 \\ &= \left(< f_n, f_m > + < L_H f_n, f_m > + < L_H f_m, f_n >\right)/2 \\ &= \left(< f_n, f_m > + < L_H f_n, f_m > + < L^A_H f_n, f_m >\right)/2 \end{aligned} \tag{3.6}$$

Here, L^A_H is the adjoint operator of L_H defined for the closed surface S, given by [99]

$$L^A_H J = \oiint_S \left[\hat{n}^{'} \times J(\boldsymbol{r}^{'})\right] \times \nabla^{'} g(\boldsymbol{r}, \boldsymbol{r}^{'})\, \mathrm{d}s^{'} \tag{3.7}$$

Eventually, the approximate symmetric MFIE reads as [99]

$$\hat{n}\times H^i = \frac{1}{2}J(r) - \hat{n}\times\frac{1}{2}\oiint_S J(\boldsymbol{r}^{'})\times\nabla^{'} g(\boldsymbol{r}, \boldsymbol{r}^{'})\, \mathrm{d}s^{'} + \frac{1}{2}\oiint_S \left[\hat{n}^{'} \times J(\boldsymbol{r}^{'})\right]\times\nabla^{'} g(\boldsymbol{r}, \boldsymbol{r}^{'})\, \mathrm{d}s^{'}, \quad r \in S \tag{3.8}$$

According to [76], both A(S)MFIE and MFIE have the same generalized eigenvalue equation and the same characteristic mode solutions.

3.3 Augmented Integral Equations Formulation

In 1981, Yaghjian within his framework on internal resonances problem introduced two sets of equations, namely, the augmented electric and magnetic field integral equations to eliminate the spurious resonances found in the solution of the MFIE and EFIE when solved for the exterior region [93]. According to Yaghjian, the reasons causing both EFIE and MFIE to fail in providing a unique solution for the exterior region originate from a failure in fulfilling the boundary conditions at the surface of the scatterer, he had expressly described this in [93] as:

"*In particular, it is proven that the electric field tangent to the scatterer is not restricted to zero by the MFIE, and the magnetic field tangent to the scatterer is not restricted to equal $J \times \hat{n}$ in the EFIE solution at (and only at) the interior resonant frequencies.*

This, in turn, implies that $\hat{n}\cdot H$ *and* $(\hat{n}\cdot E-\nabla_s\cdot J/j\omega\epsilon)$ *are not necessarily restricted to zero by the exterior MFIE and EFIE, respectively, at the interior resonant frequencies.*" Therefore, in order to rectify the integral equations, Yaghjian augmented the MFIE for the exterior region using [93],

$$\hat{n}\cdot H=0, \qquad on\ S \tag{3.9}$$

Similarly, the EFIE was augmented as follow [93],

$$\hat{n}\cdot E-\nabla_s\cdot\frac{J}{j\omega\epsilon}=0, \qquad on\ S \tag{3.10}$$

Eventually, the augmented EFIE and MFIE for the exterior region read as[2] [93]

$$E^i(\boldsymbol{r})=\frac{1}{j\omega\epsilon}\,p.v.\oiint_S\left(\left(\frac{\omega}{c}\right)^2 J\,g(\boldsymbol{r},\boldsymbol{r'})-(\nabla'_s\cdot J)\nabla' g(\boldsymbol{r},\boldsymbol{r'})\right)\mathrm{d}s'+\frac{(\nabla_s\cdot J)\,\hat{n}}{2j\omega\epsilon} \tag{3.11}$$

$$H^i(\boldsymbol{r})=-\frac{1}{2}\hat{n}\times J-p.v.\oiint_S J\times\nabla' g(\boldsymbol{r},\boldsymbol{r'})\,\mathrm{d}s' \tag{3.12}$$

Here, $p.v$ stands for a circular principal value integration. Further, equation (3.11) shows that the augmented form of EFIE (i.e., AEFIE) is an integral of the second type, hence more stable than the original EFIE [93]. Moreover, the augmented integral equations proved to efficiently eliminate the spurious resonances from the solution of the exterior region for all perfectly conducting scatterers except the sphere, which according to Correia [100] presents no problem because an analytical solution for the sphere is available. Nevertheless, based on a comparison of the performances of the integral equations with a unique solution at the vicinity of a resonance of the scatterer, it has been concluded that the use of the combined field integral equation (CFIE) is preferred than the augmented equations due to its computer performance [100]. Thus, the CFIE formulation will be detailed in Sec.3.5.

3.4 PMCHWT Formulation

The scattering problem from arbitrarily shaped three-dimensional (3-D) objects has been an area of investigation and study for several decades. Remarkably, homogeneous dielectrics have had a particular interest due to their mathematical simplicity (e.g. a constant dielectric constant). Most often, homogeneous dielectrics are analyzed using the surface integral equations (SIE) method as the volume integral equations (VIE) are

[2] A detailed derivation of both AEFIE and AMFIE can be found in [93]

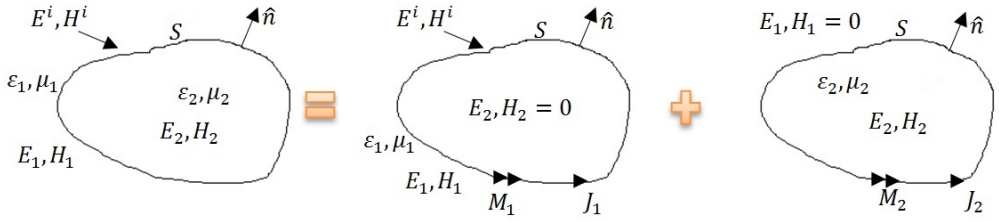

FIGURE 3.1: Surface equivalence principle of a dielectric scattering problem.

computationally expensive. The SIE is based on reducing a 3-D problem to two dimensions by expressing the solution in terms of unknown surface functions [87]. The most commonly used formulation of it is the PMCHWT approach, which resulted from the research work performed by Poggio and Miller [87], Chang and Harrington [8], and Wu and Tsai [88]. The PMCHWT formulation presents very appealing features, and it applies for a wide range of dielectric parameters (relative permittivity $\epsilon_r = 1.44$ to 80 and conductivity $\sigma = 0$ to 10^3 mho/m) [88]. A noticeable difference between VIE and PMCHWT resides in that the latter uses the magnetic currents besides the electric currents, which complicate the mathematical formalism in comparison to the VIE method as it will be shown later. Therefore, let consider a general 3-D homogeneous dielectric, characterized by a permittivity ϵ_2 and a permeability μ_2, placed in a background medium with constitutive parameters (ϵ_1, μ_1) and illuminated by the incident field (E^i, H^i), as illustrated in Fig. 3.1. Therefore, by making use of the surface equivalence principle, the original problem is subdivided into two problems, one by zeroing the field inside the body, and the other one by zeroing the field outside the body. Accordingly, the equivalent surface currents, both electric (J_1, J_2) and magnetic (M_1, M_2), must satisfy the following equalities [8]

$$J_1 + J_2 = 0 \tag{3.13}$$

$$M_1 + M_2 = 0 \tag{3.14}$$

whereas, the inner and outer electrical and magnetic fields read as follows [8]

$$E_1 = E^s + E^i = -j\omega A_1 - \nabla\phi_{1e} - \frac{1}{\epsilon_1}\nabla \times F_1 + E^i \tag{3.15}$$

$$H_1 = H^s + H^i = -j\omega F_1 - \nabla\phi_{1m} + \frac{1}{\mu_1}\nabla \times A_1 + H^i \tag{3.16}$$

$$E_2 = -j\omega A_2 - \nabla\phi_{2e} - \frac{1}{\epsilon_2}\nabla \times F_2 \tag{3.17}$$

$$H_2 = -j\omega F_2 - \nabla\phi_{2m} + \frac{1}{\mu_2}\nabla \times A_2 \tag{3.18}$$

In the precedents equations, the pair (E^s, H^s) represent the scattered fields, and the subscript '1' indicates the medium outside the body and the subscript '2' designates the inner region of the body volume, while $A_{1,2}$ represents the vector potential due to the electric current (defined by (2.5)). Whereas, $F_{1,2}$ stands for the vector potential due to the magnetic current, and $\phi_{(1,2)e/m}$ is the scalar potential due to the electric ρ_e or the magnetic ρ_m charge, and they are given in function of the Green's function g previously defined in (2.7), as it follows [101]

$$F_x(\boldsymbol{r}) = \epsilon_x \iint_S M_x(\boldsymbol{r}') \, g_x(\boldsymbol{r}, \boldsymbol{r}') \, \mathrm{d}s' \tag{3.19}$$

$$\phi_{xe}(\boldsymbol{r}) = \frac{1}{\epsilon_x} \iint_S \rho_e(\boldsymbol{r}') \, g_x(\boldsymbol{r}, \boldsymbol{r}') \, \mathrm{d}s' \tag{3.20}$$

$$\phi_{xm}(\boldsymbol{r}) = \frac{1}{\mu_x} \iint_S \rho_m(\boldsymbol{r}') \, g_x(\boldsymbol{r}, \boldsymbol{r}') \, \mathrm{d}s' \tag{3.21}$$

where, the subscript 'x' indicates the medium region 1 or 2 (i.e., outside or inside the body). Moreover, a more compact expressions of the fields E^s, H^s, E_2, H_2 are achieved using the operator notations and the matrix form equation as follows [8]

$$\begin{bmatrix} -L_{1e} & -C_1 \\ C_1 & -L_{1m} \end{bmatrix} \begin{bmatrix} J_1 \\ M_1 \end{bmatrix} = \begin{bmatrix} E^s \\ H^s \end{bmatrix} \tag{3.22}$$

$$\begin{bmatrix} -L_{2e} & -C_2 \\ C_2 & -L_{2m} \end{bmatrix} \begin{bmatrix} J_2 \\ M_2 \end{bmatrix} = \begin{bmatrix} E_2 \\ H_2 \end{bmatrix} \tag{3.23}$$

where the expressions of the operators L_{1e}, L_{1m}, C_1, L_{2e}, L_{2m}, C_2 can be straightforwardly done from equations 3.15, 3.16, 3.17, and 3.18. Moreover, the incident fields E^i and H^i can be derived using the boundary conditions of tangential components as [8]

$$\hat{n} \times (E^s + E^i - E_2) = 0 \tag{3.24}$$

$$\hat{n} \times (H^s + H^i - H_2) = 0 \tag{3.25}$$

Hence, by defining the operators in (3.22) and (3.23) to be tangential operators, and taking the tangential components of the fields and the currents, the following equations are obtained [8]

$$\begin{bmatrix} L_{1e} + L_{2e} & C_1 + C_2 \\ -(C_1 + C_2) & L_{1m} + L_{2m} \end{bmatrix} \begin{bmatrix} J_1 \\ M_1 \end{bmatrix} = \begin{bmatrix} E^i \\ H^i \end{bmatrix} \tag{3.26}$$

Unfortunately, the obtained matrix equation (3.26) is not symmetric, therefore, not suitable for CMT uses. Alternatively, equation (3.26) can be forced into symmetry as follows [8]

$$\begin{bmatrix} L_e & jC \\ -jC & L_m \end{bmatrix} \begin{bmatrix} J \\ jM \end{bmatrix} = \begin{bmatrix} E^i \\ jH^i \end{bmatrix} \tag{3.27}$$

Here, $L_e = L_{1e} + L_{2e}$, $L_m = L_{1m} + L_{2m}$, $C = C_1 + C_2$, $J_1 = J$, and $M_1 = M$.
Now, the equation (3.27) represents the usual operator equation needed for CMT development, which can be written in a more compact form as follows [7]

$$[T][f] = [g^i] \tag{3.28}$$

Admittedly, the unknown currents f can be expanded for each mode n as the superposition of two basis functions, one for the electric current f^e, and the other for the magnetic current f^m, i.e.,[8]

$$f_n = \sum_j (I_j f_j^e + V_j f_j^m) \tag{3.29}$$

Whereas, the matrix $[T]$ can be defined using the real and symmetric matrices $[T_1]$ and $[T_2]$, which represent its real and imaginary parts as follows [7],

$$[T] = [T_1] + j[T_2] \tag{3.30}$$

Consequently, the generalized eigenvalue problem can be expressed as follows [8]

$$[T_2][f_n] = \lambda_n [T_1][f_n] \tag{3.31}$$

where λ_n are the eigenvalues. Interestingly, according to Miers and Lau, the formula used to obtain λ_n previously defined in (2.18) must include the dissipated power, which transforms (2.18) into the following expression [102]

$$\lambda_n = \frac{2\omega(W_m^n - W_e^n)}{P_{radiated,n} + P_{dissipated,n}} \tag{3.32}$$

In addition, The characteristic sources can be normalized to radiate unit power. Further, the orthogonality relationships can be expressed as follows [7]

$$< f_m, T_1 f_n > =< f_m^*, T_1 f_n >= \delta_{mn} \tag{3.33}$$

$$< f_m, T_2 f_n > =< f_m^*, T_2 f_n >= \lambda_n \delta_{mn} \tag{3.34}$$

$$< f_m, TJ_n > =< f_m^*, TJ_n >= (1 + j\lambda_n)\delta_{mn} \tag{3.35}$$

Likewise, the orthogonality features hold for the characteristic fields in the loss-free case, resulting in [7]

$$\frac{1}{\eta}\oiint_{S_\infty} E_m^* \cdot E_n \, \mathrm{d}s = \eta \oiint_{S_\infty} H_m^* \cdot H_n \, \mathrm{d}s = \delta_{mn} \tag{3.36}$$

where S_∞ is the sphere at infinity. It should be noted that among the problems underlined by Miers and Lau in [102] is the problem of spurious modes in the SIE formulations, particularly, the PMCHWT formulation, besides, the eigenvalues interpretation issue for penetrable objects. Therefore, the issue of the spurious modes will be alluded to in the next Subsection.

3.4.1 Spurious Modes

Eventually, the PMCHWT formulation seems to be a good partner to the characteristic modes theory in solving the scattering problems from homogeneous dielectrics, yet practicality places this speculation into remission. In fact, a number of studies found that the PMCHWT formulation suffers from the spurious (or the non-physical) modes problem [103, 104]. Consequently, many questions were raised on the nature of these spurious modes and the ways to detect them. According to [103], these non-physical modes are the modes with very small radiated power, therefore a power threshold approach is sufficient to detect the non-desired modes. Whereas, the authors in [104] believe that a threshold value using the total efficiency of the structure will perform better. Nevertheless, there is still considerable uncertainty with regard to the origin of these spurious modes. The authors in [105] assume that the PMCHWT formulation itself is the origin of spurious modes, hence they developed a new surface integral equation based theory of characteristic modes (TCM) formulations applicable for homogeneous penetrable bodies able to eliminate the non-physical modes. Meanwhile, a different explanation was provided in [106], where Huang et al. associate the non-physical modes problem to the lack of dependence relationship between the electric and magnetic currents over the surface of the body, i.e. if the electric current is found, systematically the magnetic current can be obtained using the electric current and vice versa, which is not verified by the non-physical modes, conversely to the physical modes which do obey the dependence relationship. Recently, the authors of [106] demonstrated that the internal resonances are not responsible for the non-physical modes. Thus, there is no consensus among scientific researchers on the origins of the spurious modes in the SIE formulations.

3.5 Combined Field Integral Equation Formulation

The combined field integral equation (CFIE) has evolved from the electric field integral equation (EFIE) and the magnetic field integral equation (MFIE). It is mostly used to eliminate the spurious internal resonances from the numerical solution of closed bodies [107]. Firstly, it was applied only to conducting bodies [108], whereas, dielectric bodies were modelled using the PMCHWT formulation [109]. Thereafter, Rao and Wilton extended the CFIE method to treat the three dimensional (3-D) dielectric objects [110]. Consequently, the CFIE can be applied to both conducting surfaces as well as homogeneous and inhomogeneous material bodies [111, 112], conversely to PMCHWT, which is applicable only to homogeneous bodies. Actually, the PMCHWT and CFIE might seem to represent the same approach, viz. a combination of integral equations, however, they are different. Concisely, in the PMCHWT formulation, EFIE and MFIE are coupled but not mixed, while for CFIE they are mixed [113], as it will be shown.
therefore, let consider a homogeneous dielectric body as shown in Fig.3.1, where, again the equivalence principle is used to create the two sub-problems derived from the original one, with $J_1 = -J_2 = J$ and $M_1 = -M_2 = M$. Hence, by applying the continuity conditions of the tangential components of the fields for the equivalent exterior problem at a surface S^- slightly interior to S, the scattered fields (E_1^s, H_1^s) in the medium 1 and the incident fields (E^i, H^i) are equated to zero as follows [110]

$$\left[E_1^s(J) + E_1^s(M) + E^i\right]_{tan} = 0 \tag{3.37}$$

$$\left[H_1^s(J) + H_1^s(M) + H^i\right]_{tan} = 0 \tag{3.38}$$

Similarly, by applying the continuity conditions of the tangential components of the fields for the equivalent interior problem at a surface S^+ slightly exterior to S,can be written as [110]

$$[E_2^s(-J) + E_2^s(-M)]_{tan} = 0 \tag{3.39}$$

$$[H_2^s(-J) + H_2^s(-M)]_{tan} = 0 \tag{3.40}$$

Noting that (E_2^s, H_2^s) represent the scattered fields evaluated within the inner medium. Eventually, the CFIE formulation is constructed by combining these above mentioned equations ((3.37) to (3.40)) into two categories, one of which is for the equivalent exterior problem, while the other one for the interior problem, such that [110, 114]

$$\alpha\left[E_1^s(J) + E_1^s(M) + E^i\right]_{tan} + \eta_1(1-\alpha)\hat{n} \times \left[H_1^s(J) + H_1^s(M) + H^i\right]_{tan} = 0 \tag{3.41}$$

$$\alpha\left[E_2^s(-J) + E_2^s(-M)\right]_{tan} + \eta_2(1-\alpha)\hat{n} \times \left[H_2^s(-J) + H_2^s(-M)\right]_{tan} = 0 \tag{3.42}$$

Where α is the linear combination factor ranging from 0 to 1, while $\hat{n}$ is the unit normal vector to the surface. Noting that, if $\alpha = 0$, the equations (3.41) and (3.42) reduces to the usual MFIE formulation as the contribution of the electrical field would be eliminated, and if $\alpha = 1$, then the CFIE reduces to EFIE formalism as all expressions involving the magnetic field would be removed [110]. Therefore, the equations ((3.41), (3.42))can be re-written for the mediums $l = 1, 2$ as follows [114]

$$\alpha EFIE_l + \eta_l(1-\alpha)\hat{n} \times MFIE_l \tag{3.43}$$

Although, the choice of α is critical to the method application, it is stated in [100, 107] that the numerical results are relatively unaffected by the value attributed to this constant.

Moreover, the implementation of the CFIE requires the use of two sets of basis functions [110], $f_n^{\pm}$ and $\hat{n}^{\pm} \times f_n^{\pm}$, with f_n is the RWG basis function [52] defined in Appendix. A. These two sets carry out the expansion of the electric and magnetic currents, respectively. Myriad manipulations of the expansion and testing functions were proposed in order to improve the performances of the method, either by recasting the CFIE formulation, or by investigating the role of the combination coefficients (α and $(1-\alpha)$), which resulted in several alternatives derived from the original CFIE approach [113, 114]. More importantly, not all the alternatives of the CFIE method are immune to the internal resonance problem [115].

Furthermore, alike the PMCHWT, the CFIE was applied in the implementation of the characteristic modes theory by making use of the impedance matrices provided by the EFIE and MFIE, $[Z_E]$ and $[Z_H]$, respectively [76, 97, 105, 116]. Therefore, for closed perfectly conducting objects the characteristic modes theory can be formulated according to the following matrix eigenvalue equation [97]

$$\Big[\alpha[Z_E] + (1-\alpha)\eta_1[Z_H]\Big][I_n] = (1+j\lambda_n)\Big[\alpha[R_E] + (1-\alpha)j\eta_1[X_H]\Big][I_n] \tag{3.44}$$

where $[X_H]$ is the imaginary part of $[Z_H]$, and $[R_E]$ is the real part of $[Z_E]$. Roughly equivalent eigenvalue equations are developed in [105] for penetrable bodies derived from a degenerate formulation from the CFIE formulation.

Undoubtedly, the computational effort required to construct the matrices associated with CFIE or PMCHWT is doubled as both EFIE and MFIE are solved, in addition, such an increase in the number of unknowns implies an increase in the system storage. Therefore, the examination of other alternatives might be of interest. To that end, the single source integral equation formulation will be detailed in the following Section 3.6.

3.6 Single Source Integral Equation Formulation

The single source integral equation (SSIE) method is based on the use of a single unknown equivalent surface current [117], which halves the number of unknowns needed for the numerical solution of penetrable objects, and consequently render it a very appealing formulation to be used for electromagnetic scattering problems, especially, for the homogeneous dielectrics. Among the pioneering publications on this method, the work of Maystre [118] that treated the problem of diffraction by a 2-D dielectric body, followed by the work of Marx [119] on the determination of scattered and transmitted transient electromagnetic waves by a 3-D dielectric body. Thereafter, Glisson in [120] used the equivalence principle to develop the mathematical formalism of the SSIE in the frequency domain. Unfortunately, according to [121], Glisson and Sholy had demonstrated in their work [122] that the SSIE method seemed to suffer from internal resonance problem or the non-uniqueness of the solution at irregular frequencies. Therefore, special emphasis was given to suppress the spurious solution by several investigators, such as Mautz who successfully developed an integral equation whose solution is always unique [123]. A few years later, Yeung implemented the SSIE formulation and validated the formulation through some numerical applications of the scattering problem from dielectric spheres [117]. Also, he provided a detailed derivation of the MoM matrix using the single source approach. Likewise, the application of the SSIE to inhomogeneous bodies had a particular focus in the framework of Swatek and Ciric, who provided new recursive formulations of the single source surface integral equations to study inhomogeneous cylinders [121]. Thus far, work is still ongoing to take profit from the SSIE method. Recently, the authors in [124] proposed a new formalism of the method for the scattering problem from 3-D homogeneous dielectrics by making use of both the surface integral representation of the electromagnetic field developed in the theory of the single source integral equations and the volume equivalence principle.

Equally to all surface integral equations, the SSIE is based on the surface equivalence principle, hence, the original scattering problem is decomposed as shown in Fig. 3.2. The

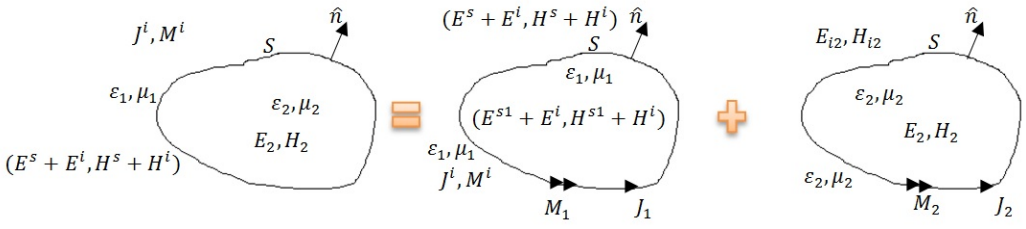

FIGURE 3.2: Decomposition of the original scattering problem into an exterior and an interior equivalent problems designated by the subscripts 1 and 2. This figure was reproduced based on Fig. 1 from [120].

disparity of this formulation as it will be shown is that one of the equivalent currents, i.e. the electric or the magnetic current on the surface S of the body, will be zeroed, whether for the exterior or for the interior problem, allowing to express the fields using a single equivalent surface current. Therefore, to build the SSIE formulation, the relationships between the electromagnetic fields and the equivalent currents, shown in Fig. 3.2, can be expressed as [120]

$$J_1 = \hat{n} \times (H^s - H^{s1}) \tag{3.45}$$

$$M_1 = (E^s - E^{s1}) \times \hat{n} \tag{3.46}$$

$$J_2 = \hat{n} \times (H_{i2} - H_2) \tag{3.47}$$

$$M_2 = (E_{i2} - E_2) \times \hat{n} \tag{3.48}$$

where the subscripts 1 and 2 are used to denote quantities related to the equivalent exterior and interior problems, respectively. The equivalent electric currents are denoted by J_1 and J_2, whereas M_1 and M_2 are the equivalent magnetic currents. The pair (E^s, H^s) represent the scattered fields, while (E_2, H_2) are the fields internal to the dielectric body. The auxiliary Maxwellian fields $(E^{s1}, H^{s1}, E_{i2}, H_{i2})$ were used in the expressions above to ensure the uniqueness of the equivalent currents [120]. In fact, the SSIE formulation is founded on the appropriate choice of the auxiliary fields. Accordingly, E^{s1} is chosen such that its tangential component on the surface S is equal to the tangential component of E^s [120], i.e.,

$$\hat{n} \times E^{s1} = \hat{n} \times E^s \tag{3.49}$$

Therefore, by inserting (3.49) into (3.46), the exterior equivalent magnetic current is set to zero as it is shown below [120]

$$M_1 = (E^s - E^s) \times \hat{n} = 0 \tag{3.50}$$

However, the auxiliary fields related to the interior problem (E_{i2}, H_{i2}) are chosen to be equal to zero. Consequently, J_2 and H_2 are reduced to [120]

$$J_2 = -\hat{n} \times H_2 \tag{3.51}$$

$$H_2 = -E_2 \times \hat{n} \tag{3.52}$$

Hence, all the remaining fields can be related together through the boundary conditions such that [120]

$$\hat{n} \times (E^s + E^i) = \hat{n} \times E_2 \tag{3.53}$$

$$\hat{n} \times (H^s + H^i) = \hat{n} \times H_2 \tag{3.54}$$

Note that, both the electrical field integral equation (EFIE), and the magnetic field integral equation (MFIE) can be obtained from (3.53) and (3.54). These above mentioned equations can be solved for J_1, whereas J_2 and M_2 can be found in terms of the single source J_1 and the exterior fields using the following equations [120]

$$J_2 = -\hat{n} \times (H^s + H^i) \tag{3.55}$$

$$M_2 = -(E^s + E^i) \times \hat{n} \tag{3.56}$$

Note that, similar formalism of the SSIE could be obtained by choosing $J_1 = 0$ [120]. Furthermore, the formulation of the SSIE presented in this section following the work of Glisson in [120] was not tested in terms of stability and the uniqueness of the solution, which inspired Yeung in [117] to perform the numerical implementation of the SSIE formulation and to investigate the internal resonance problem. According to Yeung [117], the CFIE based single integral equation is found to eliminate the error in the solution for frequencies that coincide with an internal resonance.

3.7 Conclusion

This chapter discussed the most commonly known surface integral equation methods used to implement the characteristic modes theory. Usually, the equivalence principle and the MoM are used to formulate and solve the surface integral equations, where the choice of an appropriate surface integral equation is mainly dependent on the intended use. For instance, it was shown that the MFIE is more suitable for closed surfaces conversely to its counterpart the EFIE, which can be applied for both open and closed surfaces. Although, both MFIE and EFIE suffer from the internal resonance problem at the resonance frequencies of the cavity formed by the closed surface. Consequently, the PMCHWT formulation used for homogeneous dielectrics is also affected by this issue as its formulation is based on coupling MFIE and EFIE. A possible countermeasure to circumvent the internal resonance issue is the use of the augmented equations of MFIE and EFIE, or even the CFIE method, which are found to be immune to the internal resonances problem, with a privilege granted to the CFIE formulation. However, the use of the CFIE method might be undesirable as it requires an increase in the computational time and system storage, where the total number of unknowns of the MoM matrix is two times greater than the total number of the elements of the meshed surface. Hence, although it is seldom to find the CMT implementation based on the SSIE formulation, it might be a good alternative to the existing implementations.

Chapter 4

Resolution of the Matrix [R] Deficiencies for PEC Bodies

4.1 Introduction

This chapter is devoted to highlighting one of the main problems encountered in the modal decomposition process, namely, the deficiencies of the real part of the impedance matrix, which affects tremendously the accuracy of the obtained characteristic modes. In this thesis framework, a new method is proposed to overcome the indefiniteness issue of the real part of the impedance matrix. The proposed approach is based on reconstructing the real part matrix using the spherical vector waves [125]. Hence, the real part matrix is expressed as the product of the spherical modes projection matrix and its transposed matrix. Several numerical examples are presented to evaluate the performances of the proposed approach, and good results are obtained.

4.2 Major Deficiencies

Basically, the characteristic modes theory formulation starts by defining the corresponding generalized eigenvalue problem (GEP). Usually, the GEP is expressed in terms of the real and imaginary parts of the impedance matrix represented by $[R]$ and $[X]$ matrices. These two matrices are deemed to be the principal contributors in the modal decomposition. Theoretically, $[R]$ and $[X]$ are assumed to be Hermitian[1] , real, and symmetric [5]. However, in practice, due to numerical inaccuracies, they are not symmetrical [6], even when the Galerkin procedure is used (i.e. the expansion functions are chosen to be equal

[1] A hermitian matrix is equal to its conjugate transpose, e.g. $[R]^H \equiv [R^T]^* = [R]$

to the testing functions). To mitigate this issue, Harrington and Mautz in [6] performed an averaging of the off-diagonal elements of the impedance matrix, with no noticeable effect of this averaging in radiation and scattering problems. The same procedure was followed in [71] to obtain the symmetric version of $[R]$ using

$$[R_{sym}] = \frac{1}{2}([R] + [R^T]) \tag{4.1}$$

Furthermore, and in compliance with the theory, the matrix $[R]$ must be positive semi-definite (i.e., all of its eigenvalues must be non-negative), as it is related to the radiated power ($P_{rad} \geq 0$) by

$$P_{rad} =< J^*, RJ > \tag{4.2}$$

However, in practice the matrix $[R]$ is found to suffer from indefiniteness (i.e. some of its eigenvalues might be negative), which renders the process of characteristic modes decomposition very challenging. Again, in order to relieve this issue, Harrington and Mautz suggested in [6] to diagonalize the $[R]$ matrix leaving,

$$[\mu] = [U^T R U] \tag{4.3}$$

where $[U]$ is an orthogonal matrix (i.e. $[U^T] = [U^{-1}]$), and $[\mu]$ is a diagonal matrix containing the eigenvalues of $[R]$ in descending order (i.e. $\mu_1 \geq \mu_2 \geq ...$), whereupon, the negative entries of $[\mu]$ were zeroed. Interestingly, this solution was investigated by Čapek et al. in [71], and they concluded that forcing $[R]$ to become positive semi-definite cannot cure the imminent fact that matrix $[R]$ is 'ill-conditioned', or in other words, exhibits a high condition number, which reduces the total number of characteristic modes obtainable from the modal decomposition. In this thesis, this problem is approached in a new manner by expressing the real part of the impedance matrix as a multiplication of the spherical modes projection matrix with its transposed matrix [70][2], as it will be shown in the following sections.

[2]The present chapter is based on [70], to which the author of this thesis contributed by writing the $[S]$ matrix implementation code by making use of the spherical wave functions used to build the theoretical background presented in [70]. Meanwhile, Vit Losenicky performed the $[S]$ matrix implementation in Matlab using the M and N functions presented in [71] for comparison purposes. Further, the author used the Advanpix Matlab toolbox to transform the $[S]$ matrix implementation into an arbitrary precision code. Moreover, the author developed the modal decomposition code using Python. While Doruk Tayli derived the expressions and performed the Python multi-precision implementation. Whereas, the manuscript with the figures and tables was prepared mostly by Doruk Tayli and Miloslav Čapek, while recommendations were given by both Lukas Jelinek and Mats Gustafsson to improve the implementations and the manuscript. These were the main tasks of the co-authors as far as the author is aware.

4.3 Theoretical Background

The proposed method aims to improve the accuracy of the modal decomposition and the obtained characteristic modes through reconstructing the matrix $[R]$ using the spherical vector waves [125]. This is accomplished by re-writing the expression of the impedance matrix $[Z]$ in function of the dyadic Green function G [126, chap.2] as

$$Z_{mn} = jk\eta \int_S \int_S f_m \cdot G(k, \boldsymbol{r}, \boldsymbol{r}') \cdot f_n \, \mathrm{d}s \, \mathrm{d}s' \tag{4.4}$$

$$G(k, \boldsymbol{r}, \boldsymbol{r}') = \left(\mathbf{I} + \frac{\nabla\nabla}{k^2}\right) \frac{e^{-jk|\boldsymbol{r}-\boldsymbol{r}'|}}{4\pi|\boldsymbol{r}-\boldsymbol{r}'|} = \left(\mathbf{I} + \frac{\nabla\nabla}{k^2}\right) g(\boldsymbol{r}, \boldsymbol{r}') \tag{4.5}$$

where j is the imaginary unit, k is the wave number, η is the free space impedance, whereas f_m and f_n are the real valued basis functions used to expand the current density, while $\mathbf{I}$ is the unit dyadic, and $\boldsymbol{r}$ and $\boldsymbol{r}'$ are the source and observation points.
Thereafter, the dyadic Green function is expressed using the spherical wave expansion, i.e., [126, chap.7]

$$G(k, \boldsymbol{r}, \boldsymbol{r}') = -jk \sum_\alpha u_\alpha^{(1)}(k\boldsymbol{r}_<) \, u_\alpha^{(4)}(k\boldsymbol{r}_>) \tag{4.6}$$

where $u_\alpha^{(1)}(k\boldsymbol{r}_<)$ and $u_\alpha^{(4)}(k\boldsymbol{r}_>)$ are the spherical wave functions [125, 127] (for more details see Appendix D). Therefore, by making use of (4.6), the impedance matrix can be expressed as

$$Z_{mn} = k^2\eta \sum_\alpha \int_S \int_S f_m(\boldsymbol{r}) \cdot u_\alpha^{(1)}(k\boldsymbol{r}_<) u_\alpha^{(4)}(k\boldsymbol{r}_>) \cdot f_n(\boldsymbol{r}') \, \mathrm{d}s \, \mathrm{d}s' \tag{4.7}$$

Noting that $u_\alpha^{(1)}(k\boldsymbol{r}) = Re\{u_\alpha^{(4)}(k\boldsymbol{r})\}$ simplifies the extraction of the real part from (4.7), hence, the elements of the real part matrix R_{mn} can be explicitly defined as

$$R_{mn} = k^2\eta \sum_\alpha \int_S \int_S f_m(\boldsymbol{r}) \cdot u_\alpha^{(1)}(k\boldsymbol{r}) u_\alpha^{(1)}(k\boldsymbol{r}') \cdot f_n(\boldsymbol{r}') \, \mathrm{d}s \, \mathrm{d}s' \tag{4.8}$$

Further, equation (4.8) can be separated into two integrals, where one of them represent a rectangular matrix $[S]$ and the other one its transpose, as it follows

$$[R] = [S^T S] \tag{4.9}$$

Note that for complex-valued spherical vector waves, the transpose $(^T)$ in (4.9) is replaced with the Hermitian transpose $(^H)$. Further, the elements of $[S]$ are given by

$$S_{m\alpha} = k\sqrt{\eta} \int_S f_m \cdot u_\alpha^{(1)}(k\boldsymbol{r}) \, \mathrm{d}s \tag{4.10}$$

The dimensions of matrix $[S]$ are in function of the total number of basis functions N_{f_n}, and the desired number of modes N_α, i.e. $N_\alpha \times N_{f_n}$, with N_α given by [128]

$$N_\alpha = 2L(L+2) \tag{4.11}$$

Here, L stands for the highest order of spherical mode. Notice that the parameter N_α is limited from below by the convergence and the number of desired modes, but also from above since the spherical Bessel function in $u_\alpha^{(1)}(k\boldsymbol{r})$ decays rapidly with l as

$$j_l(ka) \approx \frac{2^l l!}{(2l+1)!}(ka)^l, \quad ka \ll l \quad \text{where} \quad l = \{1, ..., L\} \tag{4.12}$$

Moreover, the radiated far-field $F(\hat{\boldsymbol{r}})$ can be expressed using the spherical vector harmonics as it follows,

$$F(\hat{\boldsymbol{r}}) = \frac{1}{k}\sum_\alpha j^{l-\tau+2} f_\alpha Y_\alpha(\hat{\boldsymbol{r}}) \tag{4.13}$$

where $Y_\alpha(\hat{\boldsymbol{r}})$ are the spherical vector harmonics defined in Appendix D. While, the expansion coefficients f_α are given by

$$[f_\alpha] = [S][I_n] \tag{4.14}$$

where the column matrix $[I_n]$ contains the current density coefficients I_n. In addition, the total time-averaged radiated power of a lossless antenna can be expressed as a sum of expansion coefficients such that,

$$P_r \approx \frac{1}{2}[I_n^H][R][I_n] = \frac{1}{2}\Big|[S][I_n]\Big|^2 = \frac{1}{2}\sum_\alpha |f_\alpha|^2 \tag{4.15}$$

4.4 Numerical applications

The evaluation of the performances of the proposed method will be performed using three PEC structures, namely, a spherical shell, a rectangular plate, and a helicopter. Each one of these objects will be studied for several electrical sizes, and different number of basis functions. A summary of the parameters attributed to each example considered in this section is shown in Table 4.1. It is worth mentioning that the value attributed to the order of spherical modes trades between accuracy and computational efficiency, where increasing L improves the accuracy, and decreasing L provides computational gain. Fig.4.1 presents the convergence of $[R]$ for Example R2. To prove the efficiency of the proposed approach, a comparison in terms of the computational time[3] needed

[3]Computations are done on a workstation with $i7-3770$ CPU @ 3.4 GHz and 32 GB RAM, operating under Windows 7. Note that the Computation time for the matrix $[X]$ is omitted as it takes longer than the matrix $[R]$, due to Green function singularity.

Structure	Example	ka	N_{f_n}	N_α
Spherical shell Fig. 9 in [129]	S1	1/2	750	240
	S2	1/2	750	880
	S3	3/2	750	880
	S4	1/2	3330	240
	S5	1/2	3330	880
Rectangular plate Fig. 10 in [129] ($L/W = 2$)	R1	1/2	199	510
	R2	1/2	655	510
	R3	1/2	2657	240
	R4	1/2	2657	1920
Helicopter	H1	1/2	18898	240
	H2	7	18898	720

TABLE 4.1: Summary of examples used throughout this chapter, where ka is the electrical size, N_{f_n} is the number of basis functions, and N_α is number of spherical modes calculated as (4.11). The order of the symmetric quadrature rule used to compute the non-singular integrals in (4.4) is $N_q = 3$ [130].

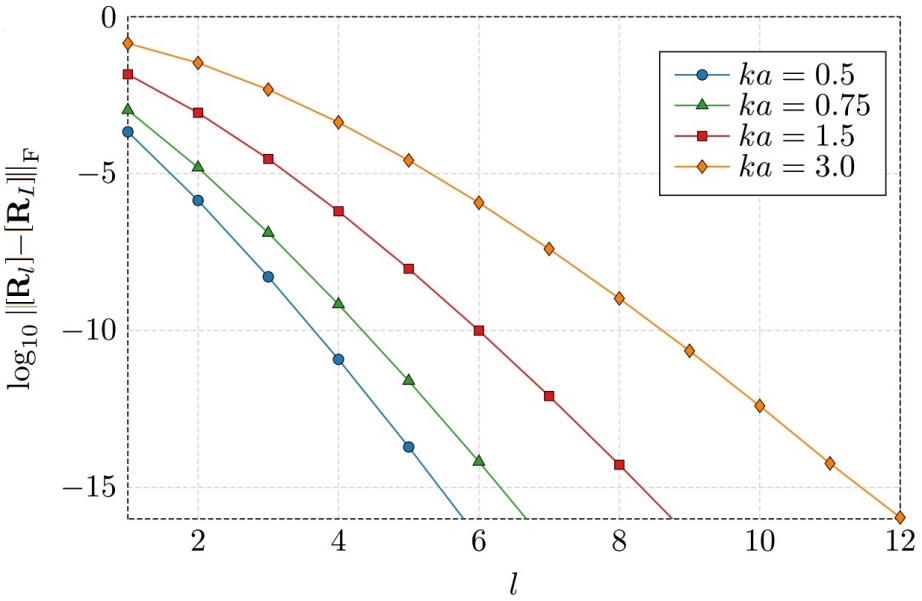

FIGURE 4.1: Convergence of the matrix $[R_l] = [S_l^T S_l]$ to the matrix $[R_L] = [S_L^T S_L]$ on the rectangular plate (Example R2) for different order of spherical modes $l = \{1, ..., L\}$ and multiple electric sizes $ka \in \{0.5, 0.75, 1.5, 3.0\}$, with the highest spherical mode order $L = 12$. The superscript ^{F} denotes the Frobenius norm. The convergence is computed with quadruple precision using the mpmath Python library [131]

.

	Time to assemble matrices in IDA (s)			
Example	$[Z]$	$[R]$	$[S]$	$[R] = [S^T S]$
S1	2.58	0.09	0.009	0.011
S4	14.2	1.78	0.039	0.083
R3	11.1	1.11	0.035	0.068
H1	200	54.5	0.236	1.66

TABLE 4.2: Time to assemble matrices in IDA [133]. Simulation setup for the examples in table I, $N_q = 3$ and $L = 10$ ($N_\alpha = 240$), matrix multiplication $[S^T S]$ is performed with DGEMM from the intel MKL library [134].

to construct the involved matrices[4] is performed, as it is apparent from Table 4.2. As expected, the matrix $[Z]$ requires the most computational resources, as it includes both matrices $[R]$ and $[X]$. The computation of the matrix $[R]$ using MoM is faster than the matrix $[Z]$ since the underlying integrals are regular. The computation of the matrix $[R]$ using (4.9) takes the least amount of time for most of the examples. The computational gain is notable for structures with more degrees-of-freedom (d-o-f), N_{f_n}. Further, the expression proposed in (4.9) will be used to perform the modal decomposition. Therefore, let consider the following standard eigenvalue problem

$$[R][I_n] = \xi_n [I_n] \tag{4.16}$$

where ξ_n are the eigenvalues of the matrix $[R]$ (i.e., of the radiation modes [135]), and $[I_n]$ are the eigenvectors. Furthermore, let consider the singular value decomposition (SVD) of the matrix $[S]$ given by

$$[S] = [U][\Lambda][V^H] \tag{4.17}$$

where $[U]$ and $[V]$ are unitary matrices, and $[\Lambda]$ is a diagonal matrix containing singular values of matrix $[S]$. Inserting (4.9) and (4.17) into (4.16), then multiplying from the left with $[V^H]$ yields

$$[\Lambda^H][\Lambda][\tilde{I}_n] = \xi_n [\tilde{I}_n] \tag{4.18}$$

where the eigenvectors are rewritten as $[\tilde{I}_n] \equiv [V^H][I_n]$, and the eigenvalues are $\xi_n = \Lambda^2_{nn}$. A comparison of procedure (4.16) and (4.18) is shown in Table 4.3. For high order n, the classical procedure (4.16) with double numerical precision yields in non-physical modes with negative eigenvalues ξ_n (negative radiated power) or with incorrect current profile (as compared to the use of quadruple precision). Using double precision, the number of modes which resemble physical reality (called "properly calculated modes" in Table 4.3) is much higher[5] for the new procedure (4.18). It is also worth mentioning that the new

[4] The matrices used in modal decomposition have been computed using in-house solvers AToM [132] and IDA [133].

[5] Quantitatively, the proper modes in Table 4.3 are defined as those having less than 5% deviation in eigenvalue ξ_n as compared to the computation with quadruple precision.

Example (see Table 4.1)	Number of properly calculated modes				
	$[R][I_n] = \xi_n[I_n]$			$[X][I_n] = \lambda_n[R][I_n]$	
	(4.16)	(4.18)	(4.19)	$[R] = [S^T S]$	(4.23)
S2	59	284	**70**(5)	96(6)	**284**(11)
S3	96	364	**105**(6)	197(9)	**389**(13)
S5	59	311	**70**(5)	96(6)	**306**(11)
R1	31	109	**29**	35	**37**
R2	29	117	**26**	33	**98**
R4	28	116	**22**	26	**98**

TABLE 4.3: Comparison of the number of modes correctly found by the classical and the novel methods for the examples listed in Table 4.1, where columns 2–3 summarize the radiation modes and columns 4–6 summarize the CMs. Values in parentheses depicts the number of non-degenerated TM and TE modes found on spherical shell. The main outcome of the table, comparison of the CMs is highlighted by bold type.

procedure, by design, always gives positive eigenvalues ξ_n. Nevertheless, the generalized eigenvalue problem (GEP) with the matrix $[R]$ on the right hand side, i.e., serving as a weighting operator [136], is much more involved as the problem cannot be completely substituted by the SVD. Yet, the SVD of the matrix $[S]$ in (4.17) plays an important role in CM decomposition. In the conventional approach, the CM decomposition is defined as

$$[X][I_n] = \lambda_n[R][I_n] \tag{4.19}$$

which is known to suffer from the indefiniteness of the matrix $[R]$ [71], therefore delivering only a limited number of modes. The first step is to represent the solution in a basis of singular vectors $[V]$ by substituting the matrix $[R]$ in (4.19) as (4.9), with (4.17) and multiplying (4.19) from the left by the matrix $[V^H]$

$$[V^H][X][V][V^H][I_n] = \lambda_n[\Lambda^H][\Lambda][V^H][I_n] \tag{4.20}$$

Formulation (4.20) can formally be expressed as a GEP with an already diagonalized right hand side [137]

$$[\tilde{X}][\tilde{I}_n] = \lambda_n[\tilde{R}][\tilde{I}_n] \tag{4.21}$$

that is $[\tilde{X}] \equiv [V^H][X][V]$, $[\tilde{R}] \equiv [\Lambda^H][\Lambda]$, and $[\tilde{I}_n] \equiv [V^H][I_n]$.
Since the matrix $[S]$ is in general rectangular, it is crucial to take into account cases where $N_\alpha < N_{f_n}$, (4.11). This is equivalent to a situation in which there are limited number of spherical projections to recover the CMs. Consequently, only limited number of singular values Λ_{nn} exist. In such a case, the procedure similar to the one used in [5] should be undertaken by partitioning (4.21) into two linear systems as follows

$$[\tilde{X}][\tilde{I}_n] = \begin{bmatrix} \tilde{X}_{11} & \tilde{X}_{12} \\ \tilde{X}_{21} & \tilde{X}_{22} \end{bmatrix} \begin{bmatrix} \tilde{I}_{1n} \\ \tilde{I}_{2n} \end{bmatrix} = \begin{bmatrix} \lambda_{1n}\tilde{R}_{11}\tilde{I}_{1n} \\ 0 \end{bmatrix} \tag{4.22}$$

where $\tilde{I}_{1n} \in \mathbb{C}^{N_\alpha}$, $\tilde{I}_{2n} \in \mathbb{C}^{N_{f_n}-N_\alpha}$, and $N_\alpha < N_{f_n}$. The Schur complement is obtained by substituting the second row of (4.22) into the first row

$$[\tilde{X}_{11} - \tilde{X}_{12}\tilde{X}_{22}^{-1}\tilde{X}_{21}][\tilde{I}_{1n}] = \lambda_{1n}[\tilde{R}_{11}][\tilde{I}_{1n}] \tag{4.23}$$

with expansion coefficients of CMs defined as

$$[\tilde{I}_n] = \begin{bmatrix} \tilde{I}_{1n} \\ -\tilde{X}_{22}^{-1}\tilde{X}_{21}\tilde{I}_{1n} \end{bmatrix} \tag{4.24}$$

As far as the matrices $[U]$ and $[V]$ in (4.17) are unitary, the decomposition (4.21) yields CMs implicitly normalized to

$$[\tilde{I}_n^H][\tilde{R}][\tilde{I}_m] = \delta_{nm} \tag{4.25}$$

which is crucial since the standard normalization cannot be used without decreasing the number of significant digits. In order to demonstrate the use of (4.23), various examples from Table 4.1 are calculated and compared with the conventional approach (4.19).
The CMs of the spherical shell from Example S2 are calculated and shown as absolute values in logarithmic scale in Fig. 4.2. It is shown that the number of the CMs calculated by classical procedure (FEKO, AToM) is limited to the lower modes, especially considering the degeneracy $2l + 1$ of the CMs on the spherical shell [71]. The number of properly found CMs is significantly higher when using (4.23) than the conventional approach (4.19) and the numerical dynamic is doubled. Notice that, even (4.19) where the matrix $[R]$ calculated from (4.9) yields slightly better results than the conventional procedure. This fact is confirmed in Fig. 4.3 dealing with Example R2, where the multiprecision package Advanpix [138] is used as a reference. The same calculation illustrates that the matrix $[R]$ contains all information to recover the same number of modes as (4.23), but this can be done only at the expense of higher computation time[6].
While (4.23) preserves the numerical dynamics, the computational efficiency is not improved due to the matrix multiplications to calculate the $[\tilde{X}]$ term in (4.22). An alternative formulation that improves the computational speed is derived by replacing the matrix $[R]$ with (4.9) in (4.19)

$$[X][I_n] = \lambda_n[S^T S][I_n] \tag{4.26}$$

and multiplying from the left with $[S][X^{-1}]$

$$[S][I_n] = \lambda_n[S][X^{-1}][S^T S][I_n] \tag{4.27}$$

[6]For Example S2 the computation time of CMs with quadruple precision is approximately 15 hours.

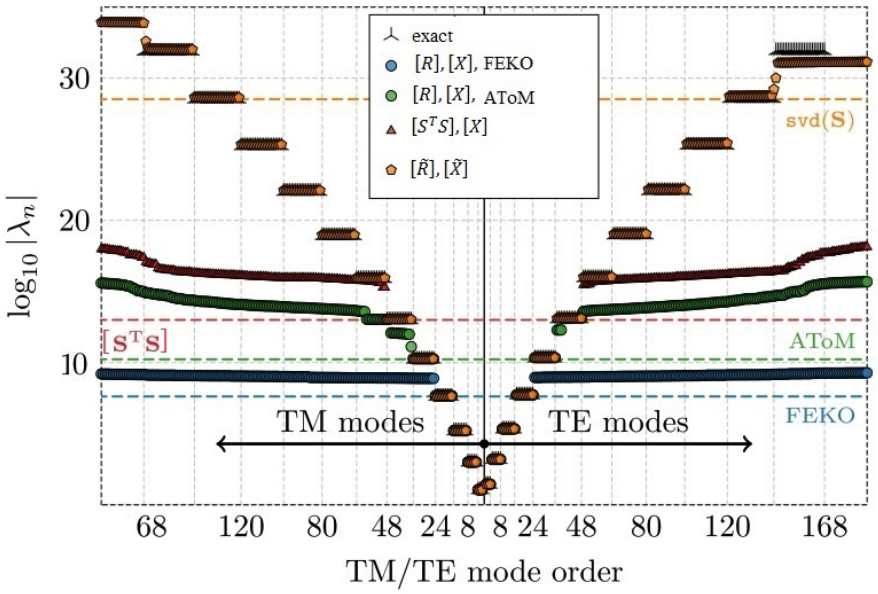

FIGURE 4.2: The absolute values of the CMs of spherical shell with electrical size $ka = 0.5$ (Example S2). Data calculated with classical procedure (4.19) are compared with (4.20), (4.23), and with the analytical results valid for the spherical shell [71].

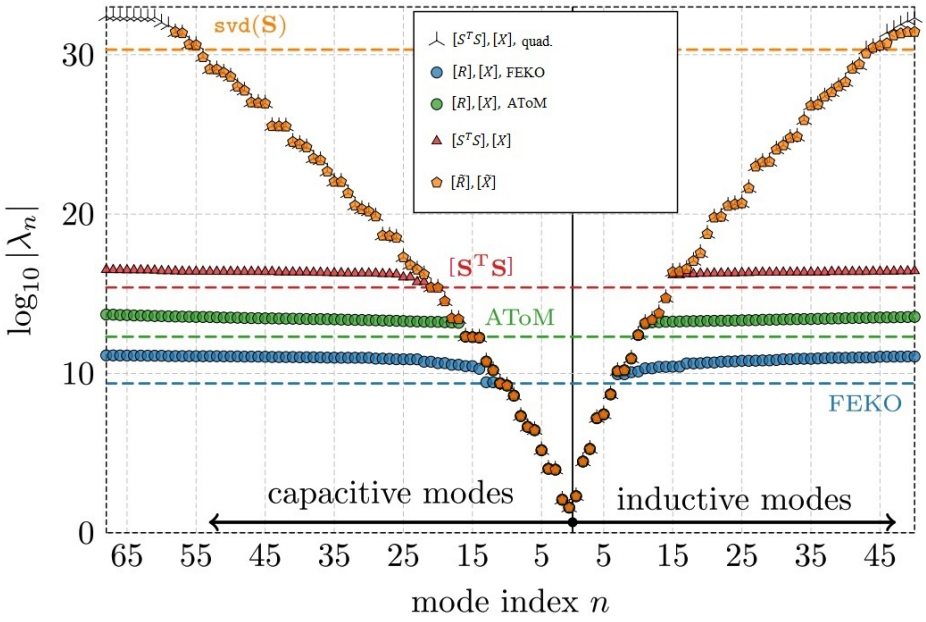

FIGURE 4.3: The absolute values of the CMs of rectangular plate (Example R2). Since unknown analytical results, the multi-precision package Advanpix has been used instead to calculate the first 150 modes from impedance matrix in quadruple precision.

The formulation (4.27) is a standard eigenvalue problem and can be written as

$$[S][X^{-1}][S^T][\hat{I}_n] = [\hat{X}][\hat{I}_n] = \xi_n[\hat{I}_n] \tag{4.28}$$

where $[\hat{X}] = [S][X^{-1}][S^T]$, $[\hat{I}_n] = [S][I_n]$, and $\xi_n = 1/\lambda_n$. As an intermediary step, the matrix $[X_S] = [X^{-1}][S^T]$ is computed, which is later used to calculate the characteristic eigenvectors $[I_n] = \lambda_n[X_S][\hat{I}_n]$. The eigenvalue problem (4.28) is solved in the basis of spherical vector waves, $[\hat{I}_n] = [S][I_n]$, that results in a matrix $[\hat{X}] \in \mathbb{C}^{N_\alpha \times N_\alpha}$. For problems with $N_\alpha \ll N_{f_n}$ the eigenvalue problem is solved rapidly compared with (4.19) and (4.23). The computation times for various examples are presented in Table 4.4 for all three formulations where a different number of CMs are compared. For Example H1 the computation time is investigated for the first 20 and 100 modes. The acceleration using (4.28) is approximately 4.7 and 14 times when compared with the conventional method (4.19). The first characteristic mode of Example H1 is illustrated in Fig. 4.4. Two tests proposed in [71] are performed to validate the conformity of characteristic current densities and the characteristic far fields with the analytically known values. The results of the former test are depicted in Fig. 4.5 for Example S2 and S5 that are spherical shells with two different d-o-f. Similarity coefficients $\chi_{\tau n}$ are depicted both for the CMs using the matrix $[R]$ (4.19) and for the CMs calculated by (4.23). The number of valid modes correlates well with Table 4.3 and the same dependence on the quality and size of the mesh grid as in [71] is observed. Qualitatively the same behavior is also observed in the latter test, depicted in Fig. 4.6, where similarity of characteristic far fields is expressed by coefficient $\zeta_{\tau n}$ [71]. These coefficients read

$$\zeta_{\tau n} = \max_l \sum_{\sigma m} |\tilde{f}_{\tau\sigma mln}|^2 \tag{4.29}$$

where $\tilde{f}_{\tau\sigma mln}$ is calculated using (4.14). The results for characteristic far fields computed from the conventional procedure (4.19) and the procedure presented in this work (4.23) are illustrated in Fig. 4.6. Lastly, the improved accuracy of using (4.23) over (4.19), is demonstrated in the Fig. 4.7 which shows current profiles, corresponding to a rectangular plate (Example R2), of a selected high order mode (a collection of the first 30 modes is presented in [129]). It can be seen that for modes with high eigenvalues (numerically saturated regions in Fig. 4.3), the surface current density in left panel, calculated via (4.19), shows numerical noise, while the evaluation via (4.23) still yields a correct current profile. Moreover, the matrix $[S]$ contains projections onto TE and TM spherical waves in its odd ($\tau = 1$) and even rows ($\tau = 2$), respectively. The separation of TE and TM spherical waves can be used to construct resistance matrices $[R^{TE}]$ and $[R^{TM}]$, where only odd and even rows of matrix $[S]$ are used to evaluate (4.9). Matrices $[R^{TE}]$ and $[R^{TM}]$ can be used in optimization, e.g., in such a case when the antennas have to radiate

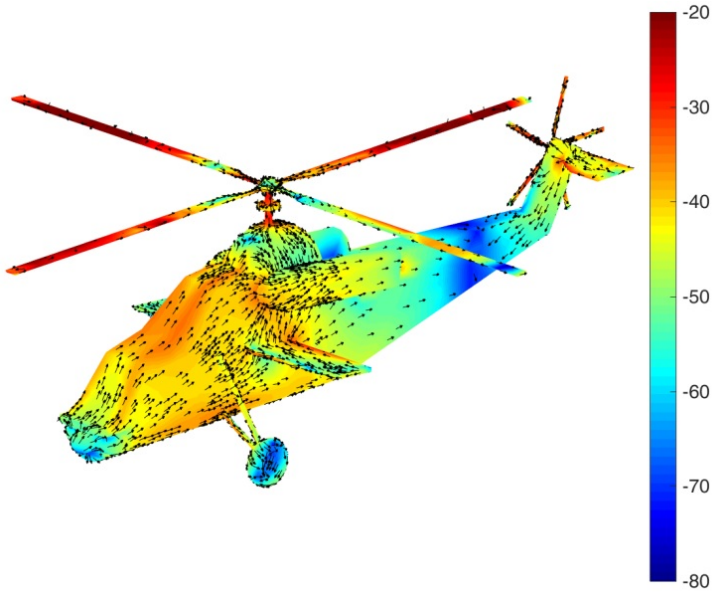

FIGURE 4.4: Current density of the first characteristic mode of a helicopter at $ka = 7$ (Example H2), mesh grid has been taken from [84].

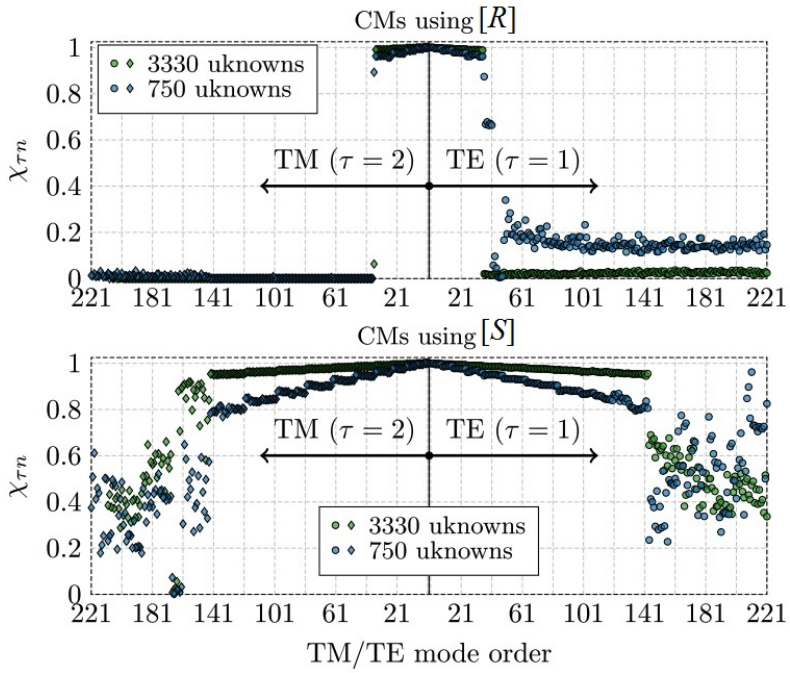

FIGURE 4.5: Similarity of numerically evaluated characteristic currents for a spherical shell with two different discretizations (Example S2 and S5) and the analytically known currents [71]. The coefficients $\chi_{\tau n}$ were calculated according to [71], top panel depicts results for the conventional procedure (4.19), bottom panel for the procedure from this work.

Example (see Table 4.1)	N_λ	Time to calculate N_λ CMs (s)		
		(4.19)	(4.23)	(4.28)
S1	10	0.36	0.18	0.12
S2	300	3.3	2.0	1.1
S4	10	2.8	2.5	0.78
S4	100	13	2.1	0.72
R1	100	0.29	0.28	0.42
R3	50	7.2	1.3	0.49
H1	20	130	150	28
H1	100	500	150	35
H2	100	350	160	35

TABLE 4.4: Comparison of computation time required by various methods capable to calculate first N_λ CMs. The calculations were done on windows server 2012 with $2 \times XEON\ E5-2665$ CPU @ 2.4 GHz and $72-GB$ RAM.

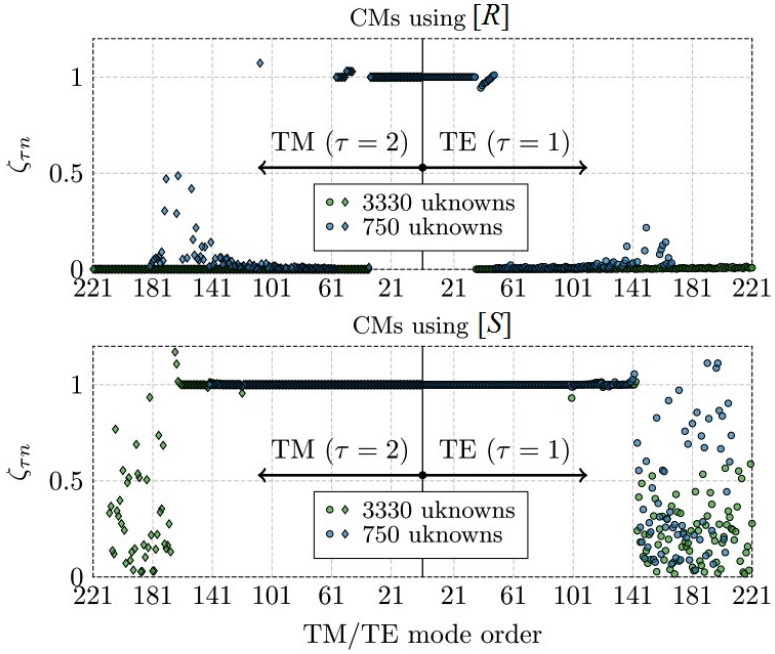

FIGURE 4.6: Similarity of numerically and analytically evaluated characteristic far fields for a spherical shell (S2 and S5) and analytically known far fields [71]. Top panel depicts results using (4.19), bottom panel are the results using (4.23).

TM-modes only [135]. With this feature, characteristic modes consisting of only TM (or TE) modes can easily be found. This is shown in Fig. 4.8, in which the spherical shell (Example S2) and rectangular plate (Example R2) are used to find only TM (capacitive) and TE (inductive) modes, respectively. In case of a spherical shell this separation could have been done during the post-processing. For a generally shaped body this separation however represents a unique feature of the proposed method.

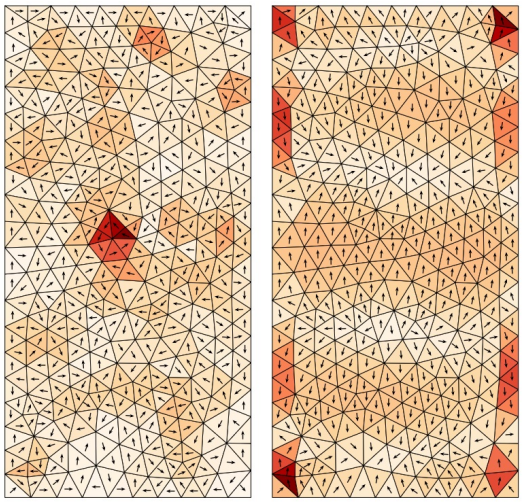

FIGURE 4.7: Comparison of the higher-order CMs of the rectangular plate (Example R2) with the most similar characteristic number, left panel: conventional procedure (4.19), right panel: procedure from this paper (4.23). The first 30 modes evaluated via both procedures are available as interactive collection (available in Adobe Acrobat Reader) in [129], cf. Fig.4.3.

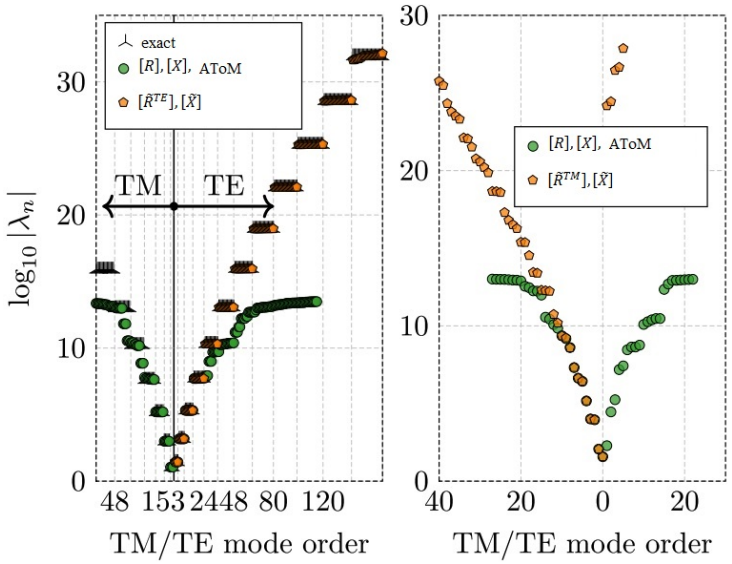

FIGURE 4.8: Left pane: the absolute values of the CMs of a spherical shell (Example S2) if only odd rows of the matrix S were kept. Right pane: the absolute values of the CMs of a rectangular plate (Example R2) if only even rows of the matrix $[S]$ were kept.

4.5 Conclusion

In this chapter, a new method to improve the accuracy of modal decomposition has been presented. It is based on reconstructing the real part of the impedance matrix using the projection of the vector spherical harmonics. The proposed method offers several appealing features such as

- Accelerating the CMs computation.
- Improving the accuracy of the derived CMs.
- Solving the indefiniteness issue of the matrix $[R]$.
- Estimating the number of CMs prior to the decomposition by making use of the total number of spherical modes N_α used.
- Allowing an independent choice of the parameters N_α and N_{f_n}, as the matrix $[S]$ is rectangular.
- Optimal for applications involving the modal decomposition of the matrix $[R]$.
- Allows the prescription of the radiation pattern of optimized current by restricting the set of the spherical harmonics used for the construction of the matrix.

Finally, it can be easily implemented into both in-house and commercial solvers, improving thus their performance and providing antenna designers with more accurate and larger sets of characteristic modes.

Chapter 5

Tracking Methods

5.1 Introduction

Actually, the characteristic modes theory is a very promising design approach, which can provide useful insights about the radiation and scattering phenomena of arbitrarily shaped objects. However, to ensure the accuracy of the results, much more care should be given to the tracking methods used to track the characteristic modes. Therefore, in this chapter, an enhanced modal tracking method is presented. The proposed approach is based on the minimum magnitude between consecutive eigenvalues. Four numerical examples are used to evaluate the method performance, and the obtained results are discussed.

5.2 Commonly-known Tracking Methods

Generally, modal tracking is used to pursue the evolution of characteristic modes' eigenvalues over the frequency spectrum at discrete samples. Where a mode can be at resonance if its associated eigenvalue is equal to zero. Whereas, all modes featured with positive values of the eigenvalues are deemed to be inductive, and all modes with negative eigenvalues are considered capacitive. Therefore, the modal tracking process concerns the traceability of the variation of a characteristic mode between these three states over the frequency, by making use of an index attributed to each mode of the tracked modes. Worth noting that a mode might become more dominant than the others at a certain frequency step (i.e., the mode is at resonance or close to it), then become insignificant or even disappear at other frequency steps.
In the following subsections, a brief introduction to the common methods used in modal tracking will be given along with their major features and their reported limitations.

5.2.1 Correlation based methods

The majority of the existing tracking algorithms are based on the correlation concept [139]. This concept comprises the computation of the correlation coefficient between the modal quantities (e.g. eigenvectors, eigenfields, etc.) at discrete frequency points. The value of the correlation coefficient indicates whether the modes can be associated together or not, viz. a higher correlation coefficient implies that the corresponding modal quantities represent the same characteristic mode, where the similarity here is in terms of current distribution and modal field patterns [76]. Typically, for acceptance criteria a threshold value is set, where the threshold value varies depending on the needs of the user and the desired applications.

5.2.1.1 Eigenvectors Correlation

In fact, the most known type of the modal correlation methods is the approach based only on the eigenvectors due to its simplicity and low complexity. The working principle of this approach relies on the assumption that the eigenvectors are slowly changing over the frequency. Usually, the computation of the correlation coefficient between eigenvectors is performed using the Pearson' coefficient [139], which is usually used to get the degree of linearity between the variables. The Pearson' coefficient ranges from -1 to +1, with -1 indicating that the variables are negatively correlating , +1 for variables positively correlating, and 0 for no correlation. Its mathematical expression is given by [140]

$$C_r = \frac{\sum_{i=1}^{N}(X_i - \bar{X})(Y_i - \bar{X})}{\sqrt{\sum_{i=1}^{N}(X_i - \bar{X})^2 \sum_{i=1}^{N}(Y_i - \bar{Y})^2}} \tag{5.1}$$

Here, X_i and Y_i represents two column vectors, and $\bar{X}$, $\bar{Y}$ their means, respectively. Frequently, in the characteristic modes case, the elements X_i constitute the eigenvector at the previous frequency step, while Y_i are considered to be the elements of the eigenvector at the current frequency step [65]. This correlation coefficient can be calculated in Matlab using the predefined function 'corr'. In addition, for eigenvectors tracking, the absolute value of the correlation coefficient $|corr|$ might be used as the direction of the correlation is not important (More details about the modal correlation method can be found in [76, p. 65-68]).

Actually, intensive research work on the potential of the eigenvectors correlation method has been carried out. For instance, in [60] the authors proposed the use of eigenvectors correlation to perform the modes tracking, where the modes' discontinuity issue was

studied, and functions to deal with the closed modes (i.e. modes that disappeared) and the newly appearing modes were incorporated. Similarly, in [61] the modal tracking was performed using the correlation matrix [76] between eigenvectors at adjacent frequencies. The novelty of this work is the adoption of an adaptive frequency scheme. This latter aims to clarify ambiguity between sets of eigenvectors at consecutive frequency samples, in such case multiple eigenvectors at a specific frequency step are mapped to a single eigenvector at the previous frequency step. Hence, this adaptive frequency scheme is based on subdividing each frequency interval into two sub-intervals and computing the correlation matrix of the eigenvectors over each sub-interval. If any given sub-interval has some ambiguity, that same sub-interval is subdivided again.
However, the eigenvectors correlation was found to be very sensitive to changes in modal surface current distributions, and that the condition concerning the orthogonality of the eigenvectors is not fully fulfilled [67]. Also, it might fail in connecting the appropriate modes with each other and consequently generate which is known as swapped modes [141]. Furthermore, even if the orthogonality requirement is guaranteed, still the eigenvectors correlation suffers from an inevitable issue at equal eigenvalues, where the eigenvectors of the two identical eigenvalues are not clearly defined, therefore the accuracy of the results is not assured, as it will be further detailed in section 5.3.

5.2.1.2 Eigenfields Correlation

Alternatively, eigenfields correlation or the far field correlation can be used in modal tracking. This approach was first examined by Miers et. al in [63, 64]. The proposed method makes use of the standard envelope correlation coefficient given by [64]

$$\rho_{e,mn}^{CM} \approx \frac{\left| \oint_{4\pi} \left[E_{\phi,m}(\Omega) E_{\phi,n}^{*}(\Omega) + E_{\theta,m}(\Omega) E_{\theta,n}^{*}(\Omega) \right] \mathrm{d}\Omega \right|}{\left| \oint_{4\pi} G_m(\Omega)\, \mathrm{d}\Omega \right| \left| \oint_{4\pi} G_n(\Omega)\, \mathrm{d}\Omega \right|} \tag{5.2}$$

Where

$$G_m(\Omega) = |E_{\phi,m}(\Omega)|^2 + |E_{\theta,m}(\Omega)|^2 \tag{5.3}$$

$$G_n(\Omega) = |E_{\phi,n}(\Omega)|^2 + |E_{\theta,n}(\Omega)|^2 \tag{5.4}$$

Whereas $\mathrm{d}\Omega = sin(\theta)\, \mathrm{d}\phi\, \mathrm{d}\theta$, while $E_{\phi,m/n}(\Omega)$ and $E_{\theta,m/n}(\Omega)$ are the ϕ and θ polarized characteristic electric far-field patterns of the modes m and n, where the two modes are taken at two adjacent frequency steps. The main advantage of this method is that it allows a larger frequency step compared to the eigenvectors correlation, as the far-fields

are found to be relatively stable for complex structures compared to the eigencurrents, which can reduce the computational time required for tracking the characteristic modes [64]. Besides, it allows minimizing the errors generated by the variation of the currents or by the image currents found in symmetric bodies [64]. Furthermore, the research work in [64] demonstrates that the far fields correlation approach outperforms eigenvectors correlation, where fewer degenerated modes were observed (i.e., an issue which arises usually at equal eigenvalues) and no observable modes swapping (i.e., an abrupt switching of the modes' indexes, it will be further explained in subsection 5.3) compared to the eigenvectors correlation method. Moreover, the approach was successfully applied to a radiator composed of both perfect electrical conductor (PEC) and dielectric material [63]. The major drawback of this method is the need for additional computations, as the eigenfields are not a direct output of the modal decomposition. Therefore, numerical calculations of the eigenfields with a predefined resolution of the ϕ and θ components are required, which decreases the accuracy of the tracked modes [67].

5.2.1.3 Surface Current Correlation

Another interesting approach to perform the characteristic modes tracking could be implemented using the surface current correlation [67], previously known as the orthogonality property algorithm [62]. This approach makes use of two parameters, the eigenvectros and the real part of the impedance matrix of the structure under study, and it is based on the orthogonal aspect of the characteristic modes. Therefore, this approach does not require any extra calculations, conversely to the eigenfields correlation method [67]. The correlation coefficient for this approach is calculated as it follow [67]

$$\rho_{m,n} = \frac{1}{2} < [I_m(f_i)], [R(f_{i+1})][I_n(f_{i+1})] > \tag{5.5}$$

According to [62], the main drawback of this correlation coefficient (5.5) is its unbounded nature, therefore it is very difficult to set a threshold value to map the modes at adjacent frequency steps f_i and f_{i+1}, which might lead to errors in the obtained results. Further, in [62], the authors evaluated the performances of the Pearson' correlation and the orthogonality property algorithm performances. Their study revealed that the latter approach is more computationally demanding than the former, moreover, the Pearson' correlation approach (see eigenvectors correlation in 5.2.1.1) led to more accurate results. Meanwhile, based on the research work reported in [67], this tracking method requires sufficient mesh density of the structure and a small frequency step size to accurately track the modes, where the results of the tracked modes were found to change by changing the frequency step size. Taking this into consideration, the use of intelligent frequency control schemes might be of great usefulness to improve this tracking approach [67].

Finally, the fact that the eigenvectors associated with equal eigenvalues are not well defined might still affect the accuracy of the surface current correlation. A very promising solution to the aforementioned problem was proposed in [67], where the authors make use of the orthogonality (or nearly orthogonality) property of the characteristic modes to define new orthogonal eigenvectos at equal eigenvalues by rotating the eigenvectors initially obtained by the modal decomposition. However, the major drawback of this solution is the long computational time required for the computations compared to that needed in the surface current correlation method, besides some reported inaccuracies in tracking higher-order modes [67].

5.2.2 Hybrid Methods

In like manner, the potential of hybrid methods in modal tracking was also investigated. Typically, these methods are a combination of two tracking methods, where one is considered to be the main tracking approach and the other one as the backup method to check the correctness or to rectify the tracking results. For instance, in [65], the tracking is first performed by extrapolating the eigenvalue or the characteristic angle curves. Then, the quality of each mapping is checked, and if a discrepancy arises a linear correlation (Pearson' correlation) is applied to the corresponding eigenvectors to ensure successful modes tracking. Furthermore, the authors in [66] suggested the use of an eigenvalues' estimation mechanism, where the value of the eigenvalue at the next frequency step is approximated using a reference eigenvector at the current frequency step and the real and imaginary parts of the impedance matrix at the next frequency step. Thereafter, preconditioning of the eigenvectors is effectuated to discard the improper eigenvectors, then the correlation method is applied to the remaining eigenvectors, where an alterable threshold scheme for the correlation was adopted by lowering the threshold value.
Actually, these methods might be very effective in tracking the characteristic modes, and outperform the single based tracking procedures but at the cost of the required computational time, besides the substantial complexity in implementing the two tracking approaches instead of only one modal tracking mechanism.
Finally, in light of all these pioneer studies, the need to develop a tracking method that grants the accuracy of the tracked modes and featured with low complexity is critical to the survival of the characteristic modes theory from the possible disuse. Therefore, an enhanced modal tracking algorithm is suggested which is immune to degenerated modes and swapping modes, more details about the proposed approach can be found in the following subsection 5.3.

5.3 Proposed Tracking Method

In the context of modal tracking, a new tracking method is proposed. The proposed approach is intended to address the most commonly encountered problems in eigenvectors correlation method, namely swapped and degenerated modes. The proposed approach is mainly built upon the difference in magnitudes between consecutive eigenvalues, without the use of any other modal quantities. To better elucidate the working mechanism of the proposed method, a meshed structure, and its impedance matrix $[Z]$ are used, and they are obtained using Makarov' code [79]. The dimensions of $[Z]$ are $N_b \times N_b \times F$, with N_b representing the number of basis functions, and F the total number of frequency steps. Following, the generalized eigenvalue problem (5.6) related to the characteristic modes theory is solved for each frequency sample f_i [1, 5]

$$[X(f_i)][I_n(f_i)] = \lambda_n(f_i)[R(f_i)][I_n(f_i)] \tag{5.6}$$

Where, $[X]$ and $[R]$ are the imaginary and real parts of the impedance matrix $[Z]$, while $[I_n]$ and λ_n designate the eigenvectors and eigenvalues, respectively. Here, the index n is sweeping over all the basis functions of the structure. Next, $\lambda_n(f_i)$ are sorted in ascending order, then their corresponding eigenvectors are reordered accordingly. This ascending order is due to the fact that the smaller is the eigenvalue, the better is its radiation efficiency. Moreover, a preconditioning of the eigenvalues is necessary for further process. Consequently, all highly valued (e.g. matrix' entries indicated by Inf in Matlab [80]) or complex eigenvalues are excluded, together with their associated eigenvectors (see Appendix. C). Usually, the number of tracked modes N_m is very small compared to the total number of modes within the structure, therefore, the index n would henceforth sweep over N_m. Next, the difference in magnitudes between each eigenvalue at f_i and all eigenvalues at f_{i+1} is computed, and the minimum difference m_{λ_n} found indicates the most appropriate continuation of the mode at f_{i+1}. The modes with a smaller index are mapped first. Once a mode is mapped, no other associations are possible with it, this bears a close resemblance to the association process used in eigenvectors correlation matrix (see [76, p. 67-68]). Thus, in case of two modes having the exact same eigenvalue, the mode with the smaller index will be associated first with the appropriate mode at the next frequency step, then the following mode and so forth, where m_{λ_n} is given by

$$m_{\lambda_n} = min|\lambda_k(f_{i+1}) - \lambda_n(f_i)|; \quad (n, k = 1, 2, .., N_m) \tag{5.7}$$

Note that in the equation above for each value of the index n, the index k should loop over all the values in the range from 1 to N_m. Furthermore, according to the values

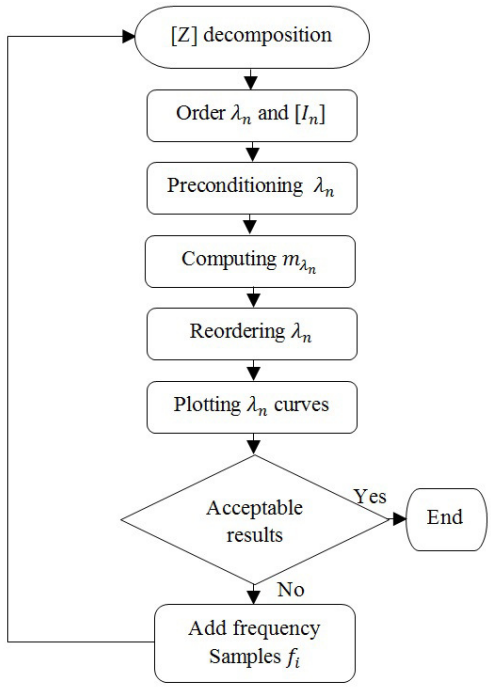

FIGURE 5.1: Illustrative flowchart of the proposed method.

	f_i	f_{i+1}
m_1	1	0.5
m_2	2	1.25
m_3	2	3

TABLE 5.1: Illustrative example of ordered eigenvalues obtained from the modal decomposition of the matrix $[Z]$.

of m_{λ_n}, the eigenvalues are reordered, and the corresponding characteristic modes are determined over the frequency range. In case of unsatisfactory results, the frequency step size is decreased, and the above described process is repeated. Fig. 5.1 represents an illustrative flowchart of the proposed tracking method. To better clarify the tracking process, let consider three modes of which two modes m_2 and m_3 are having the exact same eigenvalue at f_i as it is shown in Table 5.1. Now, by applying the proposed method, and the steps illustrated in Fig. 5.1, the difference in magnitudes between each eigenvalue at f_i and all the eigenvalues at f_{i+1} is computed (see Table 5.2). The association between modes is performed based on the minimum difference found m_{λ_n}. The modes with a smaller index are mapped first (i.e. $m_{1(f_i)}$ with $m_{2(f_{i+1})}$, $m_{2(f_i)}$ with $m_{3(f_{i+1})}$, and $m_{3(f_i)}$ with $m_{1(f_{i+1})}$). Once a mode is mapped, no other associations are possible with it. The final modes' association results are highlighted in Table 5.3.

	$m_{1(f_{i+1})}$	$m_{2(f_{i+1})}$	$m_{3(f_{i+1})}$
$m_{1(f_i)}$	0.5	0.25	2
$m_{2(f_i)}$	1.5	0.75	1
$m_{3(f_i)}$	1.5	0.75	1

TABLE 5.2: Computation of the difference in magnitudes of eigenvalues (gray colors indicate the modes in the vertical direction which have been mapped first from lightest to darkest).

	f_i	f_{i+1}
m_1	1	1.25
m_2	2	3
m_3	2	0.5

TABLE 5.3: Reordered eigenvalues after the modes' re-association.

5.4 Numerical Results

The performances of the proposed tracking method are evaluated using four numerical examples. An electrically small metallic plate is first examined. Then, a large slot antenna is considered. Thereafter, a spiral antenna example is treated. Finally, a Sierpinski fractal antenna is studied. The tracking results of the proposed method are compared to the results of the eigenvectors correlation method. Note that in all the examples considered in this section, the impedance matrices were generated using the Makarov' code [79].

5.4.1 Metallic Plate

Firstly, the proposed algorithm has been applied to a flat metallic plate ($L = 30$ mm, $W = 40$ mm), over a wide frequency bandwith [3 GHz − 10 GHz], and using 25 frequency samples, with 224 Rao-Wilton-Glisson (RWG) basis functions [52] used for the surface current density expansion, and without considering any source of excitation. The mesh file was generated using [142]. Additionally, as the electrically small antennas need only few modes to describe their radiation behavior, only the first five modes of the metallic plate are tracked. Fig. 5.2 shows the eigenvalues' variation over the frequency using the eigenvectors correlation method. It can be observed that the modes swapping occurred several times in a severe manner, for instance, the first one occurred between the third and fourth modes. This is mainly due to the large difference between the linked eigenvalues, although the correlation coefficient between their associated eigenvectors is high enough to perform the connection, as it is apparent from Fig. 5.3 and Table 5.4. In contrast, the results of the proposed approach depicted in Fig. 5.4 shows a smooth progress of the modes over the frequency without any modes swapping detected. Also,

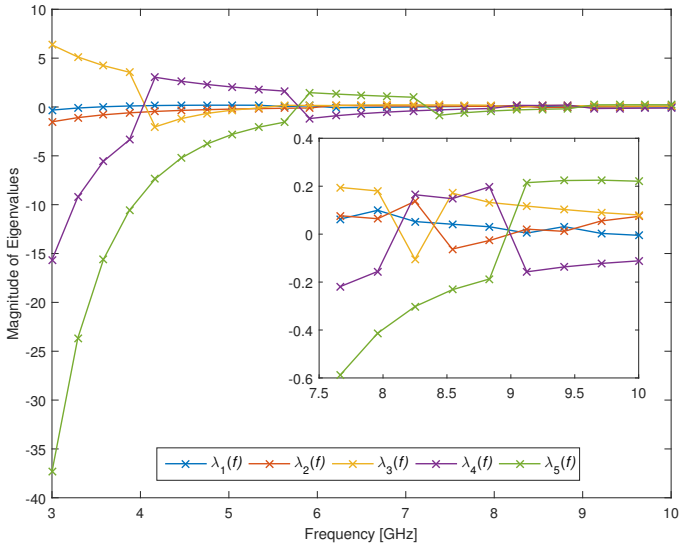

FIGURE 5.2: Tracked eigenvalues of the metal plate using the correlation method, with an inset from 7.5 GHz to 10 GHz.

	Modes indexes				
	n_1	n_2	n_3	n_4	n_5
f_3	1	2	3	4	5
f_4	1	2	4	3	5
f_5	1	2	3	4	5

TABLE 5.4: Extract from mapping matrix of the metal plate showing modes swapping between modes n_3 and n_4 using the correlation method.

it is worth mentioning that the characteristic modes are unaffected by the degenerated modes problem (e.g. see encircled part from Fig. 5.4), but how to check the correctness of the obtained results? One of the most practical methods used to check the exactness of the results is to reduce the size of the frequency step used. In order to do so, the number of frequency samples has been increased from 25 samples to 50 and 100 samples, respectively. The results are shown in Fig. 5.5, from which it is apparent that the behavior of modes didn't change by increasing the number of frequency samples to 50 samples (see left side of Fig. 5.5), although the order of modes has changed when 100 samples were used (see right side of Fig. 5.5), which proves the correctness of the obtained results. Moreover, the accuracy of the proposed tracking method can be improved by making use of a refining process based on decreasing the frequency step size over some segments of the frequency axis. Fig. 5.6 exhibits its working principle to correct tracking errors caused by non-sufficient frequency samples. Firstly, 9 samples are considered over the operating band of the metallic plate (see the left side of Fig. 5.6). In this case, the frequency segment $f_1 f_3$ will be subdivided into smaller segments, and the proposed algorithm is again applied for $f_1 f_3$ segment only, and the obtained eigenvalues are inserted into the previously computed eigenvalues between f_1 and f_3 samples. Next,

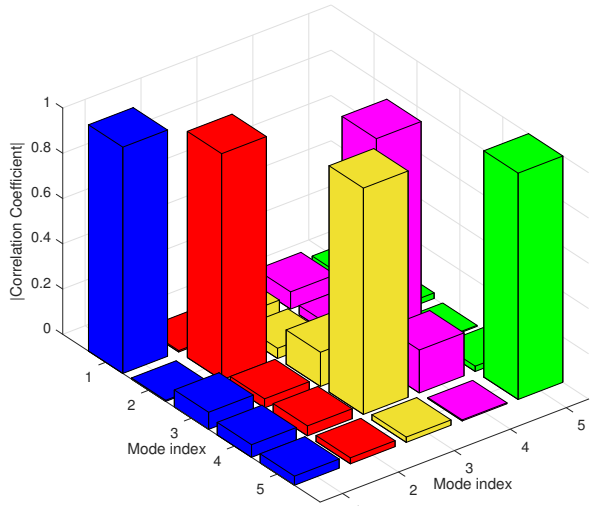

FIGURE 5.3: Correlation matrix between f_3 and f_4 frequency samples, with the pairs $[J_3(f_3), J_4(f_4)]$ (in magenta color), and $[J_4(f_3), J_3(f_4)]$ (in golden color) showing a very high correlation coefficient.

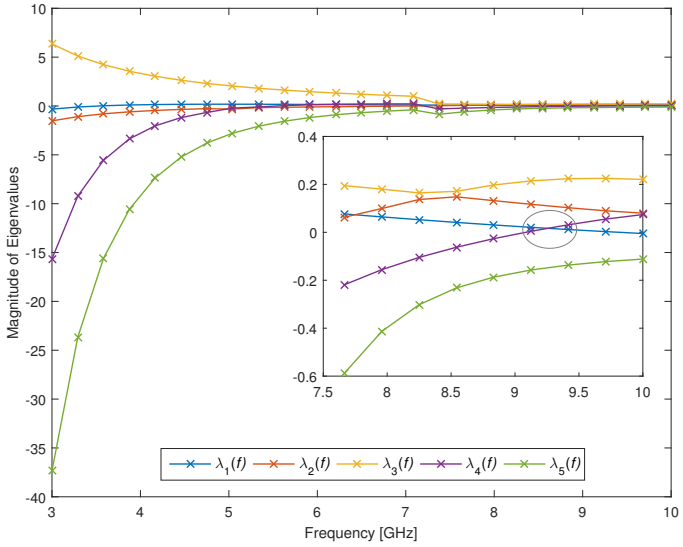

FIGURE 5.4: Tracked eigenvalues of the metal plate using the proposed method.

the eigenvalues are reordered using the newly calculated m_{λ_n} through $f_1 f_F$, and as it can be observed from the right side of Fig. 5.6 satisfactory results are obtained with fewer frequency samples.

5.4.2 Slot Antenna

Moreover, the proposed tracking method was applied on a relatively large slot antenna geometry (3×3 m^2), with a slot at the middle ($L = 2$ m, $W = 0.06$ m), and a junction bridge ($L = 0.06$ m) as it can be seen from Fig. 5.7. The slot antenna mesh file is taken

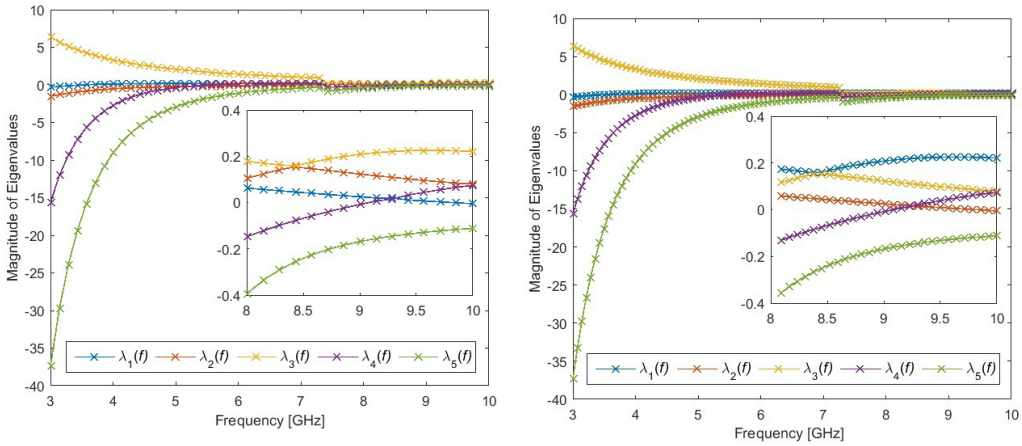

FIGURE 5.5: Eigenvalues of the metal plate using 50 samples (left side) and 100 samples (right side).

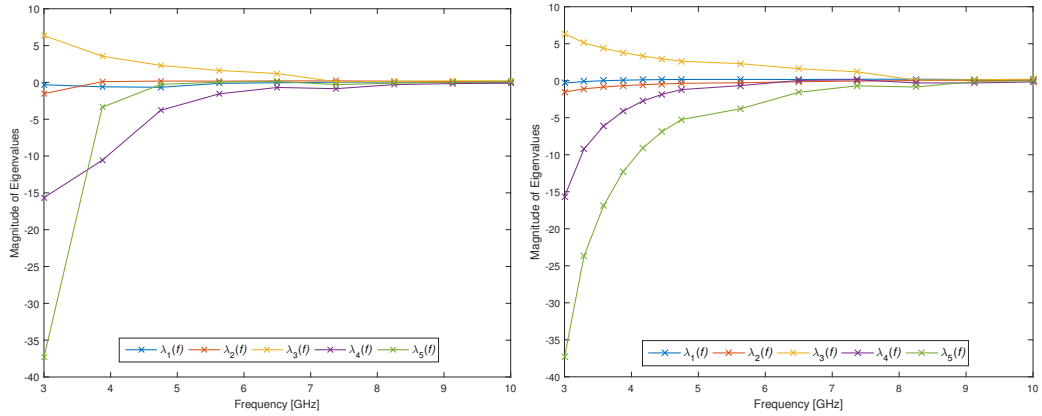

FIGURE 5.6: Eigenvalues of the metal plate without (left) and with (right) refinement of the frequency axis between the samples f_1 and f_3.

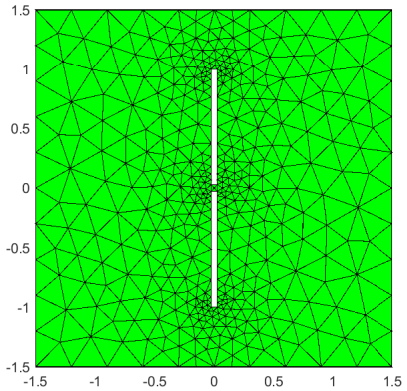

FIGURE 5.7: The mesh representation of the slot antenna.

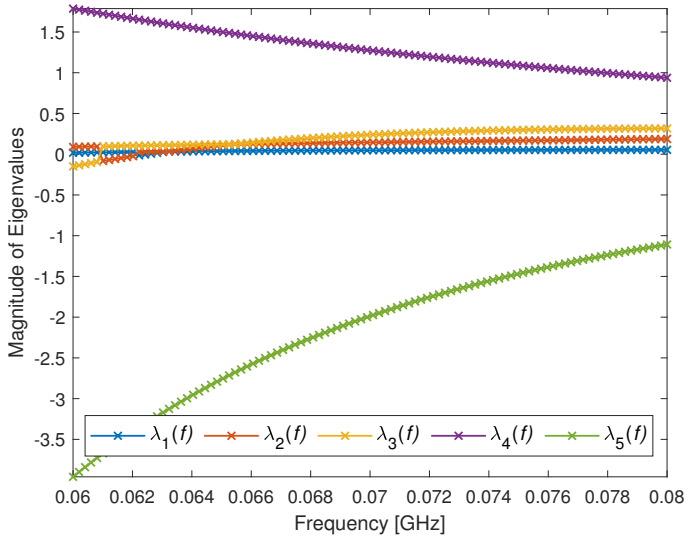

FIGURE 5.8: Tracked eigenvalues corresponding to the first five characteristic modes of the slot antenna obtained using the eigenvectors correlation method.

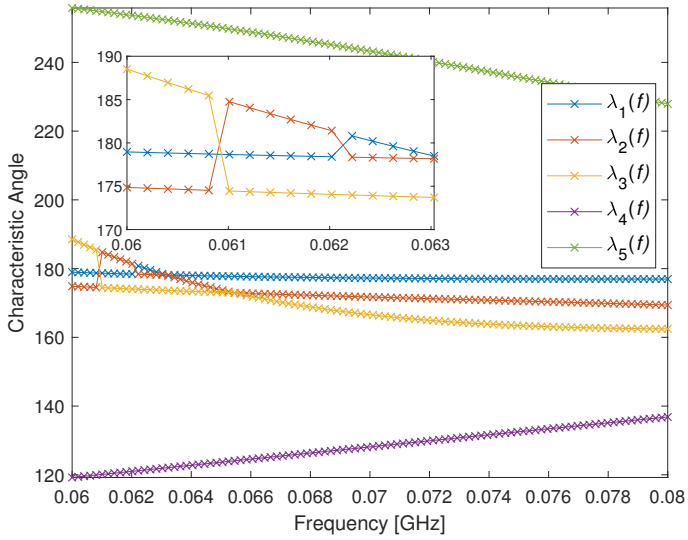

FIGURE 5.9: Illustration of the characteristic angles parameter obtained using the eigenvectors correlation method for the slot antenna example.

from [79], and it contains 816 triangles with 1176 inner edges. The eigenvalues variation was observed along with the frequency band [60 MHz – 80 MHz] , in order to include the resonance frequency of the slot antenna at 75 MHz. Meanwhile, the examined band is subdivided into 100 frequency samples. It should be noted that for this example 10 modes were tracked while only 5 modes are presented, as it is found that increasing the number of tracked modes helps tremendously in increasing the accuracy of the modal tracking. The results of the eigenvectors correlation method and those obtained by the proposed tracking method are presented. The Fig. 5.8 depicts the eigenvalues curves obtained using the correlation method, where the swapping between the three

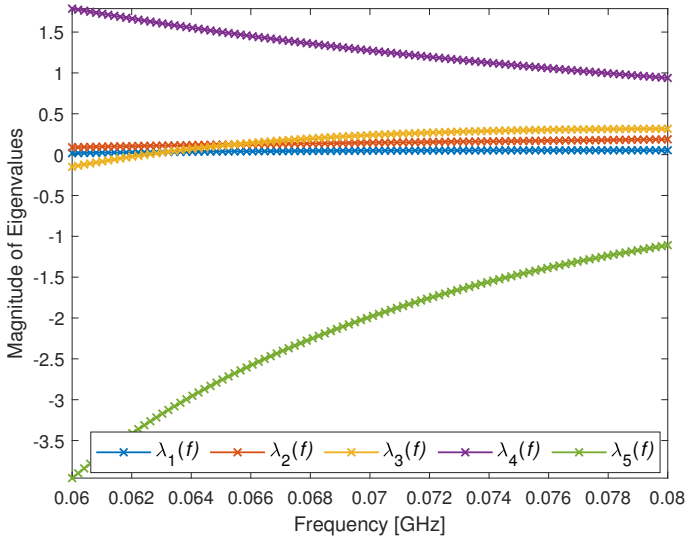

FIGURE 5.10: Tracked eigenvalues corresponding to the first five characteristic modes of the slot antenna obtained using the proposed method.

first characteristic modes can be easily detected, and it is even more noticeable in the characteristic angles plot shown in Fig. 5.9. Whereas, the proposed method resulted in more coherent curves of the eigenvalues along the frequency band studied, without any swapping or leaps between the tracked characteristic modes as it can be seen from Figs. 5.10 - 5.11. The same results are obtained using the modal significance parameter as is reported in Fig. 5.12. In addition, Fig. 5.12 provides new informations about the modal significance of each mode. For instance, the modes n_1, n_2, and n_3 have the higher modal significance along [60 MHz − 63 MHz], thereafter, only the mode n_1 keeps the higher modal significance for the rest of the examined band, while the modal significance of the modes n_2, and n_3 is slightly decreased, whereas, that of the modes n_4, n_5 is significantly increased.

5.4.3 Spiral Antenna

In this subsection, the performances of the proposed tracking method are evaluated for a wire antenna example using the spiral antenna mesh highlighted in Fig. 5.13, which was retrieved from [79]. As can be seen the spiral antenna has seven turns, with a size of 0.2 m, while the mesh file contains 600 triangles and 599 inner edges. In this example, the frequency band examined is [0.025 GHz−5 GHz], with 200 sample points. Therefore, the resulting impedance matrix has a size of $(599, 599, 200)$. Note that 40 modes where tracked, although only 5 characteristic modes will be presented. As can be seen from Fig. 5.14, the eigenvectors correlation method led to an ambiguous representation of the characteristic modes with many leaps. Whereas the proposed method resulted in a

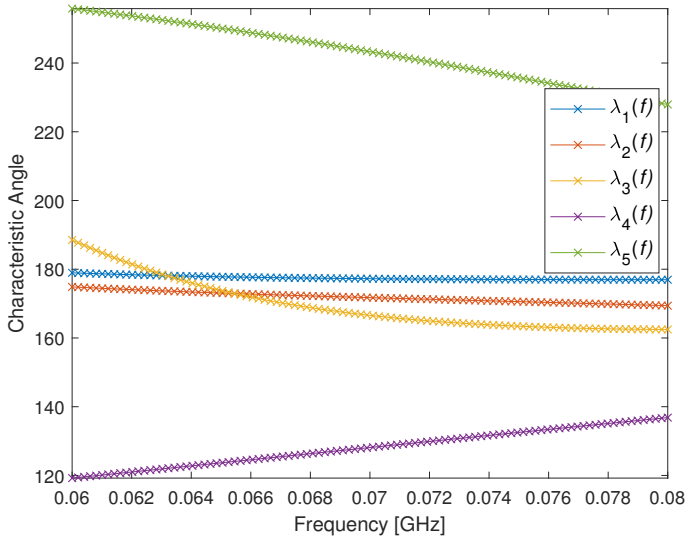

FIGURE 5.11: Representation of the characteristic angles of the slot antenna using the proposed method.

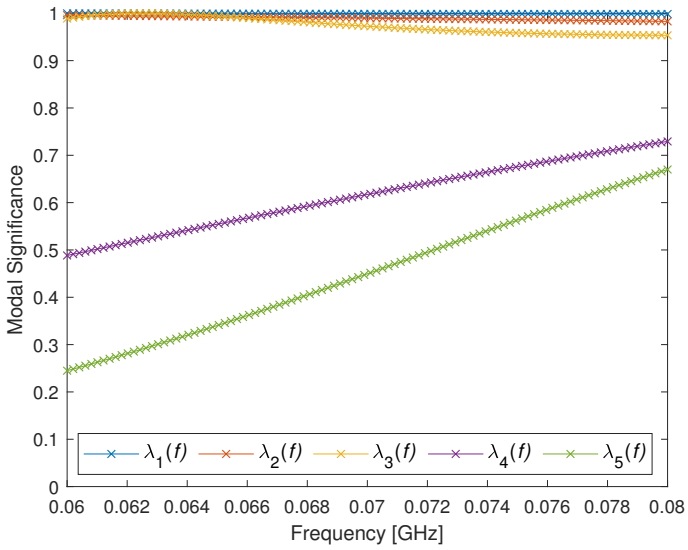

FIGURE 5.12: The modal significance of the five first characteristic modes of the slot antenna obtained using the proposed method.

smoother representation of the modes as it can be seen from Figs. 5.15 - 5.16, although it is still insufficient to predict the antenna behavior when excited. This can be due to the high complexity of the antenna geometry considered. One solution to improve the obtained results could be to reduce the size of the frequency band being examined, or to increase the total number of frequency samples, or even to refine the mesh.

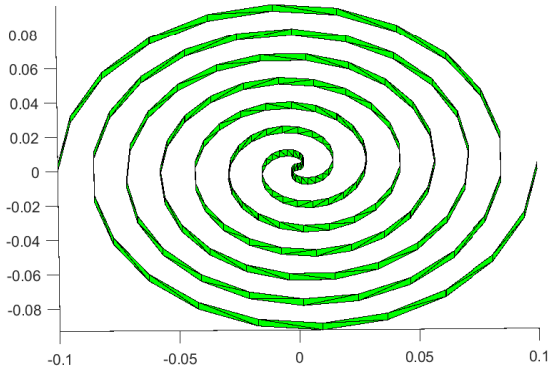

FIGURE 5.13: Discretized structure corresponding to the spiral antenna.

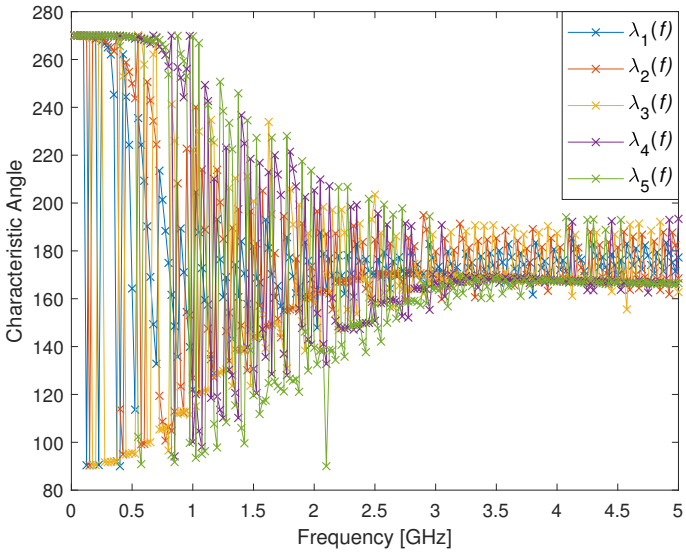

FIGURE 5.14: Characteristic angles variation along with the frequency axis obtained using the eigenvectors correlation approach for the spiral antenna example.

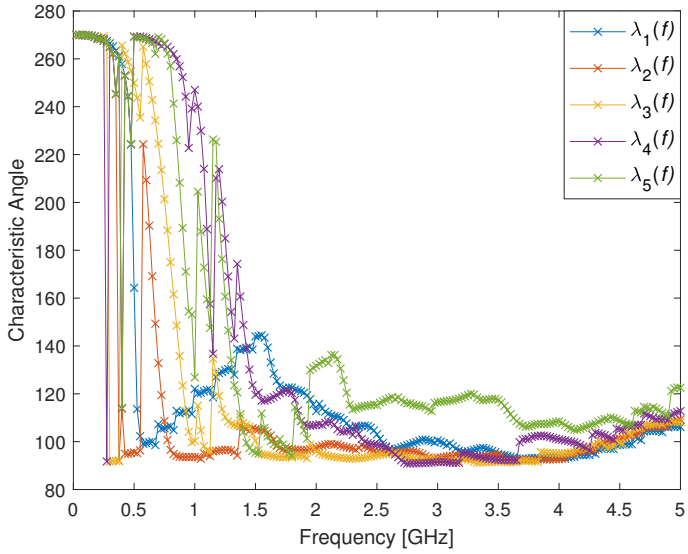

FIGURE 5.15: Representation of the characteristic angles for the spiral antenna example using the proposed method.

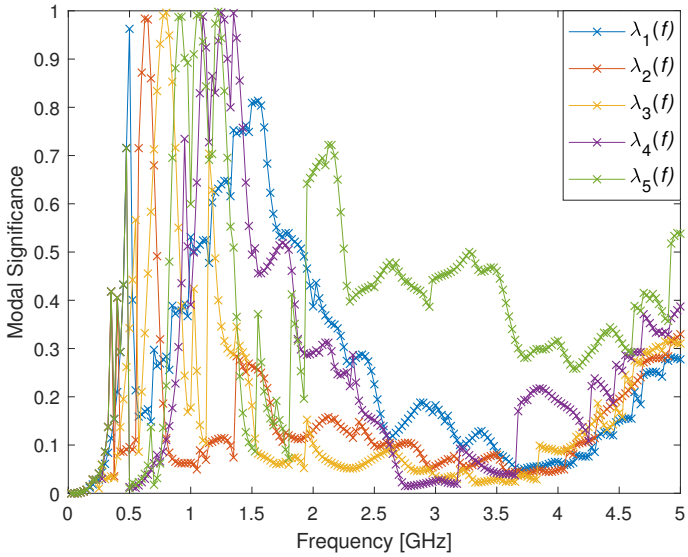

FIGURE 5.16: Illustration of the modal significance parameter for the spiral antenna obtained using the proposed method.

5.4.4 Sierpinski Fractal Antenna

This subsection is devoted to highlighting the issue of degenerated modes. Therefore, a Sierpinski fractal antenna is considered, where the mesh file[1] is retrieved from [79]. The antenna is characterised by a stage of growth equal to 2, flare angle set to 90°, with 853 RWG edge element, and 100 frequency samples over [1 GHz − 3 GHz]. It should be emphasized that for this example 25 modes were tracked even though only 5 modes are needed and eventually presented. For comparison purposes, the tracked eigenvalues obtained using the eigenvectors correlation approach are depicted in Fig. 5.17. As might be seen the correlation method yielded incoherent curves with many leaps, and intersections between the modes. Hence, to better understand the behavior of the modes at crossing points, more precisely at equal eigenvalues, Fig. 5.18 displays zooming of the intersection between the second mode and the third mode from Fig. 5.17, along with their associated eigenvectors. As it can be seen from Figs. 5.18 - 5.19 the second mode after the crossing point should continue with a mode index equal to 3, and the third mode should continue with the mode index equal to 2. This fact is also supported by Figs. 5.20 - 5.21, but as the eigenvectors are not well defined in the case of equal eigenvalues, the correlation method leaded to inaccurate tracking results. Whereas, the proposed technique produced coherent curves over the operating band, and more importantly unaffected by the degenerated modes issue as it might be deduced from Fig. 5.22, this is due to the fact that the process is systematically based on the difference between magnitudes

[1]The mesh contains two overlapping triangles, therefore they should be removed before making use of the antenna mesh.

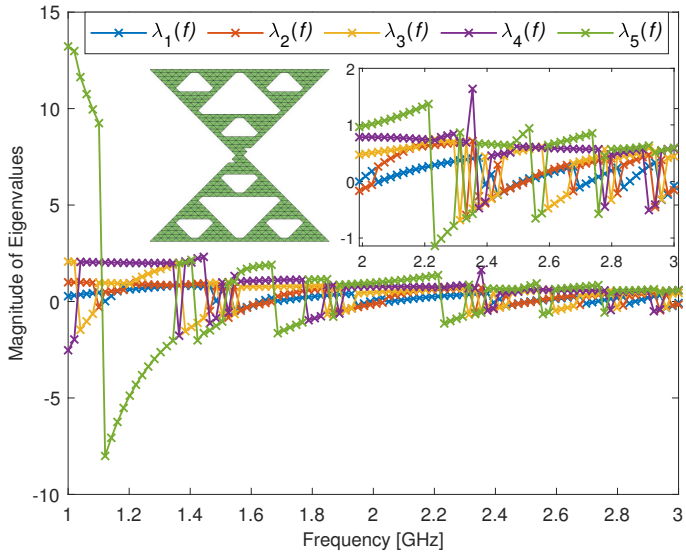

FIGURE 5.17: Eigenvalues of the fractal antenna tracked using the eigenvectors correlation algorithm.

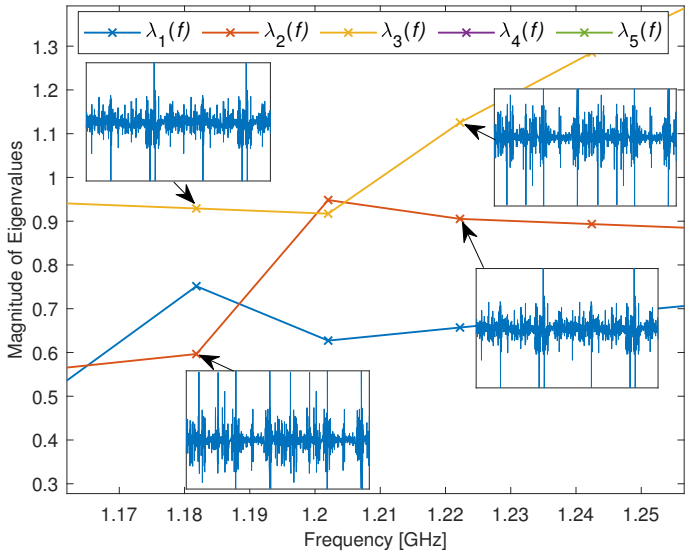

FIGURE 5.18: Zoomed intersection of modes $\lambda_2(f)$ and $\lambda_3(f)$ of the fractal antenna with insets showing the corresponding eigenvectors.

of eigenvalues, and doesn't distinguish between the modes, either they are degenerated or not, which have proven performance in treating such cases (i.e. degenerated modes). It is worth mentioning that in the above-mentioned example of the correlation-based tracking method, the eigenvectors distribution was used to prove the switching between modes. In fact, This could be used for the proposed tracking approach or other tracking procedures to measure the correctness of the obtained results. Further, the modal significance of the tracked characteristic modes is shown in Fig. 5.23. Interestingly, the antenna has one dominant or resonant mode n_4 at 1.121 GHz with a radiation bandwidth of approximately 0.133, computed using 1.06 GHz as the lower frequency and 1.21 GHz as the upper frequency (see Fig. 5.23). This is slightly different from the results obtained in [79] which predict the resonance to be around 1.48 GHz. Furthermore, the computational time[2] of the proposed method and that of the correlation method were calculated. It is worth mentioning that the impedance matrix decomposition time was not included, and no refining frequency scheme was used for these calculations. The computations were performed using Windows 8 with Intel$^{(R)}$ core$^{(TM)}$ i7-2700K CPU @ 3.5 GHz and RAM 16 GB. The proposed method is found to be much more faster than the eigenvectors correlation method as it can be seen from Table. 5.5. Therefore, the proposed approach can accelerate the tracking process in a significant way, particularly, for dense meshes as in the case of the slot antenna.

[2]The calculations were made using the stopwatch timer functions, tic and toc from Matlab.

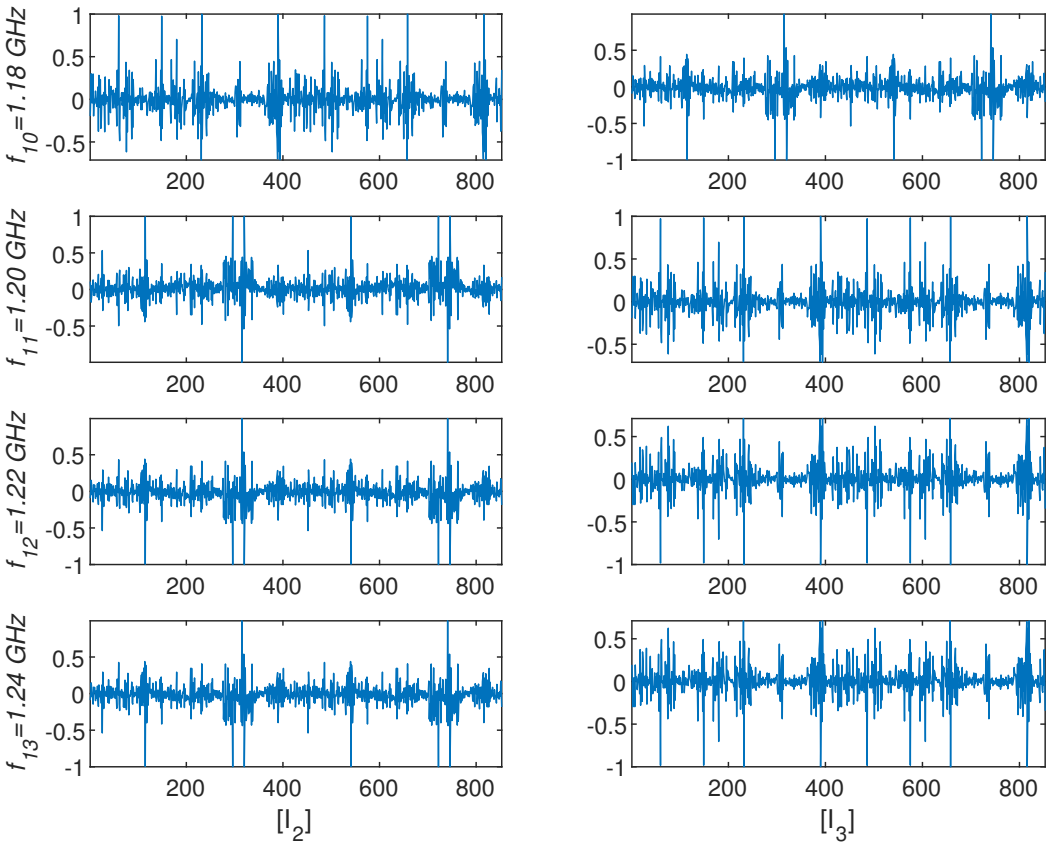

FIGURE 5.19: Illustration of the distribution of the eigenvectors $[I_2]$ and $[I_3]$ associated with the modes n_2 and n_3 at several frequencies near degeneracy at $f_{11} = 1.20$ GHz.

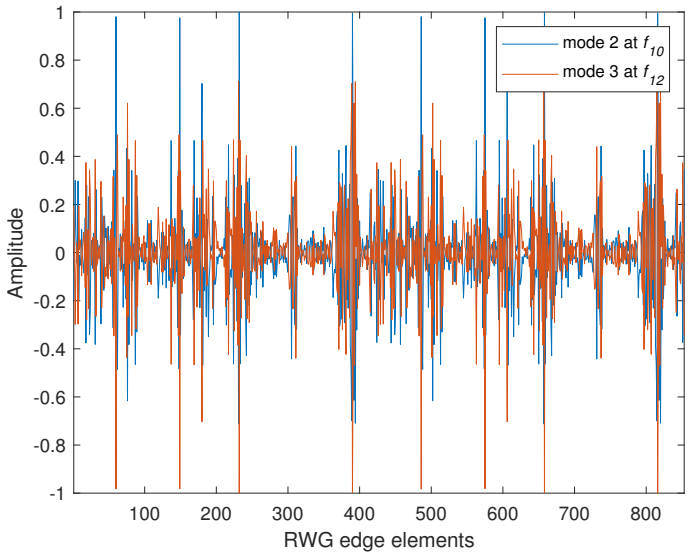

FIGURE 5.20: Distribution of the eigenvectors associated to the modes n_2 at the frequency sample f_{10} and n_3 at f_{12} for the fractal antenna example.

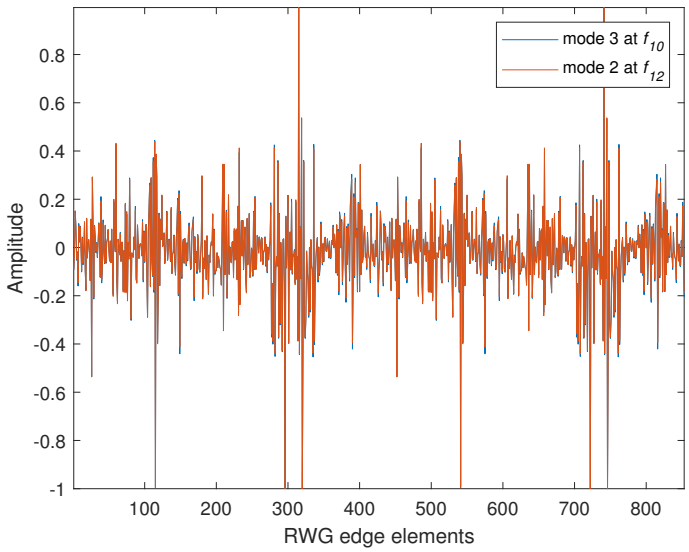

FIGURE 5.21: Distribution of the eigenvectors associated to the modes n_3 at the frequency sample f_{10} and n_2 at f_{12} for the fractal antenna example.

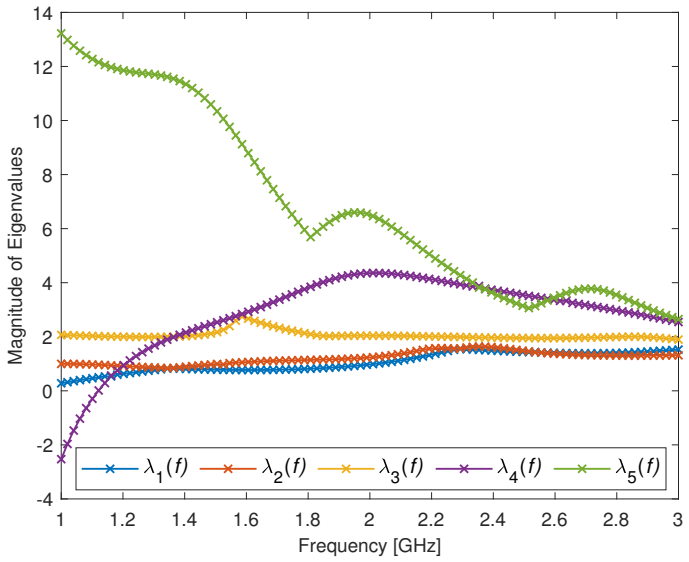

FIGURE 5.22: Tracked eigenvalues of the fractal antenna using the proposed method.

TABLE 5.5: Computational time of the tracking process using the correlation and the proposed method.

	Correlation Method (s)	Proposed Method (s)
Metal Plate	0.067	0.006
Slot Antenna	0.462	0.014
Spiral Antenna	2.206	0.027
Fractal Antenna	0.995	0.012

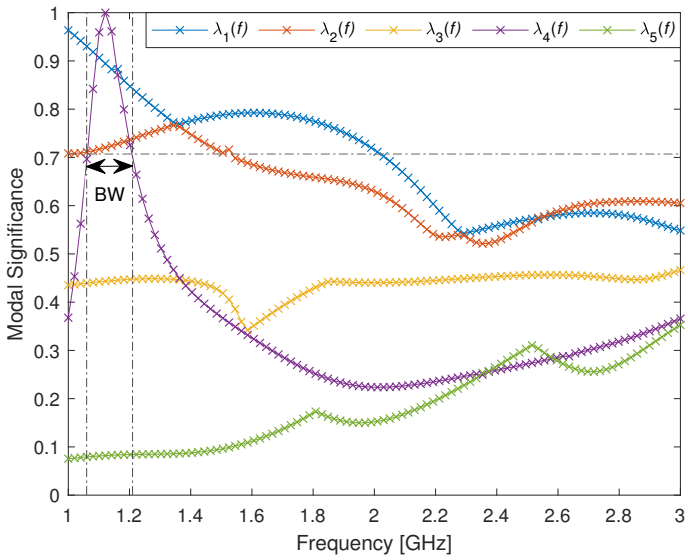

FIGURE 5.23: Representation of the modal significance parameter for the Fractal antenna obtained using the proposed method, with the black dashed lines showing the bandwidth of the resonant mode.

5.5 Performances of the Proposed Tracking Method

The proposed tracking method presents several appealing features. Firstly, it has proven its efficiency in eliminating the swapped modes issue, which is a very severe problem for the eigenvectors correlation procedure but not for the eigenfields correlation approach. Secondly, The proposed mechanism is immune to degenerated modes issue, while it is frequently encountered in the correlation-based methods, and it is related to the fact that the eigenvectors are not well defined at equal eigenvalues. Furthermore, the proposed procedure is based only on the minimum magnitude between consecutive eigenvalues, therefore no need to fulfill any orthogonality condition, conversely to the correlation-based methods, which are based on the assumptions of the orthogonality of modal quantities (i.e., eigenvectors and eigenfields). Moreover, the use of eigenvalues alone to track the characteristic modes simplifies tremendously the modal tracking process, without any need for extra computations such as the case for far fields correlation. However, a reasonable frequency step size must be set to avoid tracking failures, and in case of unsatisfactory results it is recommended to reduce the space between adjacent frequency samples. In fact, this is recommended for all the discussed tracking methods, although the eigenfield correlation tolerates a relatively large frequency step size. In addition, the results of the proposed method might be affected by the mesh density used in the computations, especially for complicated structures. Finally, a summary of the advantages and limitations of the proposed approach in comparison to the correlation-based methods is presented in Table 5.6

Main issues	Tracking Methods			
	Eigenvectors Correlation	Eigenfields Correlation	Surface current Correlation	Proposed Method
Swapped modes	Yes	No	Not reported	No
degenerated modes	Yes	Yes	Yes	No
Extra computations	No	Yes	No	No
Frequency step reduction	Yes	No	Yes	Yes
Mesh density	Yes	Not reported	Yes	Yes

TABLE 5.6: A comparison of the immunity of the proposed tracking procedure and the correlation-based methods to the main issues encountered in modal tracking. Yes is used for not eliminated problems and No for eliminated problems.

5.6 Conclusion

In this chapter, a simple yet efficient and fast algorithm was presented to shed new light on the possible uses of the eigenvalues in the modal tracking process, and to take a new look over the most challenging problems encountered in eigenvectors correlation-based tracking methods, specifically, the swapping and the degenerated modes. The proposed tracking method was implemented and assessed using four numerical examples, and the obtained results were compared with the eigenvectors correlation method. The proposed method provided generally satisfactory results and proved its efficiency in modal tracking with a high rate compared to the eigenvectors correlation method. Furthermore, the accuracy of the obtained results could be improved by making use of the refining process whether over a specific frequency segment or overall the operating band, or also by increasing the number of the characteristic modes being tracked.

Finally, the proposed method seems to be a very promising approach, nevertheless, further testing and improvements need to be performed to overcome some shortcomings of this approach, such as dealing with the discontinuity of characteristic modes.

Chapter 6

Matrix $[Z]$ interpolation

6.1 Introduction

Admittedly, as it has been explained through the previous chapters, the MoM impedance matrix $[Z]$ has a central importance in the characteristic modes theory formulation, as this latter is based mainly on diagonalising the impedance matrix $[Z]$ of the scatterer. However, computing the impedance matrix at each frequency sample is a time-consuming process, particularly for wideband frequency applications. In this chapter, the interpolation approach of the impedance matrix will be discussed for its simplicity and efficiency in terms of saving the processing time.

6.2 Pioneering Research Works

The increasing demands of highly accurate results of the characteristic modes are among the leading causes of heavy computations in the numerical implementation of the characteristic modes theory. The heaviest load is the construction of the MoM impedance matrix. Therefore, accelerating the MoM calculations is one of the most significant current discussions within the scientific community. Newman and Forrai were the first to propose an effective solution to this problem using the impedance matrix interpolation in [57], without giving any details of the approach used. Thereafter, a detailed description of the method was given latter by Newman in [58]. A few years later, a direct application of this interpolation method was performed to evaluate the performance of two complex antennas, namely a planar inverted F antenna (PIFA) and a helix antenna, for personal wireless applications, where a high reduction in terms of the CPU time was achieved [143]. Meanwhile, other approaches have been reported effective in reducing the computation time of the MoM matrix. For instance, Canning in [144] combined the

LU decomposition[1] and the pivoting method to reduce the filling time of a symmetric impedance matrix to half the computational time. Moreover, the use of analytical methods has been reported in [145, 146], these types of approaches don't require any numerical integration and accelerate the matrix-fill time significantly. Also, the use of semi-analytical approaches was suggested in [147, 148], which consist of simplifying the integrals used in building the impedance matrix from double integrals to single integrals. Whilst, the authors in [149] proposed the use of Cauchy's technique to extrapolate the currents at certain frequency points. While, the spatial interpolation was extensively investigated in [150–154]. Similarly, a combination of the Method of Moments-Physical Optics (MoM-PO) hybrid formulation and the Maehly approximation was implemented in [155], and good results were obtained in terms of CPU time compared to the traditional MoM-PO.

Among all the above-mentioned approaches, Newman's approach seems to be relatively simple to integrate into existing implementations without the need to perform any modifications, although, it is very demanding in terms of the system storage required, which can be considered as its major drawback. Fortunately, this issue has been already addressed by Karwowski and Noga in [156], who investigated the possibility of reducing the order of the matrix being interpolated. The authors proposed two approaches, one by partitioning the impedance matrix into smaller blocks and then manipulating on the resulting blocks. This partitioning mechanism can be illustrated by considering the matrix equation of an antenna current given by [156]

$$\underbrace{\begin{bmatrix} Z_{11} & Z_{12} \\ Z_{21} & Z_{22} \end{bmatrix}}_{[Z]} \begin{bmatrix} I_1 \\ I_2 \end{bmatrix} = \begin{bmatrix} U_1 \\ 0 \end{bmatrix} \tag{6.1}$$

From equation (6.1), a smaller matrix $[Z_1]$ can be obtained, which is easier to interpolate compared to the whole matrix $[Z]$. Its expression is given by [156]

$$[Z_1] = [Z_{11} - Z_{12} Z_{22}^{-1} Z_{21}] \tag{6.2}$$

The equation (6.2) is derived by making use of the following equations [156]

$$[Z_{11} I_1 + Z_{12} I_2] = [U_1] \tag{6.3}$$

$$[I_2] = [-Z_{22}^{-1} Z_{21} I_1] \tag{6.4}$$

Now, by making use of the assumption that a smaller number of unknowns is associated to the sub-domain 1 compared to that attributed to the sub-domain 2, the order of $[Z_1]$

[1] L stands for a lower triangular matrix, while U stands for an upper triangular matrix.

can be maintained smaller even for large impedance matrices [156].
While, the second approach consists in making use of Physical Optics approximations, which allow expressing $[Z_1]$ as [156]

$$[Z_1] = [Z_{11} + Z_{12}A_{21}] \tag{6.5}$$

where $[A_{21}]$ represents the influence of sources in sub-domain 1 on those in the sub-domain 2, such that [156]

$$[I_2] = [A_{21}] \cdot [I_1] \tag{6.6}$$

Effectively, both approaches resulted in a reduced computational time, nevertheless, it was found that the latter approach is faster and requires less storage space than the partitioning method [156].

6.3 Matrix Interpolation Methodology

Generally, the impedance matrix interpolation method constitutes a very appealing tool to accelerate the MoM method, hence the CMT analysis. This approach is mainly based on the fact that the elements of the impedance matrix $[Z]$ are slowly varying with the frequency, therefore, allowing the computation of the impedance matrix at relatively large frequency steps, which can be of particular importance for electrically large structures analysis. The interpolation scheme can be easily integrated into the existing implementations without any alteration of the codes, resulting in a significant reduction of the computational time. In fact, only few steps are needed to implement the interpolation method. Primarily, the impedance matrix $[Z]$ is computed and stored at relatively widely spaced frequency samples called matching points (e.g. f_1, f_5 and f_{10}) [58]. Thereafter, the intermediate values of the $[Z]$ elements are obtained using the interpolation method [143] at the desired intermediate frequency samples (e.g. f_3, f_6 and f_9). Therefore, one computes the impedance matrix at the matching points and apply the interpolation scheme to get the impedance matrix at the closet three match points [58]. This process continues along with the whole frequency band understudy.
Certainly, the choice of the interpolation function to be applied to the impedance matrix is a key factor in the interpolation scheme. For instance, Newman in [58] performed the interpolation using a quadratic function, where the elements of the impedance matrix $[Z]$ at a specific intermediate frequency f can be obtained using [157]

$$Z_{mn}(f) = a_{mn}f^2 + b_{mn}f + c_{mn} \tag{6.7}$$

Here, a_{mn}, b_{mn}, and c_{mn} are elements of the complex coefficients matrices $[a]$, $[b]$, and $[c]$. It is worth mentioning that in case of wire antennas the above formula (6.7) can be used to get only the real part of Z_{mn}, whereas the imaginary part could be obtained using the following expression [58]

$$X_{mn}(f) = A + B\ \ln f + Cf \tag{6.8}$$

where A, B, and C are constants.

However, for electrically large antennas, a further alteration needs to be performed to the interpolation approach, which is known as the improved interpolation scheme [58], where the distance between the observation point and the source point is typically greater than half the wavelength, i.e, $r_{mn} > \lambda/2$, as in that case the exponential term in the Green' function is found to dominate the frequency behavior of the $[Z]$ elements. Therefore, the impedance element Z_{mn} is substituted by a new element $Z_{mn}^{'}$, such that [58]

$$Z_{mn}^{'} = Z_{mn}/e^{-jkr_{mn}} \tag{6.9}$$

Obviously, the resulting $Z_{mn}^{'}$ element is easier to interpolate, as it slowly varies with frequency compared to the original element Z_{mn} [58]. This improved interpolation scheme was implemented by the authors in [158], to examine the wire-surface structures, and it was found that the proposed scheme has greatly reduced the computation time without loss of accuracy.

Secondly, after choosing the interpolation function to be used, an appropriate frequency step size must be set. Newman, in his description of the method, didn't provide any hints of the ideal frequency step size that can accurately describe the antenna behavior. However, he provided an estimation of the upper bound on the step size, or what can be called as the maximum interpolation step size Δf_{max}, in terms of the speed of light c in the vacuum and the maximum extent of the structure understudy L_{max} as it follows [58]

$$\Delta f_{max} = \frac{c}{2L_{max}} \tag{6.10}$$

Whereas, the authors in [157] suggested to plot the variation of some impedance matrix elements, preferably elements with small distance r_{mn} between the observation and the source points, also elements with large distance r_{mn}, and elements with mid-range distance, along the frequency spectrum in order to estimate the frequency step size at which the matrix elements can be accurately fitted by a chosen interpolation function. Eventually, it seems that the choice of the appropriate frequency step size is mainly related to the structure under consideration and its impedance matrix.

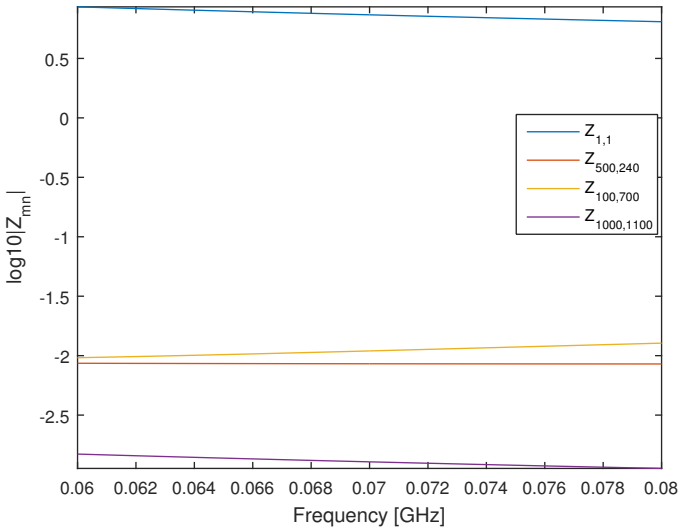

FIGURE 6.1: Magnitude variations with the frequency of selected impedance matrix elements for the slot antenna example.

6.3.1 Numerical Results

In this section, the impedance matrix interpolation method performances are evaluated using the slot antenna and the fractal antenna described in Section 5.4. A linear interpolation scheme is applied by making use of the built-in '*interp1*' Matlab function (see Appendix G) to interpolate the impedance matrix at the intermediate frequencies. Fig. 6.1 depicts the magnitude variations of the impedance matrix elements with the frequency for the slot antenna example, where the matrix elements are chosen to sweep all the matrix parts. It is apparent that the elements' magnitudes are slowly varying, while the phase of the matrix elements is almost linear (see Fig. 6.2), with the diagonal elements having almost the same behavior along the frequency range independently of their locations within the impedance matrix (i.e. top, bottom or at the center of the matrix). Similar observations can be deduced from Figs. 6.3 - 6.4 for the fractal antenna case, which is in complete agreement with the observations from [58]. Furthermore, the interpolation approach and the direct MoM method based on Makarov' code [79] were compared in terms of the computational time[2] for the slot antenna, the spiral antenna, and the fractal antenna examples (see Section 5.4). The computations were performed using Windows 8 with Intel core $I7-2700K$ CPU at 3.5 GHz and RAM 16 GB. The obtained results reveal a significant reduction of the CPU time using the linear interpolation method compared to the direct MoM, as it is shown in Table 6.1. The efficiency of the linear interpolation is more noticeable for dense meshes as is the case of the slot antenna, where the time needed to construct the whole impedance matrix is approximately half of that taken by the MoM.

[2]The calculations are performed using the '*cputime*' Matlab function.

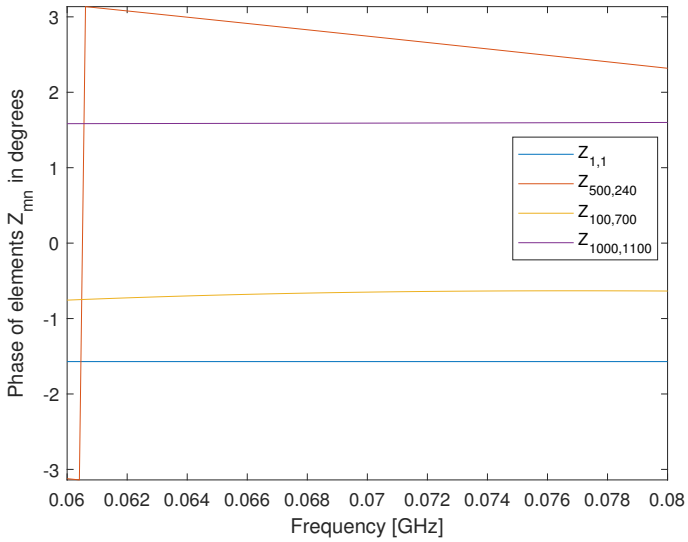

FIGURE 6.2: Phase variations with the frequency of selected impedance matrix elements for the slot antenna example.

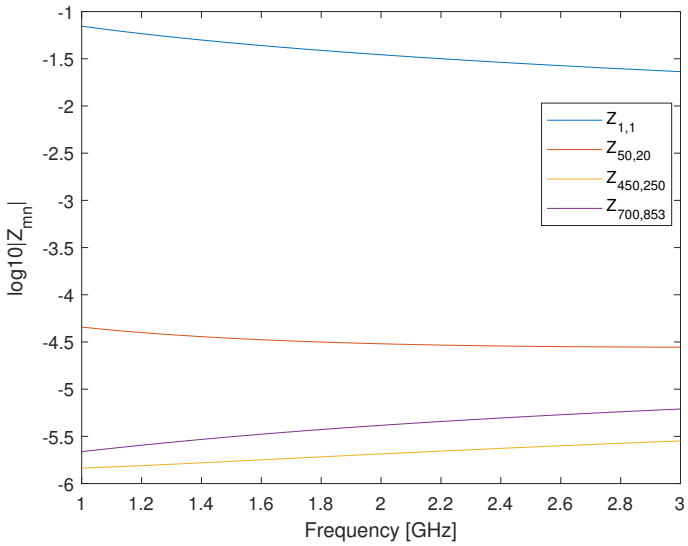

FIGURE 6.3: Magnitude variations with the frequency of selected impedance matrix elements for the Fractal antenna example.

TABLE 6.1: Assessment of the CPU time needed to construct the impedance matrix $[Z]$ using both the direct MoM method and the linear interpolation approach.

	Time in (s)	
Structure	Direct MoM	Interpolation
Slot Antenna	316.39	171.23
Spiral Antenna	251.81	143.39
Fractal Antenna	199.03	109.26

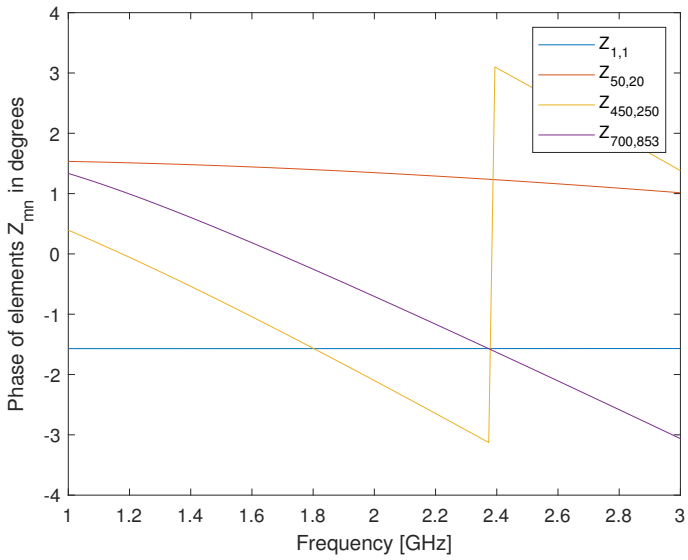

FIGURE 6.4: Phase variations with the frequency of selected impedance matrix elements for the Fractal antenna example.

6.4 Conclusion

In this chapter, the impedance matrix interpolation method has been reviewed. The method consists in computing the impedance matrix for some selected frequency samples, which are relatively distant from each other, and to interpolate the matrix elements at some chosen intermediate frequencies. It has been shown that the interpolation approach can be very useful in accelerating the impedance matrix filling time, particularly for wideband applications. Further, the method integration into existing solvers is straightforward. Nevertheless, the implementation of the interpolation method is very demanding in terms of storage memory.

Chapter 7

Conclusions and Future Work

7.1 Conclusions

In conclusion, the main goal of this work was to illustrate the usefulness of the characteristic modes theory in predicting the response of an arbitrarily shaped scatterer in the presence of an electromagnetic field. This theory uses the modal decomposition of the impedance matrix to gather data about the characteristic modes' contributions, the resonance frequency of the scatterer, and many other valuable pieces of information. The theory is well established, however, its numerical implementation suffers from some numerical inaccuracies as it has been highlighted in chapter 4, where the deficiencies of the real part of the impedance matrix raise many questions about the accuracy of the obtained results. One solution was proposed to overcome the indefiniteness issue. The proposed solution consists of rebuilding the real part matrix from the spherical modes projection matrix and its transpose. Consequently, a much more accelerated characteristic modes computation was obtained, with higher accuracy and a noticeable increase in the total number of the characteristic modes obtained.

Furthermore, the problem of modal tracking was examined, where the ramifications of swapping and degenerated modes encountered in the eigenvectors correlation method has been highlighted. In fact, it has been demonstrated that these issues can result in a misleading description of the behavior of the characteristic modes along with the frequency. Taken together, these findings suggest that the computation of the correlation coefficient between the eigenvectors is not a reliable predictor of the modes variations in function of the frequency. Hence, the need for a new measure to track more precisely the characteristic modes. In this dissertation, the use of the eigenvalues' magnitudes was proposed to track the modes over the frequency axis. The obtained results were satisfactory. Furthermore, the proposed approach has proved to be immune to the swapping

and degenerated modes problems.
Finally, the potential of the use of the impedance matrix interpolation in reducing the computational time needed has been demonstrated.

7.2 Future Work

Undoubtedly, the characteristic modes theory is a promising research area, with many open issues. Thus far, it has proved its efficiency in describing the radiation and scattering from the perfectly conducting bodies, yet it is not fully exploited in analysing the lossless dielectrics, and the lossy dielectrics. Therefore, a possible extension of the work presented here would be to adjust the proposed solution for the real part matrix to the dielectrics case.
Furthermore, another possible future work could be the improvement of the proposed tracking method to overcome its shortcomings in dealing with the discontinuity of some of the characteristic modes, and to further test the performances of the proposed method with other shapes and materials.
Finally, the impedance matrix interpolation approach seems to be very advantageous, and it could be integrated into the characteristic modes analysis. Moreover, further testing could be realised to accurately define the frequency step size needed to obtain more precise results.

Appendix A

Description of the RWG basis functions

The Characteristic modes theory is based on an operator equation, which relates the surface currents with the radiated or scattered fields. Usually, the surface currents are expanded using special expansion functions. For PEC surfaces, it is very common to use Rao-Wilton-Glisson (RWG) basis functions [52]. This choice is mainly due to its simplicity, and its divergence conforming property that makes its representation of the current physical, where the body surface is discretized using small triangular elements. Each pair of adjacent triangles define an edge element (see Figure. A.1) [79]. Thus, the vector basis function associated with an edge element is defined as [52]

$$f_p(r) = \begin{cases} \frac{l_p}{2A_p^+}\rho_p^+ \ , & \text{if } r \text{ in } T_p^+ \\ \frac{l_p}{2A_p^-}\rho_p^- \ , & \text{if } r \text{ in } T_p^- \\ 0, & \text{otherwise} \end{cases} \tag{A.1}$$

where l_p is the length of the common edge of the two adjacent triangles, and $A_p^{\pm}$ is the area of the triangle $T_p^{\pm}$. While $\rho_p^+ = r - v_p^+$, is the vector drawn from the free vertex of the positive triangle to the observation point, and $\rho_p^- = v_p^- - r$, is the vector drawn from the observation point to the free vertex of the negative triangle. More importantly, the basis function is zero outside the two adjacent triangles. Additionally, the plus or minus designation of the triangles is based on the choice of a positive current reference direction for the p^{th} edge, which is assumed to be from the positive triangle to the negative one. A remarkable feature of the RWG basis function is that the normal component to the inner edge l_p is a constant, whereas the normal component to any other edges is equal to zero, thus ensuring the current continuity across the interface of the edge element, and eliminating the fictitious charge on the inner edge [76]. Accordingly, the divergence

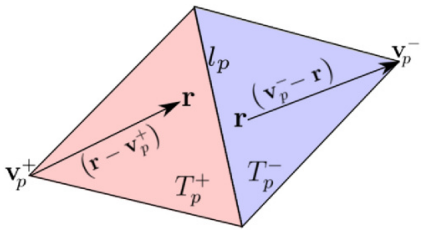

FIGURE A.1: RWG edge element

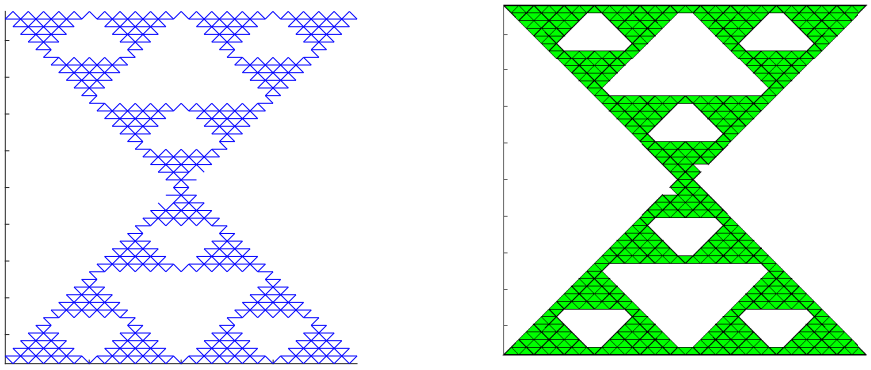

FIGURE A.2: Example of the inner edges (left side) extracted from the original mesh (right side)

of (A.1) is constant over the respective triangles, and can be expressed as [52]

$$\nabla \cdot f_p(r) = \begin{cases} \frac{l_p}{A_p^+}, & \text{if } r \text{ in } T_p^+ \\ -\frac{l_p}{A_p^-}, & \text{if } r \text{ in } T_p^- \\ 0, & \text{otherwise} \end{cases} \tag{A.2}$$

Therefore, in order to perform the numerical implementation of the MoM using the RWG basis functions, the inner edges of a given mesh should be extracted as shown in the left side of Fig. A.2, along with their lengths l_p. Further, for every two triangles sharing an inner edge a $+/-$ signs are attributed to them resulting in two categories of triangles, the plus triangles and the minus triangles. Note that a triangle might be classified within the plus and the minus triangles, i.e., a single triangle might hold the two signs simultaneously. Thereafter, the inner edges and the two categories of triangles are used in implementing the formula of the impedance operator. It should be noted that the numerical integration is simply a summation over the plus and minus triangles. More details about the MoM implementation and the source code can be found in [79].

Appendix B

Modes Decomposition using Python code

```
# importing the packages
import numpy as np
import h5py
from   scipy.linalg import eig
import math
import matplotlib.pyplot as plt # ploting package

f = h5py.File('ImpedanceMatrix.mat','r') # reading the file containing the Z matrix
Z = f['zMat'].value.view(np.complex) # transforming data into np complex array
                    # zMat is the name of the saved Z matrix within 'myMatrix.mat'

print (type (Z) )
R = Z[:,:].real
X = Z[:,:].imag

eigvals, eigvecs = eig(X, R) #  solving the generalized eigenvalue problem

eigvals = eigvals.real       # taking the real part of the eigenvalues

idx = eigvals.argsort()[::-1] # getting the index to perform the sorting process

eigvals = eigvals[idx]    # sorting the eigenvalues

eigvals = eigvals[~np.isnan(eigvals)]  # removing the Nan entries

eigvals_abs = np.absolute(eigvals)   # taking the absolute value

eigvals_log = [math.log10(y) for y in eigvals_abs] # log10 scale

# ploting the eigenvalues
plt.figure(1)
plt.plot(eigvals_log)
plt.grid(True)
plt.show()
```

Appendix C

Modes Decomposition using Matlab code

```
load('ImpedanceMatrix.mat');

X = imag(Z);

R = real(Z);

[I,Lambda]     = eig(X,R);

Lambda         = (diag(Lambda));

idxNaN         = find(isnan(Lambda));

Lambda(idxNaN)         = [];

Lambda(imag(Lambda)~=0)= [];

[LambdaSorted, index]  = sort(Lambda);

ISorted(:,:)           = I(:,index); %order the eigenvectors

LambdaSortedLog        = log10(abs(LambdaSorted));

figure(1)
plot(LambdaSortedLog); title('Eigenvalues');
grid on
```

Appendix D

Spherical wave functions

The general expression of the (scalar) spherical modes is [125]

$$u^{(p)}_{\sigma ml}(k\boldsymbol{r}) = z^{(p)}_l(kr)Y_{\sigma ml}(\hat{\boldsymbol{r}}) \tag{D.1}$$

where $\boldsymbol{r}$ is the spatial coordinate, $\hat{\boldsymbol{r}} = \boldsymbol{r}/r$, $r = |\boldsymbol{r}|$, and k the wave number, and the subscripts l denotes the degree of the wave functions (e.g., $l = 1, 2, 3 \ldots, \infty$), with m designating the wave functions order having values ranging from $-l$ to l (i.e., $m = -l, -(l-1), \ldots, 0, \ldots, (l-1), l$), while σ stand for even modes 'e' obtained by the even trigonometric azimuth functions $cos\, m\phi$, and the odd modes 'o' corresponding to $sin\, m\phi$ functions [125][126]. Furthermore, $z^{(p)}_l$ represent the radial functions, with the upper index $(^p)$ describing the type of the radial function used, i.e.,

$$\begin{aligned}
&p = 1 \implies z^{(1)}_l = j_l && \textit{Spherical Bessel function}\\
&p = 2 \implies z^{(2)}_l = n_l && \textit{Spherical Neumann function}\\
&p = 3 \implies z^{(3)}_l = h^{(1)}_l && \textit{Spherical Hankel function of the first kind}\\
&p = 4 \implies z^{(4)}_l = h^{(2)}_l && \textit{Spherical Hankel function of the second kind}
\end{aligned}$$

It is worth mentioning, that all types of $z^{(p)}_l$ functions can be implemented easily within Matlab [80], using the built in functions *besselj* and *besselh*, multiplied by a constant $\left(\sqrt{\frac{\pi}{2kr}}\right)$ [159, p.426]. In addition, $Y_{\sigma ml}$ denotes the ordinary spherical harmonics [126], and they are related to the the vector spherical harmonics [126], denoted by $Y_{\tau\sigma ml}(\hat{\boldsymbol{r}})$

as follows [126, p.350]

$$\begin{cases} Y_{1\sigma ml}(\hat{\boldsymbol{r}}) = \frac{1}{\sqrt{l(l+1)}}\nabla \times \left(\boldsymbol{r} Y_{\sigma ml}(\hat{\boldsymbol{r}})\right) \\ Y_{2\sigma ml}(\hat{\boldsymbol{r}}) = \frac{1}{\sqrt{l(l+1)}} r \nabla Y_{\sigma ml}(\hat{\boldsymbol{r}}) \\ Y_{3\sigma ml}(\hat{\boldsymbol{r}}) = \hat{\boldsymbol{r}} Y_{\sigma ml}(\hat{\boldsymbol{r}}) \end{cases} \tag{D.2}$$

where the spherical harmonics are given by [126, p.627]

$$Y_{ml}(\theta, \phi) = \sqrt{\frac{\varepsilon_m}{2\pi}} \tilde{P}_l^m(\cos\theta) \begin{Bmatrix} cos(m\phi) \\ sin(m\phi) \end{Bmatrix} \tag{D.3}$$

where $\tilde{P}_l^m(\cos\theta)$ is the normalized associated Legendre function defined in Sec. D.1, and ε_m the Neumann factor, defined as [126]

$$\varepsilon_m = \begin{cases} 1, & m = 0 \\ 2, & m > 0 \end{cases} \tag{D.4}$$

when implementing the spherical harmonics using *legendre* function from Matlab, it is highly recommended to compare the expressions of the spherical harmonics provided in the textbooks with that used within Matlab.
Therefore, the spherical wave functions can be expanded as [125][126]

$$\begin{cases} u_{1\sigma ml}^{(p)}(k\boldsymbol{r}) = R_{1l}^{(p)}(kr) Y_{1\sigma ml}(\hat{\boldsymbol{r}}) \\ u_{2\sigma ml}^{(p)}(k\boldsymbol{r}) = R_{2l}^{(p)}(kr) Y_{2\sigma ml}(\hat{\boldsymbol{r}}) + R_{3l}^{(p)}(kr) Y_{\sigma ml}(\hat{\boldsymbol{r}})\hat{\boldsymbol{r}} \end{cases} \tag{D.5}$$

where $R_l^{(p)}(kr)$ are the radial function of order l defined as [125, p.314][126, p.354]

$$R_{\tau l}^{(p)}(kr) = \begin{cases} z_l^{(p)}(kr), & \tau = 1 \\ \frac{1}{kr} \frac{(\partial kr z_l^{(p)}(kr))}{\partial kr}, & \tau = 2 \\ \sqrt{l(l+1)} z_l^{(p)}(kr)/kr, & \tau = 3 \end{cases} \tag{D.6}$$

Further, an index transformation can be performed to transform the index quadruplets into a single index denoted by α, this latter can be used to fill the $[S]$ matrix (see Chapter. 4) as follows [160]

$$\alpha = \{\tau, \sigma, m, l\} = 2(l^2 + l - 1 + (-1)^s m) + \tau \tag{D.7}$$

where $s = 1$ and $s = 2$ when $\sigma = odd$ and $\sigma = even$, respectively. While $\tau \in \{1, 2\}$, whereas $m \in \{0, ..., l\}$, and $l \in \{1, ..., L\}$.

D.1 Associated Legendre functions

In this section, the explicit expressions of the associated Legendre functions are given. Firstly, the Legendre polynomials of degree l are defined using Rodrigues' formula as [125, p.318]

$$P_l(cos(\theta)) = \frac{1}{2^l l!}\frac{d^l}{d(cos(\theta))^l}(cos(\theta)^2 - 1)^l, \quad \theta \in [0, \pi] \tag{D.8}$$

The derivative of Legendre polynomials could be used to define the associated Legendre function such that [125, p.318]

$$P_l^m(cos(\theta)) = (1 - cos(\theta)^2)^{m/2}\frac{d^m}{d(cos(\theta))^m}P_l(cos(\theta)) \tag{D.9}$$

where $l \geq m \geq 0$. The associated Legendre functions can also be obtained using recursive formulas [127, p. 401], these include

$$P_l^m(cos(\theta)) = \frac{2l-1}{l-m}cos(\theta)P_{l-1}^m(cos(\theta)) - \frac{l+m-1}{l-m}P_{l-2}^m(cos(\theta)) \tag{D.10}$$

Consequently, The derivative of associated Legendre functions is given by [127, p. 402]

$$\frac{d}{d\theta}P_l^m = \frac{1}{2}[(l-m+1)(l+m)P_l^{m-1} - P_l^{m+1}] \tag{D.11}$$

where P_l^m can be substituted by the normalized associated Legendre function $\tilde{P}_l^m$, as follows [125, p.318]

$$\tilde{P}_l^m = \sqrt{\frac{2l+1}{2}\frac{(l-m)!}{(l+m)!}}P_l^m \tag{D.12}$$

For $\theta = \{0, \pi\}$, the derivative of associated Legendre functions is ill defined. Therefore, the following expression has been used (see [125, p.319] for more details)

$$\frac{\partial \tilde{P}_l^m(\cos\theta)}{\partial\theta} = \begin{cases} -\sqrt{(l+1)l}\tilde{P}_l^1(\cos\theta), & m = 0 \\ \left[\sqrt{(l+m)(l-m+1)}\tilde{P}_l^{m-1}(\cos\theta) - \cos\theta\frac{m}{\sin\theta}\tilde{P}_l^m(\cos\theta)\right], & m \neq 0 \end{cases} \tag{D.13}$$

where the problematic term $\frac{m}{\sin\theta}\tilde{P}_l^m\cos\theta$ is altered by (see [125, p.319] for more details)

$$\frac{m}{\sin\theta}\tilde{P}_l^m(\cos\theta) = \begin{cases} 0, & m = 0 \\ \frac{1}{2}\sqrt{\frac{2l+1}{2l+3}}\left(\sqrt{(l+m+2)(l+m+1)}\tilde{P}_{l+1}^{m+1}\right. & \\ \qquad \left. +\sqrt{(l-m+2)(l-m+1)}\tilde{P}_{l+1}^{m-1}\right), & m \neq 0 \end{cases} \tag{D.14}$$

Appendix E

Extinction Theorem

The extinction theorem is inherent to the construction of surface integral equations for the electromagnetic scattering problems [75, 85, 161, 162]. Particularly, for the magnetic field integral equation (MFIE). The derivation in this section will follow [162], therefore, let consider a body V_2 characterised by the permittivity ϵ_2 and the permeability μ_2, bounded by the closed surface S, and immersed in a homogeneous medium V_1 with constitutive parameters ϵ_1 and μ_1, and bounded by the surface at infinity S_∞. Further, to illustrate the theorem derivation let suppose that V_2 is illuminated by an incident wave (E^i, H^i) as shown in Fig. E.1. The exterior fields E_1 and H_1 in V_1 can be expressed in function of the incident (E^i, H^i) and the scattered fields (E^s, H^s) as follows [162]

$$E_1 = E^i + E^s \tag{E.1}$$

$$H_1 = H^i + H^s \tag{E.2}$$

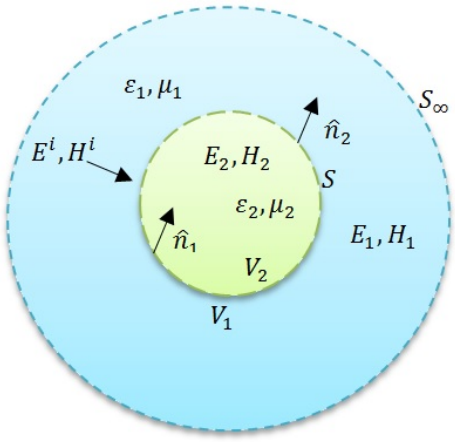

FIGURE E.1: Illustrative schematic for the scattering problem.

The electromagnetic fields defined within V_1 and V_2 satisfy the source free vector wave equation. Hence, by considering E_1 and E_2 as the solution of the vector wave equation, i.e., [162]

$$\nabla \times \nabla \times E_1 - k_1^2 E_1 = 0 \tag{E.3}$$

$$\nabla \times \nabla \times E_2 - k_2^2 E_2 = 0 \tag{E.4}$$

with $k_1^2 = \omega^2 \mu_1 \epsilon_1$ and $k_2^2 = \omega^2 \mu_2 \epsilon_2$. The integral form of the equations can be obtained by making use of the vector Green's second identity given by [162]

$$\iiint_V [P \cdot \nabla \times \nabla \times Q - (\nabla \times \nabla \times P) \cdot Q] \, \mathrm{d}v = - \oiint_S [(\hat{n} \times \nabla \times P) \cdot Q + (\hat{n} \times P) \cdot \nabla \times Q] \, \mathrm{d}s \tag{E.5}$$

For convenience, the dyadic Green's function G_1 for the the medium V_1, defined in (4.5), will be used, as it is a solution to the following vector wave equation [162]

$$\nabla \times \nabla \times \nabla G_1 - k_1^2 G_1 = \mathbf{I} \delta(\boldsymbol{r} - \boldsymbol{r}') \tag{E.6}$$

where $\mathbf{I}$ is the unit dyadic, and $\delta(\boldsymbol{r} - \boldsymbol{r}')$ is the Kronecker delta function. Therefore, by substituting P and Q in (E.5) by E_1 and G_1, the identity reads

$$\begin{aligned} &\iiint_{V_1} [E_1(\boldsymbol{r}) \cdot \nabla \times \nabla \times G_1(\boldsymbol{r}, \boldsymbol{r}') - (\nabla \times \nabla \times E_1(\boldsymbol{r})) \cdot G_1(\boldsymbol{r}, \boldsymbol{r}')] \, \mathrm{d}v = \\ &- \oiint_{S+S_\infty} [(\hat{n}_1 \times \nabla \times E_1(\boldsymbol{r})) \cdot G_1(\boldsymbol{r}, \boldsymbol{r}') + (\hat{n}_1 \times E_1(\boldsymbol{r})) \cdot \nabla \times G_1(\boldsymbol{r}, \boldsymbol{r}')] \, \mathrm{d}s \end{aligned} \tag{E.7}$$

by making use of the vector wave equations (E.3) and (E.6), the left side of (E.7) can be simplified as [162]

$$\iiint_{V_1} [E_1(\boldsymbol{r}) \cdot (\mathbf{I} \delta(\boldsymbol{r} - \boldsymbol{r}') + k_1^2 G_1(\boldsymbol{r}, \boldsymbol{r}') - k_1^2 E_1(\boldsymbol{r}) \cdot G_1(\boldsymbol{r}, \boldsymbol{r}')] \, \mathrm{d}v = \begin{cases} E_1(\boldsymbol{r}') & \text{for } \boldsymbol{r}' \in V_1 \\ 0 & \text{for } \boldsymbol{r}' \in V_2 \end{cases} \tag{E.8}$$

Further, (E.7) can be expressed in terms of the incident and scattered fields using (E.1) such that

$$\begin{aligned} E^i(\boldsymbol{r}') - &\oiint_{S_\infty} [(\hat{n}_1 \times \nabla \times E_s(\boldsymbol{r})) \cdot G_1(\boldsymbol{r}, \boldsymbol{r}') + (\hat{n}_1 \times E_s(\boldsymbol{r})) \cdot \nabla \times G_1(\boldsymbol{r}, \boldsymbol{r}')] \, \mathrm{d}s \\ &- \oiint_S [(\hat{n}_1 \times \nabla \times E_1(\boldsymbol{r})) \cdot G_1(\boldsymbol{r}, \boldsymbol{r}') + (\hat{n}_1 \times E_1(\boldsymbol{r})) \cdot \nabla \times G_1(\boldsymbol{r}, \boldsymbol{r}')] \, \mathrm{d}s \\ &= \begin{cases} E_1(\boldsymbol{r}') & \text{for } \boldsymbol{r}' \in V_1 \\ 0 & \text{for } \boldsymbol{r}' \in V_2 \end{cases} \end{aligned} \tag{E.9}$$

After some simplifications the terms in the integral over S_∞ of E^s and G_1 vanish (for details see [162]) in the above equation. Worth noting that the expression of $E^i(\boldsymbol{r}')$ can be easily derived in the absence of the scatterer, where $E_1(\boldsymbol{r}')$ is reduced into $E^i(\boldsymbol{r}')$, i.e., [162]

$$E^i(\boldsymbol{r}') = -\oiint_{S_\infty} [(\hat{n}_1 \times \nabla \times E^i(r)) \cdot G_1(\boldsymbol{r}, \boldsymbol{r}') + (\hat{n}_1 \times E^i(\boldsymbol{r})) \cdot \nabla \times G_1(\boldsymbol{r}, \boldsymbol{r}')] \, \mathrm{d}s \quad \text{(E.10)}$$

Therefore, the equation (E.9) can be rearranged as [162]

$$E^i(\boldsymbol{r}') - \iint_S [ik_1\eta_1(\hat{n}_1 \times H_1(r)) \cdot G_1(\boldsymbol{r}, \boldsymbol{r}') + (\hat{n}_1 \times E_1(\boldsymbol{r})) \cdot \nabla \times G_1(\boldsymbol{r}, \boldsymbol{r}')] \, \mathrm{d}s = \begin{cases} E_1(\boldsymbol{r}') & \text{for } \boldsymbol{r}' \in V_1 \\ 0 & \text{for } \boldsymbol{r}' \in V_2 \end{cases} \quad \text{(E.11)}$$

The equation (E.11) represent the extinction theorem, which clearly indicate that the scattered field cancels the incident field within V_2, and it defines the scattered field $E^s(\boldsymbol{r}')$ as [162]

$$E^s(\boldsymbol{r}') = -\iint_S [ik_1\eta_1(\hat{n}_1 \times H_1(\boldsymbol{r})) \cdot G_1(\boldsymbol{r}, \boldsymbol{r}') + (\hat{n}_1 \times E_1(\boldsymbol{r})) \cdot \nabla \times G_1(\boldsymbol{r}, \boldsymbol{r}')] \, \mathrm{d}s \quad \text{(E.12)}$$

Note that in the above equations $\eta_1 = \sqrt{\dfrac{\mu_1}{\epsilon_1}}$.

Analogically, expressions for the inner field $E_2(\boldsymbol{r}')$ can be derived as [162]

$$-\iint_S [ik_2\eta_2(\hat{n}_2 \times H_2(\boldsymbol{r})) \cdot G_2(\boldsymbol{r}, \boldsymbol{r}') + (\hat{n}_2 \times E_2(\boldsymbol{r})) \cdot \nabla \times G_2(\boldsymbol{r}, \boldsymbol{r}')] \, \mathrm{d}s = \begin{cases} 0 & \text{for } \boldsymbol{r}' \in V_1 \\ E_2(\boldsymbol{r}') & \text{for } \boldsymbol{r}' \in V_2 \end{cases} \quad \text{(E.13)}$$

Appendix F

Modal Tracking using Matlab code

```
function [ModesT]  = ModalTracking (Lambda,Nmodes,Steps,Isort)
%{
This function implements the Modal tracking
inputs:    Lambda : Sorted eigenvalues
           Isort  : Sorted eigenvectors
           Nmodes : number of modes required
           Steps  : number of frequency steps
output:    ModesT : matrix of tracked modes
%}
%----------------------------------
%% Eigenvectors Correlation Method
%----------------------------------
switch nargin
 case 4
  In   =  Isort(:,1:Nmodes,:);
  for thisFreq = 1:Steps-1
      for thisMode = 1: Nmodes
          corrM(thisMode,:,thisFreq)=... % computing the correlation matrix
                abs(corr(In(:,thisMode,thisFreq),In(:,:,thisFreq+1)));
      end
 end
 idxM  = zeros (Steps-1, Nmodes); % Modes indices Matrix
 for thisFreq = 1:Steps-1
     cort = corrM(:,:,thisFreq);
     for thisMode  = 1: Nmodes
         maxCol = max(cort(:,thisMode));% sort each column
         idx    = find(maxCol == cort(:,thisMode),1);
         idxM(thisFreq,thisMode)= idx ;
         cort(:,thisMode)       = -1  ;
         cort(idx,:)            = -1  ;
     end
 end
```

```
 ModesT(:,1)  = Lambda(1:Nmodes,1);
 for thisFreq = 2:Steps
     ModesT(:,thisFreq)= Lambda(idxM(thisFreq-1,:),thisFreq);
 end
%-----------------------------------
%% Proposed Tracking Method
%-----------------------------------

case 3
    ModesT           = Lambda ;
    NewModesT        = zeros (Nmodes, Steps);
    NewModesT(:,1)   = ModesT (:,1);
    for i = 1: Steps-1
        m                = repmat(ModesT(:,i), [1 Nmodes]);
        n                = repmat(ModesT(:,i+1)',[Nmodes 1 ]);
        DifferenceMatrix  = abs( m - n );
        for j = 1: Nmodes
            minV   = min(DifferenceMatrix(j,:));
            idx    = find(minV == DifferenceMatrix(j,:),1);
            NewModesT (j,i+1)       = ModesT(idx,i+1);
            DifferenceMatrix(:,idx) = 100;
        end
        ModesT(:,i+1)  =  NewModesT(:,i+1);
    end
 end
```

Appendix G

Matlab code for $[Z]$ interpolation

```
function [Zfinal,NewSteps, Fp]= Zinterpolation(Z,FStart,FStop,Steps)

%this function performs the Z matrix interpolation
%inputs:
% Z is the impedance matrix (a 3-D array)
% FStart  = 3e9;  % start of frequency range in Hz
% FStop   = 10e9; % end of frequency range in Hz
% Steps   = 4;% frequency samples

% outputs:
% Zfinal is the interpolated impedance matrix
% NewSteps is the total number of frequency samples after interpolation
% Fp is the new frequency axis obtained

NewSteps = 2*Steps-1; % new intermediate frequency samples
 for i=1:Steps
    F(i)= FStart+(i-1)*(FStop-FStart)/max(Steps-1,1); % frequency axis
 end

 for j=1:NewSteps
     Fp(j)= FStart+(j-1)*(FStop-FStart)/max(NewSteps-1,1); % new frequency axis
 end

NewF          = setdiff(Fp,F);% New frequency samples
[~,indexNewF] = ismember(NewF,Fp);

Zp            = permute(Z,[3 1 2]);
Zint          = interp1(F,Zp,Fp(indexNewF), 'linear');
Zinterpolated = permute(Zint, [2 3 1]);
Zfinal        = zeros (size(Z,1),size(Z,2),length(Fp));

final_axisF   = 1:length(Fp);
MatchPts      = setdiff(final_axisF,indexNewF);

Zfinal(:,:,indexNewF)= Zinterpolated; % inserting Z at intermediate samples
Zfinal(:,:,MatchPts) = Z; % inserting Z at primary samples
```

Bibliography

[1] R. J. Garbacz. *A generalized expansion for radiated and scattered fields*. PhD thesis, Ohio State Univ., Columbus, 1968.

[2] Raj Mittra. *Computer Techniques for Electromagnetics: International Series of Monographs in Electrical Engineering*, volume 7. Elsevier, 2013.

[3] Roger F Harrington. *Field computation by moment methods*. Wiley-IEEE Press, 1993.

[4] Walton C Gibson. *The method of moments in electromagnetics*. Chapman and Hall/CRC, 2007.

[5] R Harrington and J Mautz. Theory of characteristic modes for conducting bodies. *IEEE Transactions on Antennas and Propagation*, 19(5):622–628, 1971.

[6] R Harrington and J Mautz. Computation of characteristic modes for conducting bodies. *IEEE Transactions on Antennas and Propagation*, 19(5):629–639, 1971.

[7] R Harrington, J Mautz, and Yu Chang. Characteristic modes for dielectric and magnetic bodies. *IEEE Transactions on Antennas and Propagation*, 20(2):194–198, 1972.

[8] Yu Chang and R Harrington. A surface formulation for characteristic modes of material bodies. *IEEE transactions on antennas and propagation*, 25(6):789–795, 1977.

[9] R Harrington and J Mautz. Control of radar scattering by reactive loading. *IEEE Transactions on Antennas and Propagation*, 20(4):446–454, 1972.

[10] R Harrington and J Mautz. Pattern synthesis for loaded n-port scatterers. *IEEE Transactions on Antennas and Propagation*, 22(2):184–190, 1974.

[11] R Harrington and J Mautz. Optimization of radar cross section of n-port loaded scatterers. *IEEE Transactions on Antennas and Propagation*, 22(5):697–701, 1974.

[12] RF Harrington and JR Mautz. Characteristic modes for aperture problems. *IEEE transactions on microwave theory and techniques*, 33(6):500–505, 1985.

[13] N Inagaki and R Garbacz. Eigenfunctions of composite hermitian operators with application to discrete and continuous radiating systems. *IEEE Transactions on Antennas and Propagation*, 30(4):571–575, 1982.

[14] D Pozar. Antenna synthesis and optimization using weighted inagaki modes. *IEEE transactions on antennas and propagation*, 32(2):159–165, 1984.

[15] Duixian Liu, Robert J Garbacz, and David M Pozar. Antenna synthesis and optimization using generalized characteristic modes. *IEEE transactions on antennas and propagation*, 38(6):862–868, 1990.

[16] Jonathan Ethier and Derek A McNamara. The use of generalized characteristic modes in the design of mimo antennas. *IEEE Transactions on Magnetics*, 45(3): 1124–1127, 2009.

[17] E Newman. Small antenna location synthesis using characteristic modes. *IEEE Transactions on Antennas and Propagation*, 27(4):530–531, 1979.

[18] Brian A Austin and Kevin P Murray. The application of characteristic-mode techniques to vehicle-mounted nvis antennas. *IEEE Antennas and Propagation Magazine*, 40(1):7–21, 1998.

[19] David Anthony Strohschein. *Application of characteristic mode analysis to variable antenna placement on devices operating in the near-resonant range*. PhD thesis, the University of New Hampshire, 2002.

[20] Martin Hilbert, Mark A Tilston, and Keith G Balmain. Resonance phenomena of log-periodic antennas: characteristic-mode analysis. *IEEE transactions on antennas and propagation*, 37(10):1224–1234, 1989.

[21] Karim Y Kabalan, Ali El-Hajj, and Roger F Harrington. Characteristic mode analysis of a slot in a conducting plane separating different media. *IEEE transactions on antennas and propagation*, 38(4):476–481, 1990.

[22] K Kabalan, R Harrington, H Auda, and J Mautz. Characteristic modes for slots in a conducting plane, te case. *IEEE transactions on antennas and propagation*, 35(2):162–168, 1987.

[23] K Kabalan, R Harrington, J Mautz, and H Auda. Characteristic modes for a slot in a conducting plane, tm case. *IEEE transactions on antennas and propagation*, 35(3):331–335, 1987.

[24] KY Kabalan, ALI EL-HAJJ, and RF Harrington. Scattering and penetration characteristic mode for a dielectric filled conducting cylinder with longitudinal slot. *AEU. Archiv für Elektronik und Übertragungstechnik*, 47(3):137–142, 1993.

[25] Karim Y Kabalan, Ali El-Hajj, Shahwan Khoury, and Asaad Rayes. Electromagnetic coupling to conducting objects behind apertures in a conducting body. *Radio Science*, 32(3):881–898, 1997.

[26] Werner L Schroeder, T Famdie, and Klaus Solbach. Utilisation and tuning of the chassis modes of a handheld terminal for the design of multiband radiation characteristics. *IEE Wideband and Multi-band Antennas and Arrays(Ref. No. 2005/11059)*, 2005.

[27] Jonathan Ethier, Eric Lanoue, and Derek McNamara. Mimo handheld antenna design approach using characteristic mode concepts. *Microwave and Optical Technology Letters*, 50(7):1724–1727, 2008.

[28] Eva Antonino Daviu. *Analysis and design of antennas for wireless communications using modal methods*. PhD thesis, Universitat Politècnica de València, 2008.

[29] Shameem Kabir Chaudhury, Heinz J Chaloupka, and Andreas Ziroff. Novel mimo antennas for mobile terminal. In *2008 European Conference on Wireless Technology*, pages 330–333. IEEE, 2008.

[30] Jonathan Ethier. *Antenna shape synthesis using characteristic mode concepts*. University of Ottawa (Canada), 2012.

[31] Marta Cabedo Fabres. *Systematic design of antennas using the theory of characteristic modes*. PhD thesis, Universitat Politècnica de València, 2008.

[32] Celestin Tamgue Famdie. *Small Antennas Radiation Performance Optimization in Mobile Communications*. PhD thesis, Universität Duisburg-Essen, Fakultät für Ingenieurwissenschaften, 2007.

[33] Shen Wang. *Characteristic modes analysis for antenna parameters optimization*. PhD thesis, Yokohama National University, 2015.

[34] Bryan Dennis Raines. *Systematic design of multiple antenna systems using characteristic modes*. PhD thesis, The Ohio State University, 2011.

[35] Khaled Ahmad Obeidat. *Design methodology for wideband electrically small antennas (ESA) based on the theory of characteristic modes (CM)*. PhD thesis, The Ohio State University, 2010.

[36] Jacob J Adams and Jennifer T Bernhard. A modal approach to tuning and bandwidth enhancement of an electrically small antenna. *IEEE Transactions on Antennas and Propagation*, 59(4):1085–1092, 2011.

[37] Jonathan Ethier and Derek A McNamara. An interpretation of mode-decoupled mimo antennas in terms of characteristic port modes. *IEEE Transactions on Magnetics*, 45(3):1128–1131, 2009.

[38] Hui Li, Yi Tan, Buon Kiong Lau, Zhinong Ying, and Sailing He. Characteristic mode based tradeoff analysis of antenna-chassis interactions for multiple antenna terminals. *IEEE Transactions on Antennas and Propagation*, 60(2):490–502, 2012.

[39] Hui Li, Zachary Thomas Miers, and Buon Kiong Lau. Design of orthogonal mimo handset antennas based on characteristic mode manipulation at frequency bands below 1 ghz. *IEEE Transactions on Antennas and Propagation*, 62(5):2756–2766, 2014.

[40] Dong-Woo Kim and Sangwook Nam. Systematic design of a multiport mimo antenna with bilateral symmetry based on characteristic mode analysis. *IEEE Transactions on Antennas and Propagation*, 66(3):1076–1085, 2018.

[41] Farhan Ammar Ahmad. Review of isolation enhancement with the help of theory of characteristic modes. *arXiv preprint arXiv:1811.06452*, 2018.

[42] Krishna Kumar Kishor and Sean Victor Hum. A pattern reconfigurable chassis-mode mimo antenna. *IEEE Transactions on Antennas and Propagation*, 62(6): 3290–3298, 2014.

[43] Khaled Ahmad Obeidat. *Design methodology for wideband electrically small antennas (ESA) based on the theory of characteristic modes (CM)*. PhD thesis, The Ohio State University, 2010.

[44] Chukwuka Ozuem, Divitha Seetharamdoo, M Hassanein Rabah, and Hedi Sakli. Stored energy evaluation of metamaterials based on theory of characteristic mode. *12th European Conference on Antennas and Propagation (EuCAP 2018)*, 2018.

[45] Chukwuka Ozuem, Divitha Seetharamdoo, M Hassanein Rabah, and Hedi Sakli. Methodology for quantifying metamaterial stored energy using theory of characteristic mode. In *2018 IEEE International Symposium on Antennas and Propagation & USNC/URSI National Radio Science Meeting*, pages 1121–1122. IEEE, 2018.

[46] Mhamad Hassanein Rabah. *Design methodology of antennas based on metamaterials and the theory of characteristic modes: application to cognitive radio*. PhD thesis, Lille 1, 2015.

[47] Jacob J Adams. *Characteristic modes for impedance matching and broadbanding of electrically small antennas*. PhD thesis, University of Illinois at Urbana-Champaign, 2011.

[48] Jacob J Adams and Jennifer T Bernhard. Broadband equivalent circuit models for antenna impedances and fields using characteristic modes. *IEEE Transactions on Antennas and Propagation*, 61(8):3985–3994, 2013.

[49] Celestin Tamgue Famdie, Werner L Schroeder, and Klaus Solbach. Numerical analysis of characteristic modes on the chassis of mobile phones. In *2006 First European Conference on Antennas and Propagation*, pages 1–6. IEEE, 2006.

[50] E Antonino-Daviu, M Cabedo-Fabres, M Ferrando-Bataller, and JI Herranz-Herruzo. Analysis of the coupled chassis-antenna modes in mobile handsets. In *IEEE Antennas and Propagation Society Symposium, 2004.*, volume 3, pages 2751–2754. IEEE, 2004.

[51] E Antonino-Daviu, M Cabedo-Fabres, M Ferrando-Bataller, A Valero-Nogueira, and M Martinez-Vazquez. Novel antenna for mobile terminals based on the chassis-antenna coupling. In *2005 IEEE Antennas and Propagation Society International Symposium*, volume 1, pages 503–506. IEEE, 2005.

[52] Sadasiva Rao, D Wilton, and Allen Glisson. Electromagnetic scattering by surfaces of arbitrary shape. *IEEE Transactions on antennas and propagation*, 30(3):409–418, 1982.

[53] Yikai Chen and Chao-Fu Wang. Surface integral equation based characteristic mode formulation for dielectric resonators. In *2014 IEEE Antennas and Propagation Society International Symposium (APSURSI)*, pages 846–847. IEEE, 2014.

[54] Pasi Ylä-Oijala, Henrik Wallén, Dimitrios C Tzarouchis, and Ari Sihvola. Surface integral equation-based characteristic mode formulation for penetrable bodies. *IEEE Transactions on Antennas and Propagation*, 66(7):3532–3539, 2018.

[55] D Schaubert, D Wilton, and A Glisson. A tetrahedral modeling method for electromagnetic scattering by arbitrarily shaped inhomogeneous dielectric bodies. *IEEE Transactions on Antennas and Propagation*, 32(1):77–85, 1984.

[56] Binbin Yang and Jacob J Adams. Quality factor calculations for the characteristic modes of dielectric resonator antennas. In *2017 United States National Committee of URSI National Radio Science Meeting (USNC-URSI NRSM)*, pages 1–2. IEEE, 2017.

[57] EDWARDH Newman and David Forrai. Scattering from a microstrip patch. *IEEE Transactions on Antennas and Propagation*, 35(3):245–251, 1987.

[58] Edward H Newman. Generation of wide-band data from the method of moments by interpolating the impedance matrix (EM problems). *IEEE Transactions on Antennas and Propagation*, 36(12):1820–1824, 1988.

[59] Qi I Dai, Junwei Wu, Hui Gan, Qin S Liu, Weng Cho Chew, and EI Wei. Large-scale characteristic mode analysis with fast multipole algorithms. *IEEE Transactions on Antennas and Propagation*, 64(7):2608–2616, 2016.

[60] Miloslav Capek, Pavel Hazdra, Pavel Hamouz, and Jan Eichler. A method for tracking characteristic numbers and vectors. *Progress In Electromagnetics Research*, 33:115–134, 2011.

[61] Bryan D Raines and Roberto G Rojas. Wideband characteristic mode tracking. *IEEE Transactions on Antennas and Propagation*, 60(7):3537–3541, 2012.

[62] DJ Ludick, U Jakobus, and M Vogel. A tracking algorithm for the eigenvectors calculated with characteristic mode analysis. In *Antennas and Propagation (EuCAP), 2014 8th European Conference on*, pages 569–572. IEEE, 2014.

[63] Zachary Miers and Buon Kiong Lau. Tracking of characteristic modes through far-field pattern correlation. In *Antennas and Propagation & USNC/URSI National Radio Science Meeting, 2015 IEEE International Symposium on*, pages 1470–1471. IEEE, 2015.

[64] Zachary Miers and Buon Kiong Lau. Wideband characteristic mode tracking utilizing far-field patterns. *IEEE Antennas Wireless Propag. Lett*, 14:1658–1661, 2015.

[65] DJ Ludick, JV Tonder, and U Jakobus. A hybrid tracking algorithm for characteristic mode analysis. In *Electromagnetics in Advanced Applications (ICEAA), 2014 International Conference on*, pages 455–458. IEEE, 2014.

[66] Zhao Yang, Donglin Su, Yaoyao Li, and Yan Liu. An improved method for tracking of characteristic modes. In *Computational Electromagnetics (ICCEM), 2016 IEEE International Conference on*, pages 103–105. IEEE, 2016.

[67] Eugen Safin and Dirk Manteuffel. Advanced eigenvalue tracking of characteristic modes. *IEEE Transactions on Antennas and Propagation*, 64(7):2628–2636, 2016.

[68] H Alroughani, JLT Ethier, and DA McNamara. Numerical experiments in tracking the characteristic modes of dielectric objects. In *2016 IEEE/ACES International*

Conference on Wireless Information Technology and Systems (ICWITS) and Applied Computational Electromagnetics (ACES), pages 1–2. IEEE, 2016.

[69] H Alroughani. An enhanced algorithm in tracking characteristic modes of dielectric objects. In *2017 International Applied Computational Electromagnetics Society Symposium-Italy (ACES)*, pages 1–2. IEEE, 2017.

[70] Doruk Tayli, Miloslav Capek, Lamyae Akrou, Vit Losenicky, Lukas Jelinek, and Mats Gustafsson. Accurate and efficient evaluation of characteristic modes. *IEEE Transactions on Antennas and Propagation*, 66(12):7066–7075, 2018.

[71] Miloslav Capek, Vit Losenicky, Lukas Jelinek, and Mats Gustafsson. Validating the characteristic modes solvers. *IEEE Transactions on Antennas and Propagation*, 65(8):4134–4145, 2017.

[72] Zhaojun Bai, James Demmel, Jack Dongarra, Axel Ruhe, and Henk van der Vorst. *Templates for the solution of algebraic eigenvalue problems: a practical guide*. SIAM, 2000.

[73] Gilbert W Stewart and Sun Ji-guang. *Matrix perturbation theory*. Academic Press, Computer Science and Scientific Computing, 1990.

[74] R J Garbacz and R H Turpin. A generalized expansion for radiated and scattered fields. *IEEE transactions on Antennas and Propagation*, 19(3):348–358, 1971.

[75] Weng Cho Chew, Mei Song Tong, and Bin Hu. Integral equation methods for electromagnetic and elastic waves. *Synthesis Lectures on Computational Electromagnetics*, 3(1):1–241, 2008.

[76] Yikai Chen and Chao-Fu Wang. *Characteristic modes: Theory and applications in antenna engineering*. John Wiley & Sons, 2015.

[77] R Harrington and J Mautz. Radiation and Scattering from Bodies of Revolution. *Interaction Notes 188*, July 1969.

[78] CA Balanis. Advanced engineering electromagnetics. *Wiley*, 2012.

[79] Sergey N Makarov. *Antenna and EM Modeling with MATLAB*. Wiley-Interscience,, 2002.

[80] MATLAB. *version 8.6 (R2015b)*. The MathWorks Inc., Natick, Massachusetts, 2015.

[81] Python Software Foundation. Python language reference, version 2.7, 2010.

[82] Miloslav Capek, Pavel Hazdra, Michal Masek, and Vit Losenicky. Analytical representation of characteristic mode decomposition. *IEEE Transactions on Antennas and Propagation*, 65(2):713–720, 2017.

[83] JLT Ethier and DA McNamara. Modal significance measure in characteristic mode analysis of radiating structures. *Electronics letters*, 46(2):107–108, 2010.

[84] Altair. (2016). Feko. altair. *Online: http://www.feko.info*, .

[85] F Harrigton Roger. Time-harmonic electromagnetic fields. *IEEE Press series on Electromagnetic Wave Theory*, 2001.

[86] Jürgen Nitsch, Frank Gronwald, and Gunter Wollenberg. *Radiating nonuniform transmission-line systems and the partial element equivalent circuit method*. John Wiley & Sons, 2009.

[87] Andrew J Poggio and Edmund K Miller. *Integral equation solutions of three-dimensional scattering problems*. MB Assoc., 1970.

[88] Te-Kao Wu and Leonard L Tsai. Scattering from arbitrarily-shaped lossy dielectric bodies of revolution. *Radio Science*, 12(5):709–718, 1977.

[89] Tomás Bernabeu Jiménez. *Contribution to the physical interpretation of characteristic mode resonances. Application to dielectric resonator antennas*. PhD thesis, Universitat Politècnica de València, 2017.

[90] Tapan K Sarkar, Eric L Mokole, and Magdalena Salazar-Palma. An expose on internal resonance, external resonance, and characteristic modes. *IEEE Transactions on Antennas and Propagation*, 64(11):4695–4702, 2016.

[91] Andrew F Peterson. The "interior resonance" problem associated with surface integral equations of electromagnetics: Numerical consequences and a survey of remedies. *Electromagnetics*, 10(3):293–312, 1990.

[92] WC Chew and JM Song. Gedanken experiments to understand the internal resonance problems of electromagnetic scattering. *Electromagnetics*, 27(8):457–471, 2007.

[93] Arthur D Yaghjian. Augmented electric-and magnetic-field integral equations. *Radio Science*, 16(06):987–1001, 1981.

[94] David B Davidson. *Computational electromagnetics for RF and microwave engineering*. Cambridge University Press, 2010.

[95] Su Yan, Jian-Ming Jin, and Zaiping Nie. Improving the accuracy of the second-kind fredholm integral equations by using the buffa-christiansen functions. *IEEE transactions on Antennas and Propagation*, 59(4):1299–1310, 2011.

[96] A Haluk Nalbantoglu. New computation method for characteristic modes. *Electronics Letters*, 18(23):994–996, 1982.

[97] Qi I Dai, Qin S Liu, Hui UI Gan, and Weng Cho Chew. Combined field integral equation-based theory of characteristic mode. *IEEE Transactions on Antennas and Propagation*, 63(9):3973–3981, 2015.

[98] Adel A Mohsen, A-RA Helaly, and Hany M Fahmy. The corrected induced surface current for arbitrary conducting objects at resonance frequencies. *IEEE transactions on antennas and propagation*, 43(5):448–452, 1995.

[99] LM Correia and AM Barbosa. An approximate (symmetric) magnetic field integral equation for the analysis of scattering by conducting bodies. In *International Symposium on Antennas and Propagation Society, Merging Technologies for the 90's*, pages 902–905. IEEE, 1990.

[100] LM Correia. A comparison of integral equations with unique solution in the resonance region for scattering by conducting bodies. *IEEE transactions on antennas and propagation*, 41(1):52–58, 1993.

[101] Allen W Glisson, Darko Kajfez, and Joseph James. Evaluation of modes in dielectric resonators using a surface integral equation formulation. *IEEE transactions on microwave theory and techniques*, 31(12):1023–1029, 1983.

[102] Zachary Miers and Buon Kiong Lau. On characteristic eigenvalues of complex media in surface integral formulations. *IEEE Antennas and Wireless Propagation Letters*, 16:1820–1823, 2017.

[103] H Alroughani, JLT Ethier, and DA McNamara. Observations on computational outcomes for the characteristic modes of dielectric objects. In *2014 IEEE Antennas and Propagation Society International Symposium (APSURSI)*, pages 844–845. IEEE, 2014.

[104] Zachary T Miers and Buon Kiong Lau. Computational analysis and verifications of characteristic modes in real materials. *IEEE Transactions on Antennas and Propagation*, 64(7):2595–2607, 2016.

[105] Pasi Ylä-Oijala, Henrik Wallén, Dimitrios C Tzarouchis, and Ari Sihvola. Surface integral equation-based characteristic mode formulation for penetrable bodies. *IEEE Transactions on Antennas and Propagation*, 66(7):3532–3539, 2018.

[106] Shaode Huang, Jin Pan, and Yuyue Luo. Investigations of non-physical characteristic modes of material bodies. *IEEE Access*, 6:17198–17204, 2018.

[107] Branko M Kolundžija and Antonije R Djordjević. *Electromagnetic modeling of composite metallic and dielectric structures*. Artech House, 2002.

[108] Joseph R Mautz and Roger F Harrington. H-field, e-field, and combined field solutions for bodies of revolution. Technical report, Syracuse Univ NY Dept of Electrical and Computer Engineering, 1977.

[109] P Huddleston, L Medgyesi-Mitschang, and J Putnam. Combined field integral equation formulation for scattering by dielectrically coated conducting bodies. *IEEE transactions on antennas and propagation*, 34(4):510–520, 1986.

[110] Sadasiva M Rao and Donald R Wilton. E-field, H-field, and combined field solution for arbitrarily shaped three-dimensional dielectric bodies. *Electromagnetics*, 10(4): 407–421, 1990.

[111] John M Putnam and Louis N Medgyesi-Mitschang. Combined field integral equation formulation for inhomogeneous two-and three-dimensional bodies: The junction problem. *IEEE Transactions on Antennas and Propagation*, 39(5):667–672, 1991.

[112] A Kishk and Lotfollah Shafai. Different formulations for numerical solution of single or multibodies of revolution with mixed boundary conditions. *IEEE Transactions on Antennas and Propagation*, 34(5):666–673, 1986.

[113] Pasi Ylä-Oijala. Numerical analysis of combined field integral equation formulations for electromagnetic scattering by dielectric and composite objects. *Progress In Electromagnetics Research*, 3:19–43, 2008.

[114] Pasi Yla-Oijala and Matti Taskinen. Application of combined field integral equation for electromagnetic scattering by dielectric and composite objects. *IEEE Transactions on Antennas and Propagation*, 53(3):1168–1173, 2005.

[115] Baek Ho Jung, Tapan Kumar Sarkar, and Y-S Chung. A survey of various frequency domain integral equations for the analysis of scattering from three-dimensional dielectric objects. *Electrical Engineering and Computer Science*, 65, 2002.

[116] Yikai Chen and Chao-Fu Wang. Characteristic mode analysis of pec bodies using combined field integral equation. In *2015 IEEE International Symposium on Antennas and Propagation & USNC/URSI National Radio Science Meeting*, pages 1474–1475. IEEE, 2015.

[117] Michael S Yeung. Single integral equation for electromagnetic scattering by three-dimensional homogeneous dielectric objects. *IEEE transactions on Antennas and Propagation*, 47(10):1615–1622, 1999.

[118] D Maystre. Integral methods. In *Electromagnetic theory of gratings*, pages 63–100. Springer, 1980.

[119] Egon Marx. Integral equation for scattering by a dielectric. *IEEE transactions on antennas and propagation*, 32(2):166–172, 1984.

[120] A Glisson. An integral equation for electromagnetic scattering from homogeneous dielectric bodies. *IEEE Transactions on Antennas and propagation*, 32(2):173–175, 1984.

[121] David R Swatek. *Investigation of single-source surface integral equations for electromagnetic wave scattering by dielectric bodies*. PhD thesis, The University of Manitoba, 1999.

[122] AW Glisson and BI Sholy. Numerical solution of electromagnetic scattering problems involving homogeneous dielectric bodies via a single integral equation. In *Abstract, National Radio Science Meeting, Philadelphia, PA*, 1986.

[123] Joseph R Mautz. A stable integral equation for electromagnetic scattering from homogeneous dielectric bodies. *IEEE transactions on antennas and propagation*, 37(8):1070–1071, 1989.

[124] Farhad Sheikh Hosseini Lori, Anton Menshov, Reza Gholami, Jamiu Babatunde Mojolagbe, and Vladimir I Okhmatovski. Novel single-source surface integral equation for scattering problems by 3-d dielectric objects. *IEEE Transactions on Antennas and Propagation*, 66(2):797–807, 2018.

[125] J. E. Hansen. *Spherical Near-Field Antenna Measurements*. IET Electromagnetic waves series no. 26. Stevenage, UK: Peter Peregrinus Ltd, 1988.

[126] Gerhard Kristensson. *Scattering of electromagnetic waves by obstacles*. The Institution of Engineering and Technology, 2016.

[127] Julius Adams Stratton. *Electromagnetic theory*. John Wiley & Sons, 2007.

[128] Frank Jensen and Aksel Frandsen. On the number of modes in spherical wave expansions. *Proc. 26th AMTA*, 2(1):489–494, 2004.

[129] Tayli D, Capek M, Akrou L, Losenicky V, L.Jelinek, and Gustafsson M. Accurate and efficient evaluation of characteristic modes. *submitted, arXiv:1709.09976. [Online]. Available: https://arxiv.org/abs/1709.09976*, 2017.

[130] DA Dunavant. High degree efficient symmetrical gaussian quadrature rules for the triangle. *International journal for numerical methods in engineering*, 21(6): 1129–1148, 1985.

[131] Fredrik Johansson et al. mpmath: a python library for arbitrary-precision floating-point arithmetic (version 0.18), december 2013, 2013.

[132] (2017) Antenna Toolbox for MATLAB (AToM). Czech technical university in prague. *[Online]. Available: www.antennatoolbox.com.*

[133] Tayli D. (2017) ida (integrated development toolset for antennas. *Lund University.*

[134] Intel. (2017). Intel math kernel library 2017 update 3. *[Online]. Available: https://software.intel.com/en-us/mkl.*

[135] Miloslav Capek, Mats Gustafsson, and Kurt Schab. Minimization of antenna quality factor. *IEEE Transactions on Antennas and Propagation*, 65(8):4115–4123, 2017.

[136] JH Wilkinson. The algebraic eigenvalue problem. *Oxford University Press*, 1988.

[137] G Angiulli and F Venneri. Use of the simultaneous diagonalization technique in the Ax =λBx eigenproblem applied to the computation of the characteristic modes. *ACES Journal*, 17(3):232–238, 2002.

[138] Advanpix. (2016). Multiprecision computing toolbox for matlab. *[Online]. Available: http://www.advanpix.com/*, .

[139] Arun Kumar Sharma. *Text book of correlations and regression.* Discovery Publishing House, 2005.

[140] G Hall. Pearson's correlation coefficient. *other words*, 1(9), 2015.

[141] Lamyae Akrou and Henrique JA da Silva. Enhanced modal tracking for characteristic modes. *IEEE Transactions on Antennas and Propagation*, 67(1):356–360, 2019.

[142] Makarov Sergey N., Kulkarni Shashank, and Marut Andrew G. Matlab antenna toolbox draft 05, antenna lab, ece, wpi. *[Online]. Available: http://ece.wpi.edu/mom/index.html.*

[143] Kathleen Virga and Yahya Rahmat-Samii. Wide-band evaluation of communications antennas using [z] matrix interpolation with the method of moments. In *IEEE Antennas and Propagation Society International Symposium. 1995 Digest*, volume 2, pages 1262–1265. IEEE, 1995.

[144] FX Canning. Direct solution of the EFIE with half the computation. *IEEE Transactions on Antennas and Propagation*, 39(1):118–119, 1991.

[145] ZH Liu, Eng Kee Chua, and Kye Yak See. Accurate and efficient evaluation method of moments matrix based on a generalized analytical approach. 2009.

[146] Lale Alatan, MI Aksun, Karthikeyan Mahadevan, and M Tuncay Birand. Analytical evaluation of the mom matrix elements. *IEEE transactions on microwave theory and techniques*, 44(4):519–525, 1996.

[147] Luciano Tarricone, Mauro Mongiardo, and Francesco Cervelli. A quasi-one-dimensional integration technique for the analysis of planar microstrip circuits via mpie/mom. *IEEE Transactions on Microwave Theory and Techniques*, 49(3): 517–523, 2001.

[148] Jerry R Smith and Mark S Mirotznik. Analytical simplification of the 2-d method of moments impedance integral. *IEEE transactions on antennas and propagation*, 52(12):3288–3294, 2004.

[149] Krishnamoorthy Kottapalli, Tapan K Sarkar, R Adve, Y Hua, EK Miller, and GJ Burke. Accurate computation of wideband response of electromagnetic systems utilizing narrowband information. *Computer physics communications*, 68(1-3): 126–144, 1991.

[150] TW Nuteson, K Naishadham, and R Mittra. Spatial interpolation of the moment matrix in electromagnetic scattering and radiation problems. In *Proceedings of IEEE Antennas and Propagation Society International Symposium*, pages 860–863. IEEE, 1993.

[151] Krishna Naishadham, Todd W Nuteson, and Raj Mittra. Parametric interpolation of the moment matrix in surface integral equation formulation. *International Journal of RF and Microwave Computer-Aided Engineering: Co-sponsored by the Center for Advanced Manufacturing and Packaging of Microwave, Optical, and Digital Electronics (CAMPmode) at the University of Colorado at Boulder*, 9(6): 474–489, 1999.

[152] Soon Jae Kwon and Raj Mittra. Impedance matrix generation by using the fast matrix generation technique. *Microwave and Optical Technology Letters*, 51(1): 204–213, 2009.

[153] Glge Ogucu, Raj Mittra, and Kai Du. An interpolation algorithm to reduce the reduced matrix fill-time in CBFM. *IEEE Antennas and Wireless Propagation Letters*, 8:457–460, 2009.

[154] Shunchuan Yang and Donglin Su. Fast green function evaluation for method of moment. *arXiv preprint arXiv:1901.04162*, 2019.

[155] J Ling, S Gong, S Qin, W Wang, and Y Zhang. Wide-band analysis of on-platform antenna using mom-po combined with maehly approximation. *Journal of Electromagnetic Waves and Applications*, 24(4):475–484, 2010.

[156] A Karwowski and A Noga. Using the mom impedance matrix interpolation with domain decomposition to increase computational efficiency of the wide-band performance evaluation of antennas. In *2010 IEEE Antennas and Propagation Society International Symposium*, pages 1–4. IEEE, 2010.

[157] Kathleen L Virga and Yahya Rahmat-Samii. Efficient wide-band evaluation of mobile communications antennas using [Z] or [Y] matrix interpolation with the method of moments. *IEEE Transactions on Antennas and Propagation*, 47(1): 65–76, 1999.

[158] Lv Zheng-liang, Gong Shu-xi, Ma Ji, and Wang Xing. Impedance matrix interpolation based on method of moments for solving radiation problem over a frequency band. In *2012 International Conference on Microwave and Millimeter Wave Technology (ICMMT)*, volume 3, pages 1–3. IEEE, 2012.

[159] John David Jackson. *Classical electrodynamics*. John Wiley & Sons, 2007.

[160] Mats Gustafsson and Sven Nordebo. Characterization of MIMO antennas using spherical vector waves. *IEEE Transactions on Antennas and Propagation*, 54(9): 2679–2682, 2006.

[161] Leung Tsang, Jin Au Kong, and Kung-Hau Ding. *Scattering of electromagnetic waves: theories and applications*, volume 27. John Wiley & Sons, 2004.

[162] K. Sarabandi. Ewald-oseen extinction theorem. http://www.eecs.umich.edu/courses/eecs730/lect/EOExtTheo_W09_port.pdf, 2009. Accessed: 2019-04-19.